PhD degree in Systems Medicine (curriculum in Molecular Oncology)

European School of Molecular Medicine (SEMM),

University of Milan and University of Naples "Federico II"

Settore disciplinare: MED/04

# Drug repurposing for the treatment of acute myeloid leukaemia with adverse prognosis

*Debora Valli*

IEO, Milan

Matricola n. R11470

*Supervisor:* Prof. Pier Giuseppe Pelicci

IEO, Milan

*Added Supervisor:* Prof. Myriam Alcalay

IEO, Milan

Anno accademico 2018-2019

# Table of contents

# List of abbreviations

| | |
|---|---|
| 4E-BP1 | Eukaryotic translation initiation factor 4E binding protein 1 |
| ADMET | Absorption, distribution, metabolism, excretion, toxicity |
| ALL | Acute lymphoblastic leukaemia |
| AML | Acute myeloid leukaemia |
| APC | Adenomatous polyposis coli |
| APL | Acute promyelocytic leukaemia |
| Ara-C | Cytosine arabinoside (cytarabine) |
| ASK1 | Apoptosis signal-regulating kinase 1 |
| ASXL1-2 | ASXL transcriptional regulator 1-2 |
| ATCC | American Type Culture Collection |
| ATF4 | Activating transcription factor 4 |
| ATF6 | Activating transcription factor 6 |
| ATP | Adenosine triphosphate |
| ATRA | All-trans retinoic acid |
| BAD | BCL2 associated agonist of cell death |
| BAK | BCL2 antagonist/killer 1 |
| BAX | BCL2 associated X |
| BCL-2 | B-cell lymphoma 2 |
| BCL-xL | B-cell lymphoma-extra large |
| BIM | BCL-2-like protein 11 |
| BiP | Binding immunoglobulin protein |
| BM | Bone marrow |
| BrdU | Bromodeoxyuridine |
| CEBPA | CCAAT/enhancer-binding protein alpha |
| CHOP | C/EBP-homologous protein |
| CI | Combination index |
| CK1α | Casein kinase 1 alpha |
| CLL | Chronic lymphocytic leukaemia |
| CML | Chronic myelogenous leukaemia |
| CN | Cytogenetically normal |
| CR | Complete morphological remission |
| CSF1R | Colony stimulating factor 1 receptor |
| CTG | CellTiter-Glow |

| | |
|---|---|
| DMSO | Dimethylsulfoxide |
| DNA | Deoxyribonucleic acid |
| DNAJB9 | DnaJ heat shock protein family (Hsp40) member B9 |
| DNAJC3 | DnaJ heat shock protein family (Hsp40) member C3 |
| DNTM3A | DNA methyltransferase 3 alpha |
| DTNB | 5,5′-dithiobis (2-nitrobenzoic) acid |
| DTT | Dithiothreitol |
| DUBs | Deubiquitinases |
| E2F1 | E2F transcription factor 1 |
| E2F7 | E2F transcription factor 7 |
| ECL | Enhanced chemiluminescence |
| EDEM1 | ER degradation Enhancing alpha-mannosidase like protein 1 |
| EDTA | Ethylenediaminetetraacetic acid |
| EFS | Event free survival |
| eIF2α | Eukaryotic translation initiation factor 2 subunit alpha |
| eIF4E | Eukaryotic translation initiation factor 4E |
| ER | Endoplasmic reticulum |
| ERAD | Endoplasmic-reticulum-associated protein degradation |
| ERK | Extracellular-signal-regulated kinase |
| ERP44 | Endoplasmic reticulum protein 44 |
| FAB | French-American-British |
| FACS | Fluorescence-activated cell sorting |
| FBS | Fetal bovine serum |
| FDA | Food and drug administration |
| FLAG-IDA | Fludarabine, Cytarabine, Idarubicin and G-CSF |
| FLT3 | Fms related tyrosine kinase 3 |
| FoxO3 | Forkhead box O3 |
| $GI_{50}$ | Growth inhibition of 50% of cells |
| GO | Gemtuzumab ozogamicin |
| GSK3β | Glycogen synthase kinase 3 beta |
| HERPUD 1 | Homocysteine inducible ER protein with ubiquitin like domain 1 |
| HSCs | Hemopoietic stem cells |
| HSCT | Haematopoietic stem cell transplantation |
| HSP | Heat shock protein |
| HSPCs | Haematopoietic stem/progenitor cells |

| | |
|---|---|
| HTS | High throughput screening |
| i.p. | Intraperitoneal |
| i.v. | Intravenous |
| $IC_{50}$ | Half maximal inhibitory concentration |
| IDH1-2 | Isocitrate dehydrogenase 1-2 |
| IL-3 | Interleukin 3 |
| IRE1α | Inositol-requiring protein 1α |
| ITD | Internal tandem duplication |
| JAK2 | Janus kinase 2 |
| JM | Juxtamembrane |
| JNK | JUN N-terminal kinase |
| LEF-1 | Lymphoid enhancer binding factor 1 |
| MAD | Median absolute deviation |
| MAPK | Mitogen-activated protein kinase |
| MCL-1 | Myeloid cell leukaemia sequence 1 |
| MDS | Myelodysplastic syndromes |
| MEC | Mitoxantrone, etoposide and cytarabine |
| MLL-PTD | MLL-partial tandem duplication |
| MRD | Minimal residual disease |
| mTOR | Mammalian target of rapamycin |
| NADPH | Nicotinamide adenine dinucleotide phosphate |
| NPI | Normalized percent inhibition |
| NPM1 | Nucleophosmin 1 |
| NSG | NOD-scid IL2Rgamma$^{null}$ |
| OD | Optical density |
| OS | Overall survival |
| PB | Peripheral blood |
| PBS | Phosphate-buffered saline |
| PCR | Polymerase chain reaction |
| PDGFR | Platelet derived growth factor receptor |
| PDK1 | 3-Phosphoinositide-dependent kinase 1 |
| PERK | Protein kinase RNA-like endoplasmic reticulum kinase |
| PI | Propidium iodide |
| PI3K | Phosphatidylinositol 3-kinases |
| PDIA3 | Protein disulfide isomerase family A member 3 |

| | |
|---|---|
| PML | Promyelocytic leukaemia |
| PP | Pyrvinium pamoate |
| PPP1R15B | Protein phosphatase 1 regulatory subunit 15B |
| RAD21 | RAD21cohesin complex component |
| RARα | Retinoic acid receptor-alpha |
| ReDO | Repurposing drugs in oncology |
| RFS | Relapse free survival |
| RIDD | Regulated Ire1-dependent decay |
| RNA | Ribonucleic acid |
| RT | Room temperature |
| RTK | Receptor tyrosine kinase |
| RUNX1 | Runt-related transcription factor 1 |
| S1P | Site-1 protease |
| S2P | Site-2 protease |
| SD | Standard deviation |
| SEM | Standard error of the mean |
| SF3B1 | Splicing factor 3b subunit 1 |
| SMC3 | Structural maintenance of chromosomes 3 |
| SRSF2 | Serine and arginine rich splicing factor 2 |
| STAG1-2 | Stroma antigen1-2 |
| STAT5 | Signal transducer and activator of transcription 5 |
| TBE | Tris-borate-EDTA |
| TBP | TATA-Box binding protein |
| TBST | Tris Buffered Saline with Tween 20 |
| TCF | Transcription factor |
| TCF4 | Transcription factor 4 |
| TET2 | Tet methylcytosine dioxygenase 2 |
| TK1 | First tyrosine kinase domain |
| TK2 | Second tyrosine kinase domain |
| TKD | Tyrosine kinase domain |
| TKI | Tyrosine kinase inhibitor |
| $TNB^{2-}$ | 5-thio-2-nitrobenzoic acid |
| TP53 | Tumour protein P53 |
| TRAF2 | TNF receptor associated factor 2 |
| TRB3 | Tribbles pseudokinase 3 |

| | |
|---|---|
| TrkA-C | Tropomyosin receptor kinase A-C |
| TrxR | Thioredoxin reductases |
| U2AF1 | U2 small nuclear RNA auxiliary factor 1 |
| UPR | Unfolded protein response |
| VEGFR | Vascular endothelial growth factor |
| WHO | World Health Organization |
| WT | Wild-type |
| XBP1 | X-box binding protein 1 |
| ZRSR2 | Zinc finger CCCH-type, RNA binding motif and serine/arginine rich 2 |

# Figures index

## Introduction



## Materials and Methods



## Results

**Appendix**

# Tables index

# Abstract

Acute myeloid leukaemia (AML) is a group of aggressive haematopoietic malignancies associated with adverse outcome. Fms-like tyrosine kinase 3 (FLT3) receptor mutations confer a particularly poor prognosis to AML patients. There is no satisfactory treatment against this disease, especially for the cases harbouring FLT3 mutations, and the quest for novel therapeutic options continues. Drug repurposing represents a powerful strategy to single out existing agents active in novel therapeutic contexts. We performed a high-throughput drug screening, designed to search for agents that inhibit the growth of AML cell lines with mutated FLT3 within libraries of FDA-approved compounds or molecules in advanced phases of clinical trials. Auranofin, an antirheumatic drug, and pyrvinium pamoate, an anthelmintic agent, were identified and chosen from the list of 290 hits for *in vitro* and *in vivo* validation. We confirmed that *in vitro* treatment with auranofin and pyrvinium pamoate reduces AML cell growth through a cytotoxic and cytostatic effect, respectively. We identified the synergies/additivities of the two molecules with standard anti-AML drugs (e.g., cytarabine, doxorubicine) and a specific FLT3 inhibitor (quizartinib). Auranofin synergised with cytarabine and its effect was additive when combined with quizartinib; pyrvinium pamoate showed an additive effect when used with doxorubicin and quizartinib. Next, we determined that both auranofin and pyrvinium pamoate act through their described mechanism of action, i.e., inhibit thioredoxin reductase (auranofin) and Wnt signalling (pyrvinium pamoate). In addition, we identified a novel mechanism of action for the two agents: the induction of the endoplasmic reticulum stress and the unfolded protein response that follows. Our results support the potential of auranofin (less so in the case of pyrvinium pamoate) for the treatment of AML patients, including those with FLT3 mutations, provided that the ongoing *in vivo* validation is successful.

# 1 Introduction

## 1.1 Acute myeloid leukaemia (AML)

### 1.1.1 Molecular landscape of AML

Acute myeloid leukaemia (AML) is a heterogeneous group of diseases characterized by genetic and epigenetic changes in hemopoietic stem cells (HSCs) or precursors that affect the balance between cell survival, proliferation and differentiation. Such changes lead to a clonal expansion of myeloid progenitors, known as blasts, in the bone marrow and in the peripheral blood.[1]

AML blasts express different cell surface markers corresponding to the specific stage of the differentiation block. In 1976, eight AML subtypes (M0 to M7) were distinguished in the French-American-British (FAB) classification based on morphology.[2] To integrate the growing knowledge of genomics and molecular biology, the World Health Organization (WHO) introduced a new classification that upon two revisions (the first in 2008 and the second in 2016), defined six major classes: AML with recurrent genetic abnormalities, AML with myelodysplasia-related changes, therapy-related myeloid neoplasms, myeloid sarcoma, myeloid proliferations related to Down syndrome and AML not otherwise specified.[3,4] The presence of cytogenetic abnormalities known as recurrent genetic abnormalities (e.g., t(8;21)(q22;q22), t(15;17)(q22;q12) and inv(16)(p13.1;q22) is associated with longer remission and better survival, while alterations of chromosomes 5, 7, 11q23 and a complex karyotype determine poor response to therapy and short overall

survival (OS).[1,5] In contrast, 40% of AML patients are cytogenetically normal (CN) and are highly heterogeneous concerning clinical outcome.[5]

The development of AML can be considered as a multicause, multistep and multipathway process.[6] Most AML arise *de novo,* but they can also occur as the consequence of exposure to anti-cancer treatments, chemicals, smoking, obesity, or in patients affected by primary haematological disorders or with hereditary/familial predisposition.[6] A two-hit model has been postulated by Gilliland and Griffin: accordingly, two types of mutations are essential to cause AML.[7] Class I mutations (e.g., *FLT3-ITD*, *c-KIT* or *NRAS* mutations), which do not block differentiation but confer a proliferative advantage as a result of aberrant activation of signalling pathways, cooperate with class II mutations (i.e., AML-specific fusion genes in the original model) that impair normal haematopoietic differentiation. Commonly, class II mutations are the initiating events followed by class I mutations that are later lesions **(Figure 1.1)**.

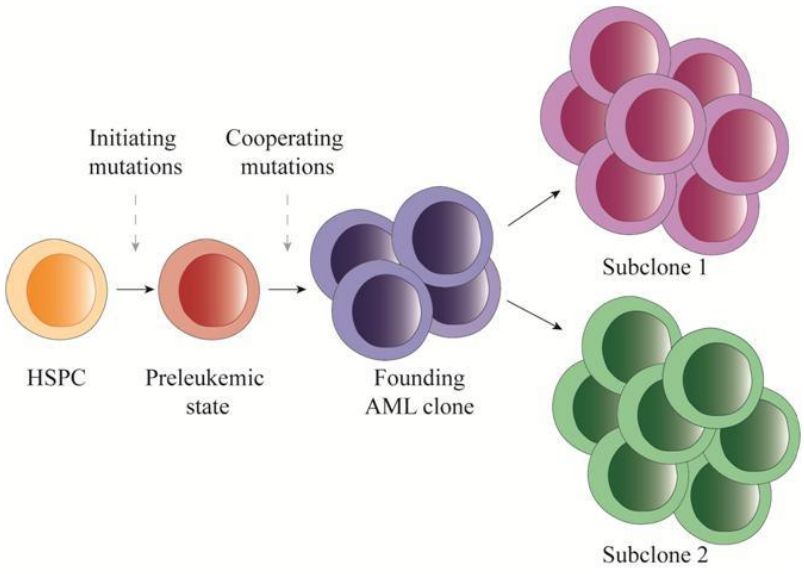


***Figure 1.1 AML evolution: the two-hit model***
*Initiating mutation blocks the differentiation of haematopoietic stem/progenitor cells (HSPCs, shown in orange) resulting in a preleukemic state. Cooperating mutations give a proliferative advantage to the preleukaemic state inducing the expansion of the founding AML clone. Subclones arise from the founding AML clone by acquiring additional mutations that confer an advantage to that cell. All the figures in the introduction section were drawn on purpose by the author.*

Recently, the advent of next generation sequencing, together with a deep knowledge of cell biology and *in vivo* animal models, allowed a better understanding of the evolution and pathogenesis of AML. It is now clear that the genetic events leading to AML are much more complex. Nearly all AML blasts have at least one "driver" mutation that endows fitness advantage with respect to normal cells; random "passenger" mutations with no effect on fitness or proliferation may also be selected and persist provided that they co-occur with a driver mutation, granting further advantages.[8] It is a patient-specific dynamic process, characterized by continuous acquisition and loss of specific genetic mutations, which results in a variety of cellular clones and subclones during the course of the disease.[9,10] Thus, the diverse combinations of driver and passenger mutations justify the heterogeneous nature of AML and clarify why, in many cases, patients who responded to initial treatment rapidly develop resistance. [11]

Some frequent molecular abnormalities have been identified and used to define the therapeutic strategy and to predict the outcome. The recurrently mutated genes in AML include DNA methylation/demethylation genes (e.g., *DNTM3A, TET2, IDH1, IDH2*), activated signalling genes (e.g., *FLT3-ITD, FLT3-TKD, NRAS, KRAS*), myeloid transcription factors (*RUNX1, CEBPA),* tumour suppressor genes (e.g., *TP*53, *NPM1),* chromatin regulation genes (e.g., *ASXL1, ASXL2),* spliceosome (e.g., *SRSF2, SF3B1, U2AF1, ZRSR2*) and cohesion (e.g., *RAD21, SMC3, STAG1-2*) genes. The specific combination of mutations or chromosomal abnormalities present in AML blasts defines the prognosis.

### 1.1.2 FLT3- tyrosine kinase receptor in AML

FLT3 is a tyrosine kinase receptor (RTK) belonging to the class III RTK family and plays a key role in the survival, proliferation and maturation of haematopoietic precursor cells. FLT3 expression is usually restricted to CD34+ haematopoietic stem and progenitor cells

(*HSPC).*[12,13] It is also highly expressed in haematological malignancies such as AML and acute lymphoblastic leukaemia (ALL), suggesting that FLT3 receptor exerts a crucial role in the survival and proliferation of leukaemic blasts.[14]

FLT3 receptor is a transmembrane protein formed of four different regions: an immunoglobulin-like domain involved in ligand binding, a transmembrane portion, a juxtamembrane (JM) domain and an intracellular region that includes the kinase domain. The tyrosine kinase domain (TKD) comprises two different domains (TK1 and TK2) connected by a flexible peptide known as activation loop (A loop). FLT3 protein undergoes post-translational modifications that favour the localization of the receptor in the plasma membrane and determine the affinity for its ligand, the FLT3 ligand (FL) **(Figure 1.2)**.[15,16]

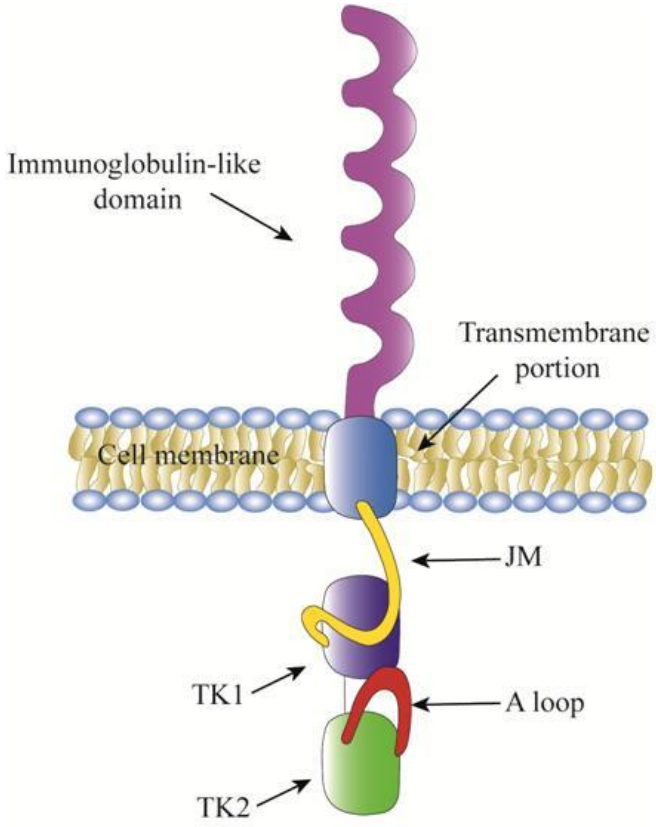


***Figure 1.2 Schematic representation of FLT3 inactive conformation***
*JM, juxtamembrane domain; TK1, first tyrosine kinase domain; TK2, second tyrosine kinase domain.*

Ligand-binding induces activation of the receptor leading to its dimerization, autophosphorylation of the TKD, and activation of downstream effectors involved in cell cycle progression, apoptosis inhibition and differentiation. In the inactive state, both the A loop and the JM domain adopt a closed conformation preventing the rotation of TK1 and TK2 and exposure of the phosphorylated sites. In the active state, tyrosine residues of the JM domain are phosphorylated and the A loop assumes an open conformation, facilitating the access of ATP to the active pocket and binding of the substrates followed by activation through phosphorylation of downstream proteins **(Figure 1.3)**.[15]

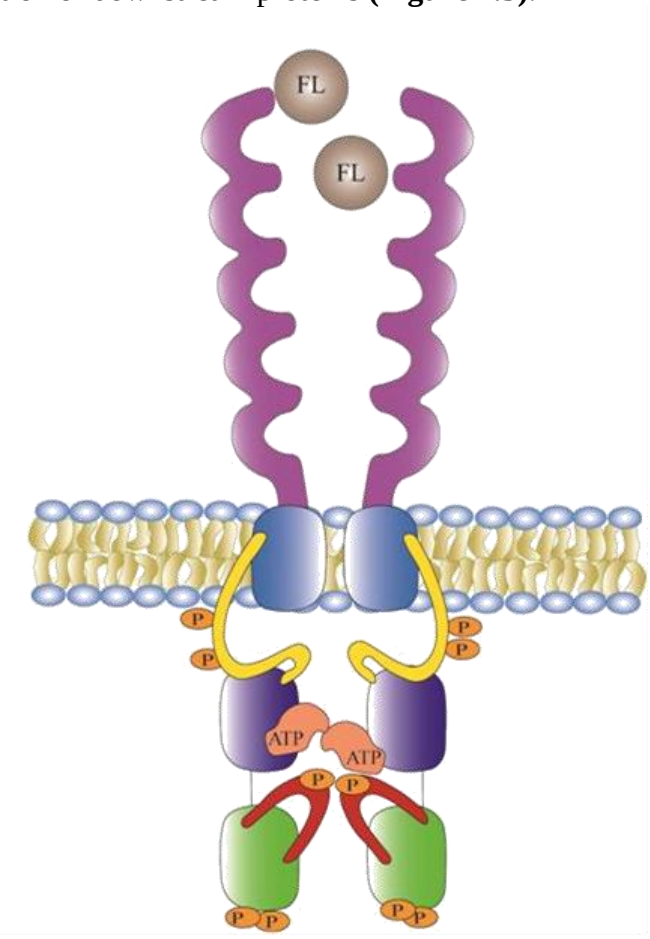


***Figure 1.3 Schematic representation of FLT3 active conformation***
*FL, FLT3 ligand; immunoglobulin-like domain (purple); P, phosphorylation site; JM, juxtamembrane domain (yellow); TK1, first tyrosine kinase domain (blue); TK2, second tyrosine kinase domain (green); A loop, activation loop (red).*

---

Phospatidylinositol-3-kinase (PI3K) and RAS signal transduction pathways are the main networks activated by FLT3 receptor, resulting in the transcription of genes involved in

cell survival and proliferation. Upon receptor stimulation, PI3K activates different downstream proteins such as 3-Phosphoinositide-dependent kinase 1 (PDK1) and AKT, which in turn phosphorylates the mammalian target of rapamycin (mTOR). The induction of cell survival involves the transcription of key genes as a result of p70S6Kinase activation and inhibition of eukaryotic translation initiation factor 4E-binding protein (4E-BP1) by mTOR.[17] Moreover, AKT blocks the apoptotic cascade by stimulating the anti-apoptotic B cell lymphoma protein 2 (BCL-2) and inactivating the pro-apoptotic BAD protein.[18] Finally, among the downstream targets of AKT, FoxO3, a member of the forkhead transcription factor family, plays an important role in the induction of the transcription of pro-apoptotic genes. The phosphorylation of FoxO3 by AKT prevents its function.[19] Cell proliferation is stimulated by the downstream effectors of RAS protein including RAF and MAPK/ ERK kinase **(Figure 1.4)**.[20]

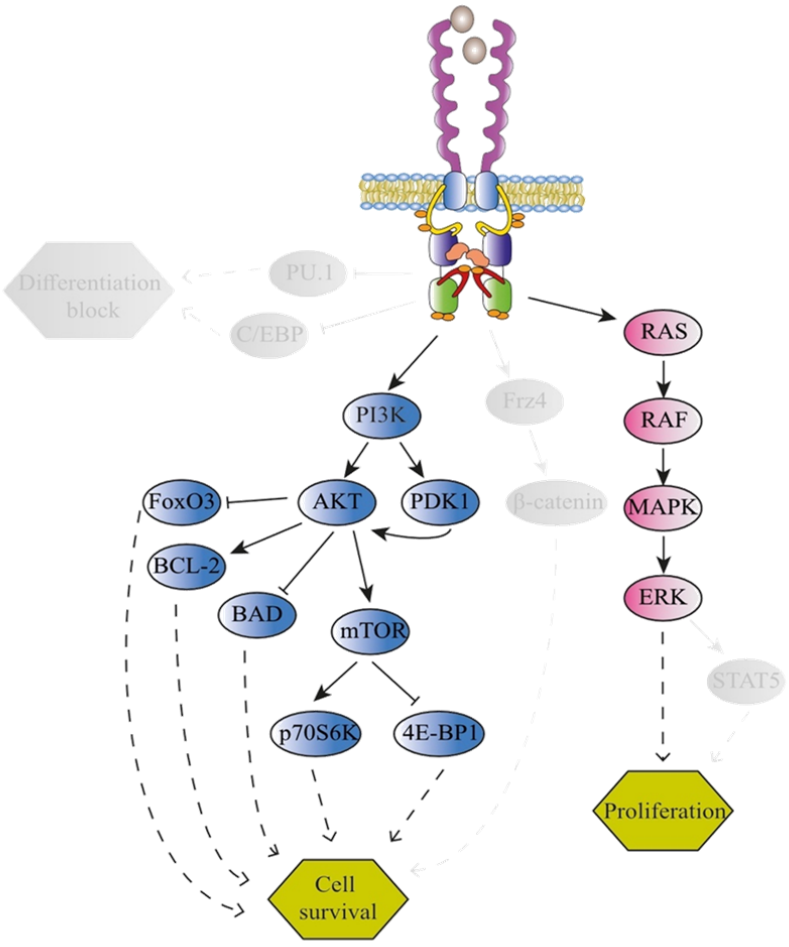


***Figure 1.4 Signalling pathways activated by wild-type FLT3 receptor***

*FLT3* mutations are the alterations most frequently found in the blast of AML patients and lead to constitutive activation of the receptor. Activating mutations include internal tandem duplications (ITD) in the JM portion of the RTK, consisting of the duplication of a variable number of bases (from 3 to 400 base pairs), in multiples of three maintaining the reading frame, in exons 14 and 15, coding for the JM domain.[21] The presence of ITDs in the TKD or point mutations in the JM in AML patients have also been reported.[22,23] FLT3-ITD receptor, but not the *wild-type* form, is mostly present in the immature form, due to glycosylation defects. Thus, FLT3-ITD receptor is also detectable in the endoplasmic reticulum and its retention is caused by inefficient folding.[24] Another activating mutation is the missense point mutation in the TKD, which occurs in exon 20 and leads to an amino acid substitution. The most common substitutions involve the aspartic acid 835 (D835) and isoleucine 836 (I836) residues.[25,26]

Both the activating mutations illustrated above prevent the association of the JM domain with the TKD, favouring ATP access to the TKD. The downstream pathways activated by the mutated receptors enhance cell survival and proliferation through the PI3K and RAS cascade, as for the *wild-type* receptor. There are three main differences between FLT3-ITD and the WT receptor: first, the mutated receptor represses transcription factors involved in normal hemopoiesis, such as PU.1 and CEBPA, causing a differentiation block.[27] Second, phosphorylated STAT5 binds to DNA and activates genes that enhance cell proliferation and inhibit apoptosis.[28] Third, it has been shown that FLT3-ITD induces the expression of the Frizzled-4 receptor even in the absence of its ligand Wnt, causing the stabilization and accumulation of β-catenin in the cytoplasm. β-catenin translocates to the nucleus and induces the transcription of its target genes including *cyclin D1* and *c-myc*, which promote cell survival and proliferation **(Figure 1.5)**.[29]

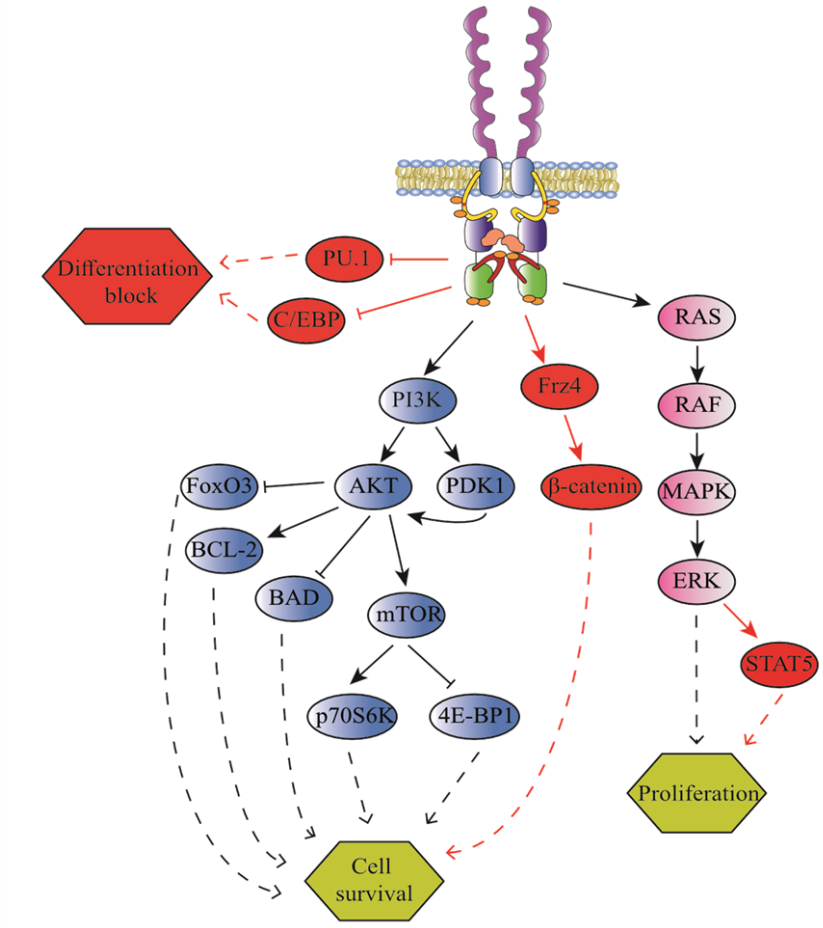


***Figure 1.5 Signalling pathways activated by FLT3-ITD receptor***

---

*FLT3-ITD* mutation is a class I mutation in the original 2 hit model as it confers proliferative and survival advantages to haematopoietic cells but does not impair differentiation. Moreover, based on the 'passengers' and 'drivers' mutation theory derived from genome sequencing studies, *FLT3-ITD* mutation is considered as a second driver mutation that cooperates with other driver mutations such as *NPM1*, *DNMT3A*, *IDH1* and *IDH2* in developing a founder clone detected at the onset of AML.[30]

Mutations of the *FLT3* gene occur in 30% of all AML patients and in 70% of CN-AML patients, and are more frequent in *de novo* cases than in secondary AML.[31–34] The frequency of *FLT3-ITD* in paediatric AML patients is lower than in adults.[35,36] On the contrary, it appears to be higher in elderly AML patients than in younger sufferers.[37]

Most *FLT3* mutations (23%) are ITD mutations. FLT3-ITDs have not been found in chronic myelogenous leukaemia (CML), juvenile myelomonocytic leukaemia, non-Hodgkin lymphoma, adult T-cell ALL, chronic lymphocytic leukaemia (CLL), or multiple myeloma.[38,39] In addition, recent data have shown that *FLT3-ITD* mutations are not detected either in a variety of solid tumours[40] as well as in normal haematopoietic cells.[41] In the vast majority of patients, *FLT3-ITD* has been found in the heterozygous state but a partial or complete loss of *wide-type* allele is also possible.

Patients bearing *FLT3-ITD* have a higher probability of relapse and poor response to therapy.[42,43] Wang et al. reported that AML patients with *FLT3-ITD* have significantly lower complete remission (CR) rates compared to patients with *wild-type* FLT3. This result is in contrast with other studies that have found no difference in the CR rates between FLT3-ITD and *wild-type* cases. The possible explanation of this contradiction is that diverse therapeutic strategies were adopted. Indeed, patients treated with more intensive induction regimes did not display any differences in terms of CR rates regardless the FLT3 status whereas patients treated with "3+7" induction therapy had different CR rates attributable to FLT3-ITD mutation.[24] The prognosis of patients with newly diagnosed *FLT3-ITD* AML is influenced by mutant-to- *wide-type* allelic ratio, insertion site, ITD length, karyotype, and the presence of a mutation in the genes such as *NPM1* and *DNMT3A*. Several studies have shown that a high allelic ratio is associated with poor survival.[31,44] Conversely, a study conducted by Linch et al., demonstrated that the risk of relapse was not correlated with the allelic ratio.[45] Thus, further studies are necessary to elucidate the prognostic impact of the allelic ratio in order to optimize the therapeutic approaches. ITD mutation in the TKD is considered an independent unfavourable prognostic factor as well as increasing ITD size is associated with a worse outcome.[46] FLT3-ITD is frequently associated with t(15;17) (q22;q12) and t(6;9)(p23;q34). In these subtypes, no clear impact is conferred by the presence of an increased percentage of blasts in the peripheral blood and in the bone marrow.[31,47]

*NPM1* and *DNMT3A* gene mutations correlate with FLT3-ITD mutations. *NPM1* mutations are associated with a good response to therapy and five-year survival. Some evidence suggests that patients with *NPM1* mutations and with low allelic ratio FLT3-ITD may have a prognosis similar to that of *wide-type FLT3* patients.[48] *DNMT3A* mutations are frequently associated with *FLT3-ITD* and *NPM1* mutations. The *DNMT3A/FLT3-ITD/NPM1* triple mutation has clinical relevance as demonstrated by its negative impact on event free survival (EFS) and OS.[49] Finally, *FLT3* mutations are considered an independent prognostic factor that affects OS and CR rates, thus the WHO recommends to assess the *FLT3* status in particular in CN-AML patients. The assay for the detection of *FLT3* activating mutation is polymerase chain reaction using as a template genomic DNA of patient's blasts derived from whole blood or bone marrow.[50]

### 1.1.3 Current treatments for AML

AML patients are classified in three different risk groups based on cytogenetic and molecular criteria. Individual factors such as age and fitness may guide the therapeutic choice defining the risk of resistance to treatment or treatment-related mortality, but chromosomal and molecular aberrations remain the strongest prognostic factors to predict outcome in AML patients and to determine the therapeutic strategy. The favourable prognosis risk group includes patients affected by acute promyelocytic leukaemia (APL), patients with balanced chromosomal abnormalities, mutated *NPM1* without *FLT3-ITD* or biallelic mutation of *CEBPA*. The intermediate risk category comprises patients with normal karyotype (other than those included in the favourable or adverse groups), t(9;11)(p22;q23), *wild-type NMP1* with or without *FLT3-ITD*, mutated *NPM1* and *FLT3-ITD*, and t(8;11)(q22;q22) with mutated *c-KIT*. Adverse risk AML includes patients with complex karyotype, inv(3)(q21;q26.2), t(6;9)(p23;q34), 11q abnormalities other than t(9;11), -5 or del(5q), and -7 or abnormal (17p). Mutated *TP53*, regardless of the

cytogenetic status, is always associated with a very poor prognosis as well as *FLT3-ITD*, *DNMT3A* or *MLL-PTD* mutations in CN-AML.[51]

Upon AML diagnosis, regardless the risk class, patients are treated with an intensive cytarabine and anthracycline regimen, the so-called "7+3" standard combination. It consists of seven days of continuous cytarabine infusion (100-200 mg/m$^2$/daily) with three days of an anthracycline, including daunorubicin (60 or 90 mg/m$^2$/daily) or idarubicin (10-12 mg/m$^2$/daily). The intent of induction chemotherapy is to achieve CR that should be evaluated 14 days after the commencement of treatment by analysing a bone marrow aspirate and core biopsy. Next, a post-remission therapy known as consolidation is applied. The main aim of consolidation therapy is to prevent relapse by eradicating minimal residual disease (MRD) still present in the bone marrow after induction therapy. There are two main options for consolidation therapy: chemotherapy and haematopoietic stem cell transplantation (HSCT). These strategies are used independently or most often in combination.[51–53]

AML therapy is tailored on the aggressiveness of the disease, but it must also take into account patients fitness and the availability of a stem cell donor. In particular, younger adults (<60 years of age) with favourable risk AML usually receive consolidation therapy with intermediate/high dose of cytarabine (1.5-3 g/m$^2$), three days a week in three or four cycles. Autologous transplantation is adopted only after an eventual relapse. In contrast, eligible patients that suffer from intermediate or high-risk AML and achieve CR after induction therapy undergo allogeneic HSCT (alloHSCT), which is the most successful long term treatment. Nevertheless, some patients are never eligible for transplant because of co-morbidities, failure to reach CR or lack of a suitable donor. Otherwise, patients receive high-dose chemotherapy followed by autologous HSCT.[51–53] Several studies investigated the effect of the addition of a third drug (i.e., gemtuzumab ozogamicin (GO), purine analogues, and sorafenib) to induction therapy or after consolidation. Results from six randomized trials of GO associated with induction or consolidation therapy are

controversial: four out six studies demonstrated an advantage in terms of OS, EFS and relapse-free survival (RFS) especially for favourable-risk AML. Purine analogues such as clofarabine and fludarabine or sorafenib addition did not show significant improvement in EFS, RFS and OS when combined with induction therapy, except in younger patients who benefited of induction+sorafenib treatment in terms of EFS and RFS.[52]

Patients who do not achieve CR after one cycle of induction therapy and those who relapse after consolidation treatment require a different treatment strategy (salvage therapy), consisting in a second cycle of induction therapy, high-dose of cytarabine, mitoxantrone-based regimens in combination with etoposide and cytarabine (MEC), or the combination of fludarabine with cytarabine, idarubicin and G-CSF (FLAG-IDA). The FLAG-IDA treatment may be a valid alternative to induction therapy with a higher CR upon one single cycle **(Figure 1.6)**.[54]

Taken together, new therapeutic strategies are undoubtedly needed.

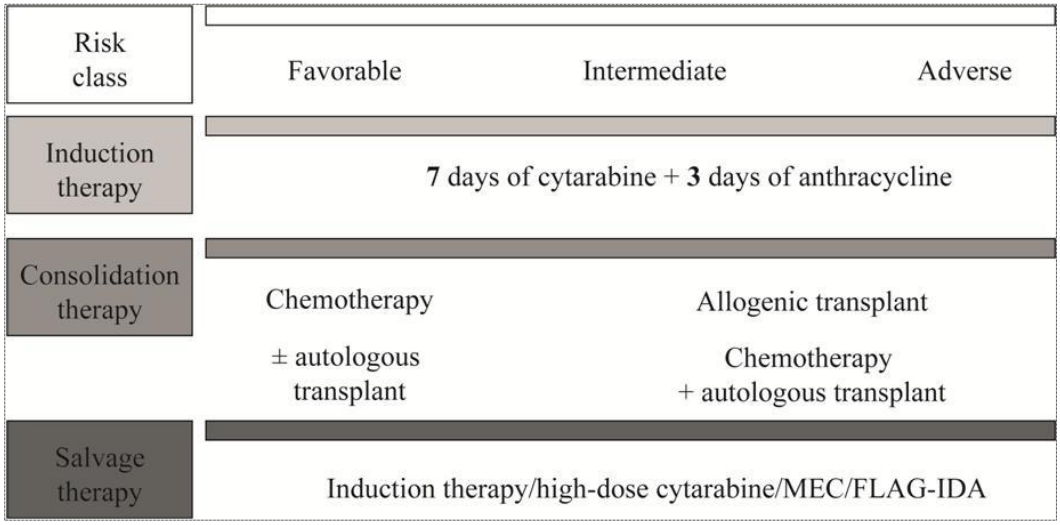


***Figure 1.6 AML risk classes and therapeutic option***

### 1.1.4 Emerging therapeutic drugs for AML: FLT3 inhibitors

Despite increasing knowledge of the molecular basis of AML, treatment options have remained basically unchanged and the outcomes for patients continue to be unsatisfactory. Several potential targets have been identified for newly diagnosed AML and, in particular, inhibition of FLT3 may represent a valid therapeutic target in AML with FLT3-ITD. Over the past few years, numerous tyrosine kinase inhibitors (TKI) targeting FLT3 receptor have been developed, and are classified into first- and second-generation based on their specificity **(Table 1.1)**.[55]

***Table 1.1 List of FLT3 inhibitors***

| Inhibitor | Generation | Target | Trial phase |
|---|---|---|---|
| **Sorafenib** | 1 | FLT3, RAF-1, PDGFR, VEGFR, c-KIT | III |
| **Sunitinib** | 1 | FLT3, PDGFR, VEFGR, c-KIT | I/II |
| **Lestaurtinib** | 1 | FLT3, Jak2, TrkA-C | II |
| **Midostaurin** | 1 | FLT3, PDGFR, VEFGR, c-KIT | III |
| **Quizartinib** | 2 | FLT3, PDGFR, CSF1R, SCFR | III |
| **Crenolanib** | 2 | FLT3, PDGFR | III |
| **Gilteritinib** | 2 | FLT3, AXL, ALK | III |

First-generation inhibitors comprise generic kinase inhibitors with no selectivity for FLT3 and include both sorafenib already approved for the treatment of advanced renal cell carcinoma (RCC) and hepatocellular carcinoma, and sunitinib, used for the treatment of RCC and imatinib-resistant gastrointestinal stromal tumour; but also lestaurtinib (CEP-701) and midostaurin (PKC412). Sunitinib is not suitable for AML treatment because it gave transient responses and had toxicity issues.[56–58] By contrast, sorafenib seems to be well tolerated with a consistent reduction in peripheral blood and bone marrow blasts.[59] The combination of sorafenib with induction therapy or with azacitidine appears as a promising approach also for relapsed/refractory AML.[60–62] Data from phase I-II clinical

trials involving relapse/refractory AML patients demonstrated a reduction in blasts count, albeit of short duration, upon lestaurtinib treatment. Surprisingly, the combination with standard chemotherapy did not improve CR rate or OS.[63,64] Midostaurin has recently been approved by Food and Drug Administration (FDA) as front-line therapy for FLT3-ITD AML. If administered as a single agent, it causes a transient decrease in bone marrow and peripheral blood blasts. However, its great success lies in the combination with standard chemotherapy (RATIFY trial) resulting in a significantly higher OS among all patients, including those with FLT3-ITD mutation.[65]

Second-generation inhibitors, such as quizartinib, crenolanib and gilteritinib, are specific, more potent and have lower toxicity associated with off-target effects. They are currently being tested in clinical trials.[55] Quizartinib, also known as AC220, has a good bioavailability and an optimal half-life (more than 24h), which allows a sustained and potent FLT3 inhibition. Phase I and II trials demonstrated a clinical response and high CR rate among young and old relapse/refractory FLT3-ITD participants.[66–68] The combination of quizartinib with conventional chemotherapy also revealed an impressive CR rate among patients with *de novo* AML.[69] Many clinical trials aimed at assessing the tolerability and the therapeutic promise of quizartinib as monotherapy, or in combination with the standard of care or with hypomethylating agents, are ongoing. Although as single agent quizartinib is very promising, patients frequently develop resistance due to the acquisition of additional mutations such as point mutations in the kinase domain.[70] Several studies have shown that crenolanib and gilteritinib are active against both types of FLT3 mutations and inhibit FLT3 receptor overcoming quizartinib drug resistance. Both compounds are well tolerated and effective as single agents.[71–74] Numerous clinical trials are under way to examine the effect of combinations with conventional therapies, hypomethylating agents or with salvage therapies.

New evidence correlates chemotherapy with high levels of FLT3 ligand, causing a reduction of FLT3 inhibition *in vivo* and the possible selection of a clone that is resistant to

chemotherapy and FLT3-addicted. This clone is responsible for relapse and ultimately for the patient's death.[75] Combination of standard chemotherapy with a general TKI followed by transplantation could, therefore, represent an approach to overcome relapse.

Another strategy for decreasing the risk of relapse is represented by the use of FLT3 TKI after HSCT. Brunner et al. demonstrated that HSCT followed by sorafenib treatment, as maintenance therapy, was associated with a significant improvement of OS and decreased rate of relapse.[76] Several other smaller, retrospective/prospective studies also support the use of sorafenib as maintenance therapy for FLT3-ITD AML patients.[76–78]

Midostaurin could also represent an effective maintenance therapy post-transplant. The phase II RADIUS trial that investigated the effect of midostaurin after alloHSCT in patients with FLT3-ITD AML showed a reduction of relapse risk at 18 months post-alloHSCT in patients who received midostaurin + standard treatment (NCT01883362). Moreover, in a phase I trial, Sandmaier et al. found a lower rate of relapse in patients treated with quizartinib after HSCT.[79] Two randomized phase III trials are ongoing, the QuANTUM-R (NCT02039726) and the QuANTUM-First (NCT02668653). The former compares quizartinib as monotherapy versus conventional salvage therapies (MEC and FLAG-IDA) in relapse/refractory FLT3-ITD patients including those who received alloHSCT, the latter evaluates the efficacy of quizartinib combined with conventional chemotherapy among FLT3-ITD patients. Clinical trials assessing the role of gilteritinib and crenolanib in the post-transplant setting compared to both placebo or salvage chemotherapy are in progress.[80]

So far, different FLT3 inhibitors have been investigated *in vitro* and *in vivo* but only sorafenib and midostaurin, both potent but nonspecific FLT3 inhibitors, are used for the treatment of patients affected by FLT3-ITD AML. Other FLT3 inhibitors and their combination with conventional chemotherapy, or in relapse/refractory patients as a bridge to transplantation, or as a maintenance therapy after HSCT will likely soon become available, but this option is not always applicable especially for elderly patients (>65 years)

who are unfit for intensive regimes. Thus, the definition of an accurate and appropriate therapeutic approach for AML patients with FLT3-ITD mutations is indispensable.

## 1.2 Drug repurposing

The demand for new therapeutic compounds against haematological malignancies and the unaffordable prices of FDA-cancer drugs have led to consider drug repurposing/repositioning as an attractive drug discovery approach.[81] This strategy is based on the exploitation of an already-approved or investigational drug for a new therapeutic indication.[82–85] The Repurposing Drugs in Oncology (ReDO) project aims at testing non-cancer drugs as a potential therapeutic strategy against cancers.[81]

### 1.2.1 Advantages and limitations

The most important advantage of repurposing is the reduction of time and costs necessary for bringing the compounds to patient's bedside. The development of a new drug can take on average 15 years and the estimated cost from research to marketing approval is 2 or 3 billion dollars. The timeframe for repurposing, instead, has been estimated to be approximately 6 years with a clear positive impact on costs.[86]

*De novo* drug discovery is made up of multiple steps and clinical trial phases. Efficacy, toxicity, pharmacokinetics and pharmacodynamics are tested by performing *in vitro* and *in vivo* studies. Upon successful completion of this pre-clinical stage, agents are tested on patients, focusing on safety (phase I clinical trial) and efficacy (phase II clinical trial). The final step (phase III clinical trial) consists in a randomised trial that compares the effect of the new drug and the standard treatment or evaluates different doses.[87] Usually, the FDA approves a new agent upon effective completion of all of the phases mentioned above.

However, recently, a new FDA program called accelerated approval (AA) warrants the marketing of products before the conclusion of confirmatory clinical trials thus speeding up the approval of drugs for the treatment of patients with serious or life-threatening oncological diseases.[88]

Most new drugs fail to achieve FDA approval because they lack efficacy, or they turn out to be unsafe for patients. A repurposed drug offers a high level of safety as its pharmacokinetics, toxicities, bioavailability, dosage, administration, off-target and adverse effects are already known.[82,83] Thus, failure rate is reduced and a phase I clinical trials may be bypassed diminishing processing time. Phase II and III clinical trials are still necessary, and represent the critical bottle-neck phases as they exclude 68% and 40% of compounds, respectively **(Figure 1.7)**.[86]

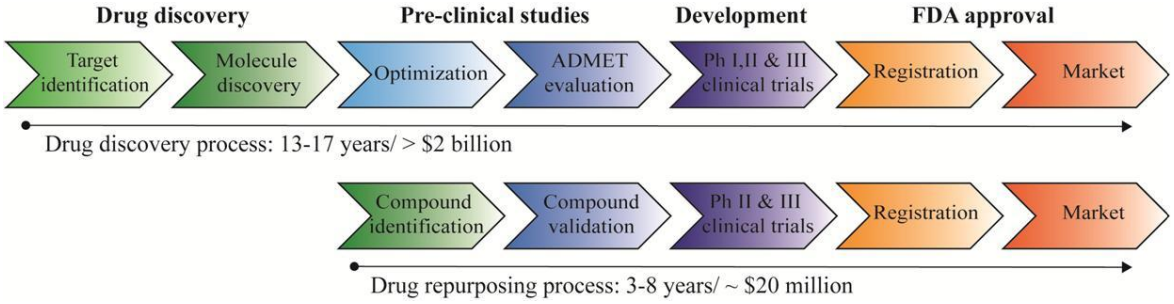


***Figure 1.7 Comparison of the phases, timescale and costs for de novo drug discovery or drug repurposing***

---

Although promising results have been achieved through the repurposing approach, some limitations have to be overcome. The drug to-be-repurposed often acts through a new mechanism of action and/or on new molecular targets,[89] therefore specific assays for the evaluation of new targets are indispensable. Moreover, a drug can elicit the desired pharmacological effect at concentrations that are much higher than those used in the "old" therapeutic setting. In such cases, a new evaluation of absorption, distribution, metabolism, excretion (ADMET) and possible toxicity and side effects, should be performed.[90]

Other barriers to drug repurposing include patent exclusivity, severe legislation and strict *modus operandi* in pharmaceutical industry.[91] A patent provides protection for up 20 years in both USA and Europe. When the patent expires, the drug enters the category of 'generic' agents as other companies can manufacture and sell it, making it available at a cost-effective price. However, an investment is indispensable for extending the license of a generic drug to patent the new use, and the new therapeutic indication of the off-patent drug must be innovative, supported by reliable data, previously unpublished and not suggested in other work. A sponsor that possesses a patent on a compound can invest in it hoping for a financial gain, while a generic compound is much less interesting.[92] Finally, a generic manufacturer who invests in a compound to-be-repurposed may perhaps be disadvantaged compared to its competitors as the cost of the drug could increase. To overcome all these issues, incentives for manufacturers who decide to license generic drugs have been proposed.[92]

### 1.2.2 Different approaches used for drug repurposing

To date, most of the successfully repurposed drugs were identified serendipitously through the study of their side effects, as for thalidomide. Thalidomide is a drug originally used for the treatment of morning sickness during pregnancy, withdrawn from the market due to its teratogenic effects and now approved for the treatment of multiple myeloma.[93] Another well-known example is the sildenafil, an angina and hypertension medication now marked as Viagra® used for the treatment of erectile dysfunction.[94] However, drug discovery and development require systematic, high-throughput and rational methods for drug repurposing.[95] Both computational and experimental approaches can be used. Computational approaches are based on the analyses of big data (e.g., gene expression, chemical structure, proteomic and genomic data). Each drug has specific characteristics including a 'signature' that derives from transcriptomic data, chemical structures and adverse effect profiles. Similarities in transcriptomic signatures may indicate that two

drugs share the same therapeutic application regardless of their chemical structure.[96,97] Analogously, drugs that have similar chemical structure could share the same biological activity.[98] Moreover, similar adverse effects caused by different drugs can suggest that these compounds act on the same targets or pathways.[99,100]

Molecular docking is a different strategy that aims at the identification of binding site complementarity between a drug and a target.[101] Taking advantage of genome-wide studies and network analyses, several genes can be recognized as targets in a specific disease.[102]

Retrospective clinical analysis is also a powerful tool to find repurposing opportunities. Data can be collected from different sources such as electronic health records, post-marketing surveillance data and clinical trials results.[103] Unfortunately, the access to all these data is still challenging due to ethical, legal, commercial and confidentiality issues.

Experimental approaches comprise two different types of screens: target-based screens and phenotypic screens. The former are based on binding assays for the identification of target interactions, mass spectrometry or affinity chromatography and can be adopted to identify novel targets of old drugs. The latter is based on cell behaviour (e.g., growth and death); typically, *in vitro* or *in vivo* phenotypic screening are exploited.[104] To date, at least ten different compound collections are available, including drugs used for the treatment of various cancers, compounds marketed in USA/Europe/or Asia, inhibitors, receptor ligands, FDA-approved drugs, or compounds in advanced phase clinical trials.

### 1.2.3 High-throughput screenings and data analysis

High-throughput screening (HTS) is a process by which a vast collection of compounds is tested in order to identify potential candidates in a rapid and accurate manner. Ninety-six- or 384-well plate formats are usually adopted for the screening whereas the number of compounds per plate can vary. A HTS includes different steps: target identification, assay design, primary and secondary screens, data analysis and drug(s) identification.[105] In a primary screen, a robot is typically adopted to add the target of interest (i.e., cells) and a

precise reagent (i.e., bioactive agents) to each well. After appropriate incubation time, the measurement of the activity (e.g., cell migration, proliferative arrest, etc.) is obtained by using an automatic plate reader. Compounds discovered in the primary screen are labelled as 'hits', and are further evaluated and eventually confirmed or discarded in a secondary screen. Confirmed hits can become drug candidates for clinical trials.

The screening procedure is complex and prone to give both false positive and false negative results. Thus, high-quality HTS and accurate analysis of results are necessary to find a reliable product. Reference controls (positive and negative) are used within each plate to assess of screen quality, identify variability between plates and establish assay background levels. Ideally, controls should be located randomly in each plate in order to avoid edge-related bias and minimize the rate of false positives and false negatives. Normalization of data allows for the comparison between measurements by removing plate-to-plate variation, and is usually performed within plate.[106]

Two different approaches can be adopted for the normalization of raw data: control-based or sample-based. Control-based normalization includes the percent of control and normalized percent inhibition (NPI) methods. The first is based on the ratio between each compound measurement ($x_i$) and the mean of the positive control measurements ($\bar{c}_+$). In the second, the difference between the mean of positive control values ($\bar{c}_+$) and compound measurement ($x_i$) is divided by the difference between the means of positive and negative controls ($\bar{c}_+ - \bar{c}_-$) **(Table 1.2)**.[106–108]

The B-score and Z-score derive from sample-based normalization methods. B-score and Z-score assume that most samples display no biological effect and can serve as control (an option not applicable in secondary screens in which positive results from primary screening are evaluated). The calculation of B-score is based on an interactive algorithm whereas the Z-score is derived from the difference between the measurement of a compound ($x_i$) and the mean of all measurements within the plate ($\bar{x}$) divided by the standard deviation of all measurements ($s_x$) **(Table 1.2)**.[106–108]

With the exception of the B-score method, all the others listed above are sensitive to outliers and are not robust because they use mean and standard deviations as statistical measures. To solve these issues, a variation based on the substitution of the mean and the standard deviation with median (~) and median absolute deviation (MAD), respectively, can be adopted **(Table 1.2)**.[106–108]

***Table 1.2 Different normalization methods***

| | | **Data normalization** | |
|---|---|---|---|
| | | Regular version | Robust version |
| **Control-based** | Percent of control | $\mathrm{PC} = \frac{x_i}{\bar{c}_+} \times 100$ | $\mathrm{PC} = \frac{x_i}{\tilde{c}_+} \times 100$ |
| | Normalized percent inhibition | $\mathrm{NPI} = \frac{\bar{c}_+ - x_i}{\bar{c}_+ - \bar{c}_-}$ | $\mathrm{NPI} = \frac{\tilde{c}_+ - x_i}{\tilde{c}_+ - \tilde{c}_-}$ |
| **Sample-based** | B-score | | $\mathrm{Bscore} = \frac{r_{ijp}}{\mathrm{MAD}_p}$ |
| | Z-score | $Z = \frac{x_i - \bar{x}}{s_x}$ | $Z = \frac{x_i - \tilde{x}}{\mathrm{MAD}}$ |

### 1.2.4 Hit identification

Following raw data analysis, a critical step is represented by the choice of compounds for further screening or investigation. There are many analytic methods for hit selection. Among them, mean ± threshold (k) SD, median ± k MAD that are equivalent to Z-score and robust Z-score, respectively; and multiple *t*-test are generally used for small-molecule screenings. Hit threshold is set to the value that is k SD (or MAD) above or below sample mean (or median) in case of mean ± k SD (median ± k MAD). It is generally 3 SD or MAD. Both statistical analyses described above have advantages and limitations. In

particular, the mean ± k SD strategy is easy to calculate but sensitive to outliers and some weak positive hits may be lost. On the contrary, the median ± k MAD method is robust to outliers and able to identify also weak hits. Finally, in the multiple *t*-test a hit is any compound for which the *t*-test between two samples in two different conditions (i.e., untreated and treated sample) is less than a predetermined threshold. It is simple to calculate but requires triplicates, normal distribution of the data and is sensitive to outliers.[106–108]

### 1.2.5 Examples of repurposed drugs in AML

Drug repurposing can be divided into 'soft repurposing' and 'hard repurposing'.[109] The former is based on the re-use of an existing anti-cancer drug for the treatment in a different oncological setting, while the latter describes the repositioning of non-cancer drugs as anti-cancer agents. Clofarabine, a purine nucleoside antimetabolite, is an example of soft repurposing as it was used for the treatment of paediatric patients with relapsed or refractory ALL whereas the new indication is for the treatment of patients affected by AML in combination with cytarabine and/or idarubicin.[110] To date, also azacitidine, a pyrimidine nucleoside analogue that impairs DNA methylation previously used for the treatment of patients with different myelodysplastic syndrome subtypes, was repurposed as AML therapy, based on data reported in the drug repurposing portal.[110]

Using a PubMed search, the ReDO project identified 291 non-cancer agents with e "hard" repurposing potential. Most of them (84%) were off-patent compounds and at least 70% had data on patients such as case reports, observational studies or clinical trials supporting their anticancer effects.[111–113] Ten compounds showed repurposing opportunities in AML. In particular, Matchett et al. found that low doses of the anthelmintic agent, albendazole, reduced the viability of AML cells with low toxicity.[114] Other two anti-parasitic agents, flubendazole[115] and mebendazole,[116] displayed activity on AML cells. Performing an *in silico* screening bromocriptine, a drug used for Parkinson's disease, was identified as a

small molecule that potentially acts against AML inducing differentiation.[117] Among oral antidiabetics, metformin exhibits great efficacy against FLT3-ITD mutated AML cells when combined with sorafenib.[118,119] Encouraging results have been reported from two clinical trials that study the combination of pravastatin, idarubicin and cytarabine in patients affected by relapsed AML .[120,121] The screening of more than a thousand of compounds from Lopac library (Sigma Aldrich) led to the identification of quinacrine, an anti-malaria agent, as a potential candidate for the treatment of AML with low toxicity in normal mononuclear cells.[122] Sharma and colleagues demonstrated that pyrimethamine, a dihydrofolate reductase antagonist used for the treatment of parasitic infections, is able to induce apoptosis and differentiation in human and murine AML cell lines without affecting normal cells both *in vitro* and *in vivo*.[123] Ribavirin, a widely used anti-viral compound, led to a clinical benefit in AML patients. It acts by targeting the oncogenic activity of the eukaryotic translation initiation factor eIF4E *in vitro*, in mouse models, and also in AML patients.[124] Finally, valproic acid, used to contrast convulsions in epilepsy, was evaluated as an anti-cancer agent. The ability of inhibiting histone deacetylase, which is often overexpressed in cancer cells, and the capacity of inducing differentiation/apoptosis in AML cells renders valproic acid a valid therapeutic agent for AML patients.[125–127]

## 1.3 Endoplasmic reticulum stress and unfolded protein response

Two of the main functions of the endoplasmic reticulum (ER) are to ensure the correct folding of proteins into their native conformation and to secrete newly synthesized proteins following post-translational modifications. Proteins that are not correctly folded are retained in the ER or targeted for degradation; accumulation of unfolded and misfolded proteins causes ER stress. To overcome ER stress, cells evolved a complex and conserved signal transduction pathway called unfolded protein response (UPR),[128] which is a self-protective process that restores the physiological activity of the ER. Indeed, under mild stress it is a pro-survival process, while continuous and chronic ER stress triggers apoptosis.

### 1.3.1 Adaptive UPR mechanism

Upon ER stress, UPR causes an expansion of the ER membrane, the induction of key components involved in protein folding and the inhibition of the influx of proteins into the ER. To date, three main stress sensors of UPR have been identified: 1) the inositol-requiring protein 1α (IRE1α), 2) protein kinase RNA-like ER kinase (PERK) and 3) activating transcription factor 6 (ATF6). Inhibition and stabilization of these three components depends on their binding to the luminal chaperone binding immunoglobulin protein (BiP) also known as GRP78.[129]

BiP has a natural high affinity for unfolded/misfolded proteins, and the accumulation of which leads to the dissociation of this chaperone from the ER sensors. This triggers homodimerization, auto-phosphorylation and activation of IRE1α and PERK, paralleled by translocation to the Golgi apparatus and activation of ATF6.[130]

The activation of IRE1α, a type I transmembrane protein, drives the processing of the mRNA encoding the unspliced X-box-binding protein 1 (Xbp1u) that generates an active transcription factor called spliced XBP1 (Xbp1s).[131–133] XBP1s in turn regulates the transcription of target genes coding for proteins that favour the folding process and modulate phospholipid synthesis, necessary for expansion of the ER membrane. Moreover, the ER-associated degradation (ERAD) pathway in which misfolded proteins are finally degraded by the proteasome is induced.[134,135] IRE1α is also an endoribonuclease that triggers degradation of mRNAs encoding proteins located in the ER to prevent increasing demand of ER protein folding by the activation of the regulated IRE1-depend decay (RIDD) **(Figure 1.8)**.[136,137]

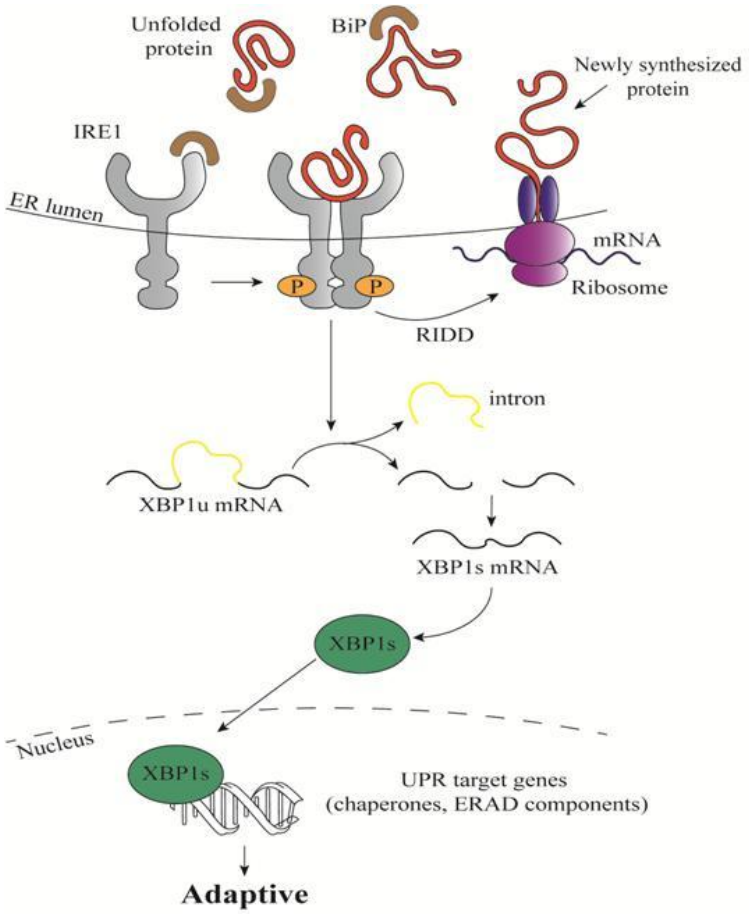


***Figure 1.8 The UPR: IRE1α activation***
*Under physiological conditions the inositol-requiring protein 1α (IRE1α) is maintained in an inactive state through the association with BiP. Upon endoplasmic reticulum stress, BiP dissociates and binds unfolded/misfolded proteins. IRE1α dimerization and auto-phosphorylation trigger the splicing of XBP1u to produce an active transcription factor, spliced XBP1 (XBP1s).*

*XBP1s favours the transcription of genes involved in protein folding and ER-associated degradation (ERAD). IRE1α also degrades a variety of mRNA through regulated IRE-dependent decay (RIDD).*

---

PERK adopts a different mechanism for the induction of specific transcription factors and UPR target genes. Indeed, PERK, a type I transmembrane protein, phosphorylates the eukaryotic translation initiator factor 2α (eIF2α) that causes a generalized cap-dependent translational repression, preventing influx of new proteins into the saturated ER lumen. Paradoxically, it induces the cap-independent translation of ATF4, a transcription factor that enters the nucleus and activates ER stress response genes involved in autophagy, amino acid metabolism and antioxidant response to maintain cell survival.[138,139] ATF4 also promotes the transcription of C/EBP homologous protein (CHOP), which mediates apoptosis both *in vitro* and *in vivo* **(Figure 1.9)**.[140,141] Several mechanisms that repress CHOP transcription during the initial phase of ER stress have been identified [142,143] including the downregulation of CHOP expression by XBP1 that supports cell survival.[144]

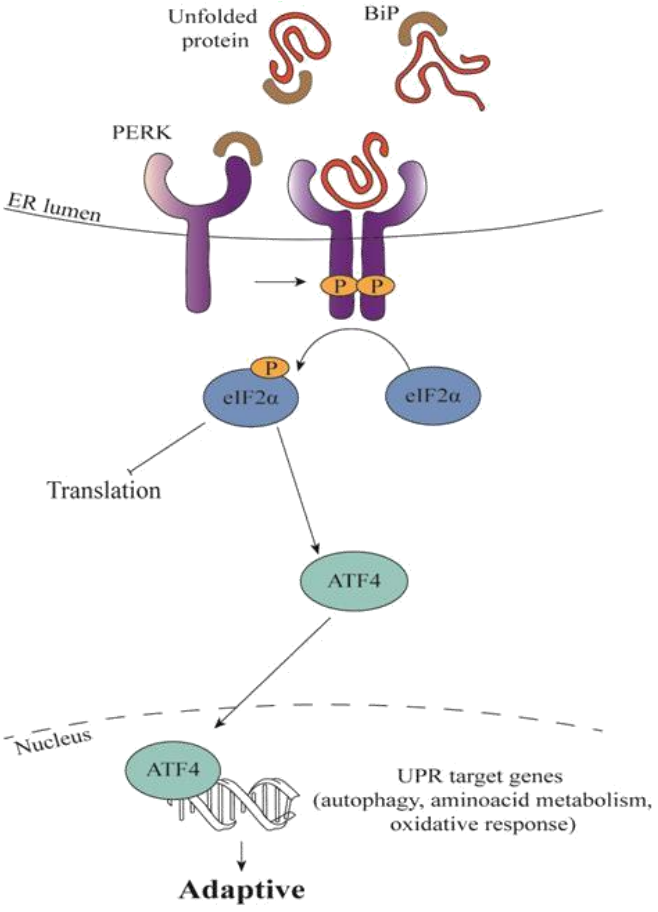

***Figure 1.9 The UPR: PERK activation***
*Under physiological conditions, the protein kinase RNA-like endoplasmic reticulum kinase (PERK) is maintained in an inactive state through the association with BiP. Upon endoplasmic reticulum stress, BiP dissociates and binds unfolded/misfolded proteins. PERK dimerization and auto-phosphorylation trigger the phosphorylation of the eukaryotic translation initiator factor 2α (eIF2α) that attenuates general protein synthesis. Phosphorylation of eIF2α causes the translation of ATF4 mRNA. ATF4 induces the transcription of genes involved in autophagy, amino acid metabolism and oxidative response.*

---

The activation of ATF6, a type II transmembrane protein, depends on site 1 and 2 proteases (S1P and S2P) that cleave ATF6 in the Golgi apparatus, releasing its cytosolic domain that controls the expression of XBP1 and of genes involved in ERAD process **(Figure 1.10)**.[132,145,146]

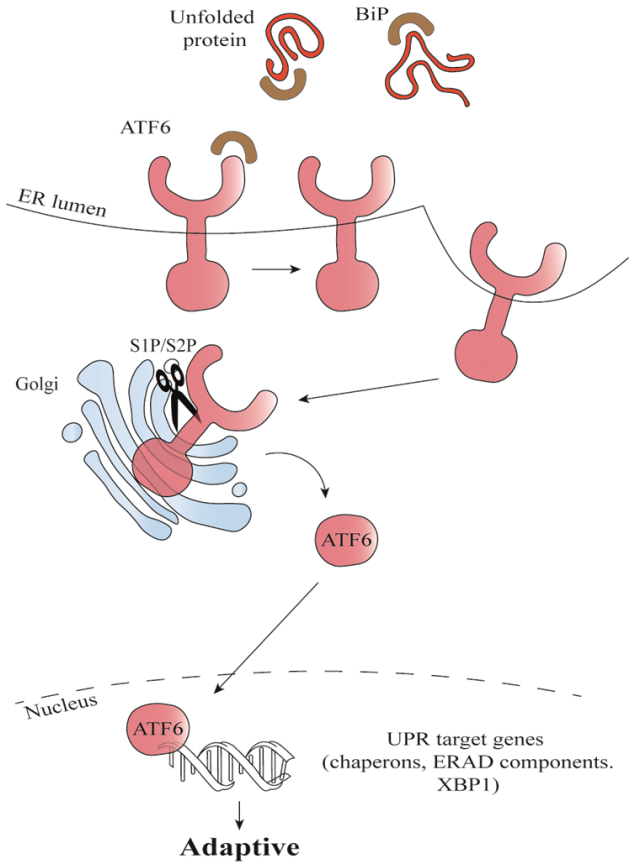


***Figure 1.10 The UPR: ATF6 activation***
*Under physiological conditions the transcription factor 6 (ATF6) is maintained in an inactive state through the association with BiP. Upon endoplasmic reticulum stress, BiP dissociates and binds unfolded/misfolded proteins. ATF6 translocates to the Golgi apparatus where it is processed by site 1 protease (S1P) and site 2 protease (S2P) triggering the release of its cytosolic domain. ATF6 induces the transcription of UPR target genes such as chaperons, ERAD components and XBP1.*

---

Thus, the first event is the phosphorylation of eIF2α mediated by PERK following by the induction of RIDD and ERAD processes. Despite a rapid activation of ATF6, the expression of its target genes (e.g., XBP1) occurs late as the cytoplasmic domain has to move to the nucleus, induce transcription and finally protein synthesis. Also, the transcription and translation of ATF4 happen during the second wave of events.

The early outcomes of UPR are the inhibition of protein synthesis, the induction of protein folding capacities and the degradation of misfolded and unfolded proteins. Collectively, all these temporal responses modulate adaptation to stress, restoring ER function and promoting cell survival.[128]

### 1.3.2 Chronic ER stress and transition to apoptosis

If ER stress is severe, prolonged and UPR fails to restore ER homeostasis, the pro-survival signalling is substituted by a pro-apoptotic programme.[147] Cell death induced by excessive or chronic ER stress is mainly dependent on the mitochondrial (intrinsic) apoptotic pathway, largely regulated by BCL-2 family, which consists of both pro- and anti-apoptotic proteins. BCL-xL, BCL-2 and MCL-1 belong to anti-apoptotic proteins whereas BAK, BAX, BIM, BAD, Noxa and Puma have pro-apoptotic functions. Following stress induction, BAX and BAK proteins change their conformation and become pore-forming proteins in the mitochondrial outer membrane that elicit the release of cytochrome *c* in the cytosol.[148,149] Upon release of cytochrome *c*, pro-caspase-9 is activated to caspase-9, which cleaves and activates its downstream effectors such as caspase-3.[150] Each branch of UPR regulates different BCL-2 family members **(Figure 1.11)**. In particular, during chronic ER stress CHOP induces the expression of pro-apoptotic proteins such as BIM and Puma[151,152] as well as the downregulation of pro-survival proteins (e.g., BCL-2, BCL-xL and MCL-1).[153] Furthermore, it promotes the translocation of BAX to mitochondria[147] triggering apoptosis. Although some mechanisms aim at the attenuation of IRE1α activation,

including Xbp1u that can act as a negative regulator of both Xbp1s and ATF6,[154] in a chronic induction state, IRE1α activates the JUN N-terminal kinase (JNK) pathway by recruiting TNF receptor associated factor 2 (TRAF2) and apoptosis signal-regulating kinase 1 (ASK1). JNK stimulates apoptosis through the inhibition and the activation of BCL-2/BCL-xL and BAD/BIM, respectively.[155,156] Moreover, the RIDD process causes the decay of specific microRNAs that normally inhibit mRNA translation of caspase-2, inducing it and resulting in apoptosis.[157] Finally, during ER stress, Noxa can be upregulated by ATF4 [158] and together with Puma it may also be directly upregulated in a p53-dependent manner.[159]

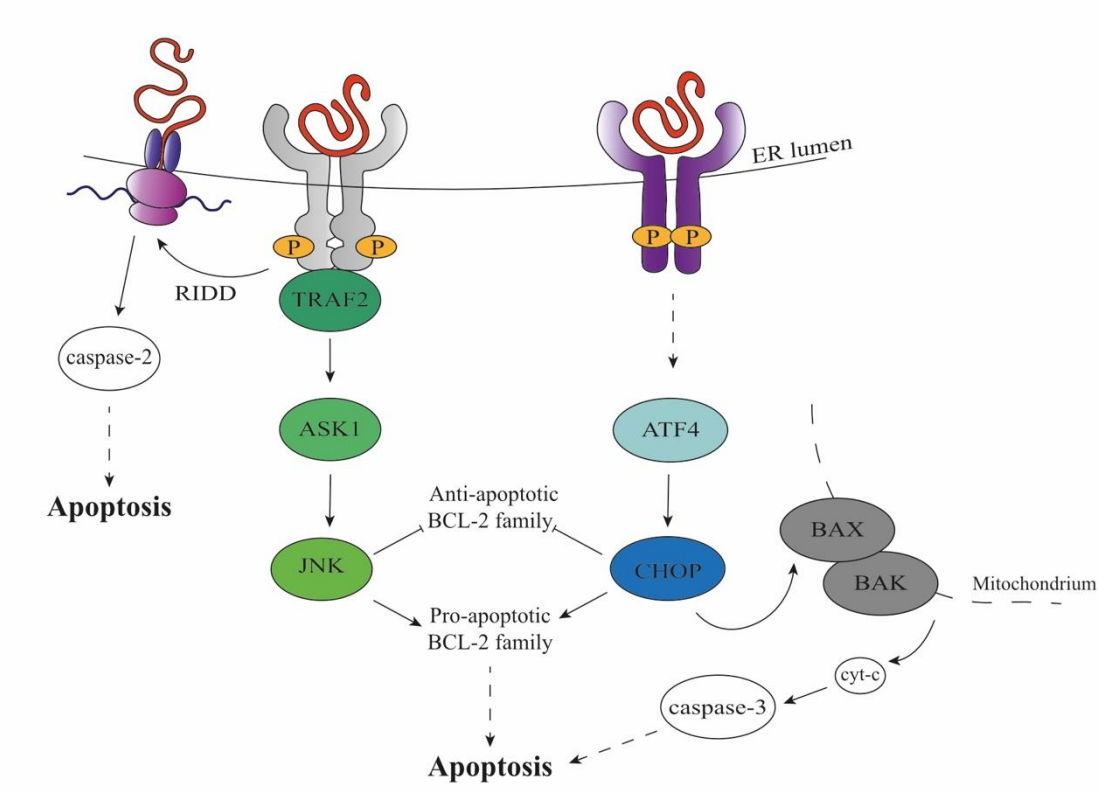


***Figure 1.11 ER stress-induced cell death***
*IRE1α (depicted in grey) recruits TRAF2 and ASK1 activating its downstream target JNK. JNK induces apoptosis by inhibiting anti-apoptotic BCL-2 family proteins. IRE1α also degrades a variety of microRNA through regulated IRE-dependent decay (RIDD) resulting in caspase 2 activation and then apoptosis. PERK (depicted in purple) activation leads to the induction of ATF4 and CHOP proteins. CHOP induces the expression of pro-apoptotic BCL-2 family proteins and favours BAX translocation in the mitochondria triggering apoptosis.*

Although the molecular mechanisms responsible for apoptosis induction have been revealed, the nature of the switch between survival (adaptive UPR mechanism) and death (under chronic ER stress) continues to be vague. Some lines of evidence showed that cell fate depends on expression level of the E2F family member, E2F1.[160] In this model, in physiological conditions, the free form of E2F1 regulates cell proliferation favouring cell cycle transition to G1-S phase and inhibits pro-apoptotic proteins such as Puma and Noxa. In the early stage of ER stress, E2F1 levels are not influenced, while some genes or factors, e.g., ATF4, ATF6, XBP1 and XBP1's target gene E2F7, are activated. ATF4 upregulates anti-apoptotic factors, such as BCL-2 and MCL-1, and in cooperation with ATF6 induces the expression of CHOP, whose function is negatively regulated by TRB3.[161] In late ER stress, ATF4 levels decline, CHOP inhibits BCL-2, and ATF6 combined with E2F7 binds the promoter of E2F1 driving its repression. Thus, the inhibition of Puma and Noxa by E2F1 stops resulting in the induction of apoptotic program.

### 1.3.3 ER stress and cancer

The response to ER stress is cell specific, depends on cell tolerance and on the environment. ER stress and UPR activation have been implicated in various human diseases such as neurodegenerative disorders, metabolic diseases and cancers. Indeed, cancer cells are characterized by uncontrolled growth and proliferation resulting in hypoxia, nutrient deprivation and oxidative stress. These conditions represent stimuli that compromise ER homeostasis inducing ER stress and UPR. The activation of UPR supports cancer cell survival and adaptation to a hostile microenvironment, and leads to cell dormancy by inhibition of cell cycle progression causing resistance to standard treatment.[162–164] For instance, melanoma cell lines and primary tumours that are resistant to therapies are characterised by high levels of ER stress markers. The oncogenic *BRAF* mutation has been associated with ER stress and induction of pro-survival signalling.[165–167] Therapy resistance is conferred by enhanced autophagy as an adaptive ER stress response.

The inhibition of ER stress decreased autophagy and re-sensitised BRAF melanoma cells to cancer therapy.[165,167]

The IRE1α/XBP1s pathway is implicated in cancer cell proliferation and survival. High levels of XBP1s have been reported in human multiple myeloma and are associated with neoplastic transformation of plasma cells and spontaneous development of multiple myeloma in mouse models.[168] The inhibition of XBP1 affects the survival of multiple myeloma cells as they become more sensitive to ER stress.[169] Moreover, an increased expression of XBP1s is reported in human breast cancers and it seems that a higher expression is found in aggressive, high proliferative and high-grade mammary tumours.[170,171] Currently, few small molecules (MKC-3946, STF-083010, A-I06 and 4μ8c) that block the RNase activity of IRE1α and the splicing of XBP1 are under investigation in multiple myeloma, acute and chronic lymphoblastic leukaemia.[172] Although, promising results have been obtained, the development of more specific and effective IRE1α inhibitors is needed.[172]

The role of ATF6 pathway is crucial in tumourigenesis, as one of its target gene is BiP. BiP, as discussed above, binds to misfolded and unfolded proteins to restore ER homeostasis. High expression levels of BiP have been found in different cancer types such as melanoma, breast, lung, prostate, brain and head and neck cancer.[173] Emerging evidence suggests that BiP can also localize to cell surface in cancer cells but not in normal cells. This discovery opens up the opportunity of targeting BiP as a possible strategy for cancer therapy.[174] Additionally, BiP overexpression confers drug resistance in multiple tumours [175] and correlates with higher pathologic grade, relapse, and poor prognosis in patients with breast, liver, prostate, colon and gastric cancers.[175]

On the contrary, the inhibition of BiP affected the ability of fibrosarcoma cells to form tumours in *xenograft* mouse models and diminished the growth rate of breast adenocarcinoma and glioma cells.[176–178] To date, five different agents (epigallocatechin

gallate, Pep42, PAT-SM6, DHA and arctigenin) are reported to inhibit BiP activity.[172,179] Pep42 and PAT-SM6 are being tested in ongoing clinical trials for the treatment of Alzheimer's disease and multiple myeloma, respectively.[172] DHA is under investigation in advanced phase clinical trials for different solid tumours such as colon cancer, lung cancer and gastric or oesophageal adenocarcinoma.[179]

Activation of the PERK branch in lymphoma models leads to cell survival[180] and deletion of PERK inhibits the formation of mammary tumours and reduces lung metastasis.[181] Two PERK inhibitors (GSK260641 and GSK2656157) have been developed and showed anti-proliferative effect in multiple myeloma and pancreatic cancer in *in vivo* studies.[172] On the contrary, it has been demonstrated that CHOP prevents tumour progression. Different studies showed how the deletion of *Chop* increased tumourigenesis in lung and hepatocellular carcinoma mouse models.[182,183]

Some evidence suggested a possible involvement of UPR in AML development. The IRE1α branch is activated in almost 20% of AML cases and patients with triggered UPR have a better survival and lower risk of relapse. Moreover, UPR related molecules are able to inhibit the translation of CEBPA mRNA which is frequently mutated leading to maturation defects.[172] The vast majority of APL patients are characterised by the fusion of retinoic acid receptor alpha (*RARα*) to the promyelocytic leukaemia (*PML*) open reading frame and express the PML-RARα chimeric protein. Khan and colleagues provided an explanation of how UPR may be a promoter of the PML-RARα activation. Under physiological conditions, RARα is able to dissociate from co-repressor (i.e., N-CoR), in the presence of specific agonist such as all-trans retinoic acid (ATRA). In the PML-RARα setting, a strong binding with the co-repressor causes its conformational change. The misfolded N-CoR protein triggers ER stress and is finally degraded through ERAD system impairing myeloid differentiation.[184]

Recently, Prof. Pier Giuseppe Pelicci's group demonstrated that inducible expression of FLT3-ITD in the Ba/F3 (Ba/F3-ITD) murine pro-B cell line results in higher basal levels of the ER stress marker BiP compared to cells expressing the *wild-type* FLT3 receptor (Ba/F3-WT) **(Figure 1.12)**. Additionally, the induction of UPR is associated with the retention of the FLT3-ITD protein in the ER (personal communication) **(Figure 1.13)**. Therefore, UPR may be a druggable target that delineates a promising novel therapeutic approach for AML patients bearing FLT3-ITD mutations.

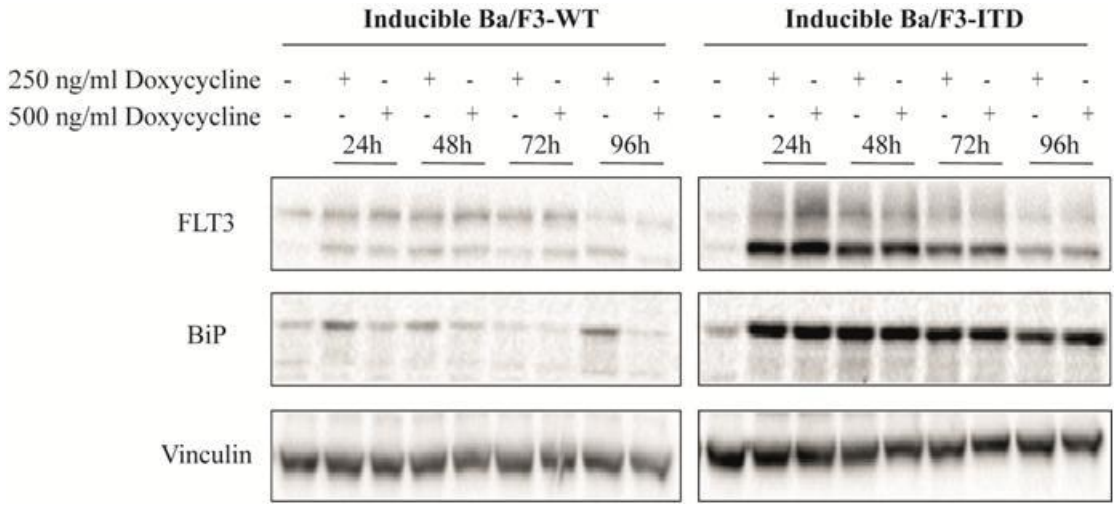


***Figure 1.12 Elevated ER stress in Ba/F3-ITD cells***
*Representative immunoblot analysis of BiP expression levels. Ba/F3-WT and -ITD cells were treated with two different concentrations of doxycycline for inducing FLT3 expression for the indicated time duration. The expression of FLT3 and BiP was analysed by SDS-PAGE and western blotting. Vinculin levels were used as a loading control.*

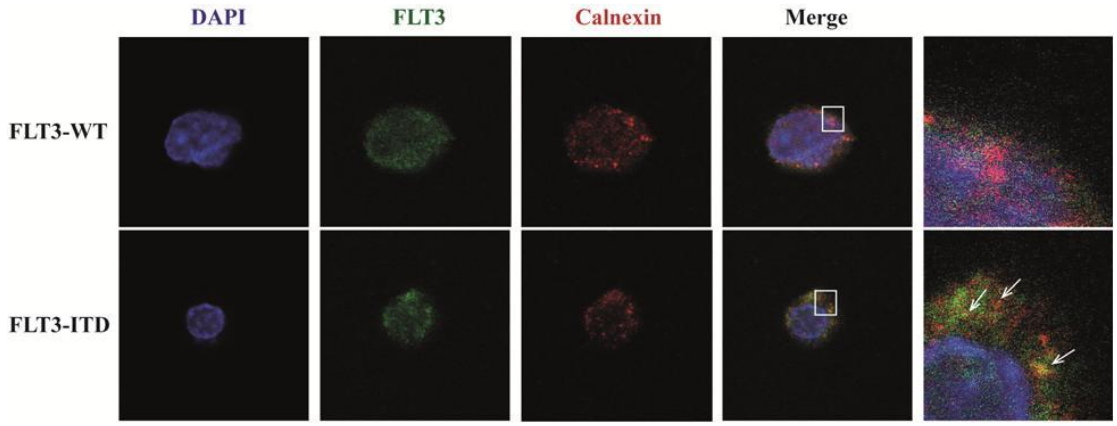


***Figure 1.13 FLT3-ITD retention in the endoplasmic reticulum***
*Immunofluorescent staining of Ba/F3 cells expressing FLT3-WT and –ITD receptor. An Alexa 488-conjugated α-FLT3 antibody was used to detect the FLT3 receptor (green) while ER was labelled using a Cy3-conjugated anti-calnexin antibody (red). The white arrows indicate the presence of FLT3-ITD receptor in the ER. DAPI (blue) was used as a counterstain for viable cell nuclei.*

---

Since UPR is a double-edge sword as it confers pro-survival advantages and induces apoptosis, an alternative therapeutic approach to attenuation of the adaptive response is enhancing of the pro-death signalling pathway. Proteasome inhibitors increase ER stress as they cause the accumulation of misfolded and unfolded proteins. Thus, cells are pushed into apoptosis. Bortezomib, an FDA-approved drug, was used successfully as monotherapy in acute leukaemias[172] and also in combination with IRE1α inhibitors to prevent the development of resistance due to the acquisition of new mutations. Other proteasome inhibitors (carfilzomib, nelfinavir, marizomib and MLN9708), pan-deacetylase inhibitors, such as panobinostat, and anti-diabetics, such as metformin, are in advanced phase clinical trials [179] for the treatment of haematological malignancies and solid tumours.

# 2 Aim of the work

The project originates from the fact that standard chemotherapy regimens cure only a minority of AML patients with adverse prognosis. FLT3-ITD mutations represent the most common type of mutations among the recurrent genetic alterations in AML, and correlate with a high leukemic burden, poor prognosis, and a significant negative impact on the management of patients.[42,43] To date, there are no effective drugs to be used for the treatment of AML patients bearing FLT3-ITD mutations. Indeed, treatment with existing inhibitors usually leads to the development of resistance due to the acquisition of new mutations.[70] The development of new effective treatment modalities is a still unmet clinical need.

The aim of this PhD project was the identification of new drugs for FLT3-ITD AML treatment by exploiting the strategy known as drug repurposing or repositioning. This aim was pursued through the completion of the following phases:

1) Screening phase: a primary HTS of three libraries of FDA-approved compounds or those in advanced stages of clinical trials that identified agents active against AML cell lines (in collaboration with the Screening Unit @IIT), followed by a secondary small-scale screening designed to narrow down the number of hits by identifying agents with selectivity for FLT3-ITD AML. This phase comprised a substantial amount of optimization of the HTS, bioinformatic statistical analysis of the data as well as extensive manual curation of the results obtained in order to make a final selection of compounds to be carried into the second phase.
2) Validation phase: the selected compounds were tested as single agents and in combination with standard therapeutics used in AML as well as with FLT3 inhibitors. The *in vitro* validation included the determination of $IC_{50}$, plotting of growth curves, characterization of the cell cycle and clonogenic activity. The *in*

*vivo* validation envisages testing the candidate drugs alone and in combination on both *xenograft* and murine AML models.

3) Mechanism of action determination phase for the two candidate drugs: the analysis of the known mechanism of action, the ability to inhibit FLT3 signalling and the analysis of a novel potential mechanism of action in collaboration with the group of Prof. P.G. Pelicci was performed.

The three phases of the project made use of different model systems: AML cell lines in the first and second phase of the project, murine models of AML in second phase of the project and of the Ba/F3 cells, a murine pro-B haematopoietic cell line transduced with FLT3-WT or FLT3-ITD, to unravel the mechanisms of action in the third phase.

# 3 Materials and methods

## 3.1 Cell lines

Human AML cell lines were maintained in appropriate media as specified on the ATCC website. Murine haematopoietic Ba/F3 cell lines expressing either FLT3-WT and -ITD generated by viral transduction were kindly donated by Pier Giuseppe Pelicci's group and grown in RPMI 1640 supplemented with 10% foetal bovine serum (FBS), 10% of WEHI-3B supernatant in the presence of penicillin (100 U/mL) and streptomycin (100 µg/mL). Cells were maintained in the logarithmic growth phase at 37°C in a humidified atmosphere containing 5% $CO_2$ at all times.

## 3.2 Chemical and Reagents

A total of 3675 compounds were tested in an initial high-throughput screening. The collection of compounds included drugs that are already approved by the FDA or in advanced-phase clinical trials. In particular, 1280 compounds were from LOPAC 1280 (Sigma-Aldrich), 75 from Selleck Catalogue of New Items and 2320 from MicroSource Spectrum collection. Drugs were dissolved in dimethylsulfoxide (DMSO). Auranofin, Ara-C, methotrexate hydrate, midostaurin hydrate, pyrvinium pamoate and thapsigargin were purchased from Sigma-Aldrich (St. Louis, MO) and dissolved in DMSO at a stock concentration of 5 mM, 100 mM, 10 mM, 10 mM, 10 mM and 1 mM, respectively. Quizartinib was acquired from Chemietek (Indianapolis, USA), dissolved in DMSO at a stock concentration of 100 mM. Doxorubicin hydrochloride was purchased from Sigma-Aldrich (St. Louis, MO) and dissolved in water at a stock concentration of 1 mM.

Dithiothreitol (DTT) was acquired from VWR Life Science, dissolved in DMSO at a stock concentration of 1 mM. All compounds were aliquoted and stored at -80°C.

CellTiter-Glo assay kit was purchased from Promega Corporation (Madison, WI, USA), Thioredoxin Reductase Assay Kit was purchased from Abcam (Cambridge, United Kingdom), BrdU flow kit was purchased from BD Pharmingen™, the 7AAD viability dye was purchased from Beckman Coulter (Brea, California, USA).

Antibodies used for immunoblotting were acquired from the following sources: anti-ATF4 (D4B8), anti-βCatenin (6B3), anti-BiP (C50B12), anti-phosho-βCatenin (Ser33/37/Thr41), anti-GSK3β (27C10), anti-phospho-GSK3β (Ser9), anti-CHOP (9C8) Cell Signaling Technology (CST, Danvers, Massachusetts, USA); anti-Lamin B1 (Abcam, Cambridge, United Kingdom), anti-Vinculin clone H (Sigma-Aldrich, St. Louis, MO).

Antibodies used for flow cytometry analysis were acquired from following sources:

PE anti-mouse CD45 (Clone 30-F11) (BD Pharmingen™), APC anti-human CD45, Pacific Blue anti-human CD45 (Beckman Coulter, Brea, California, USA).

## 3.3 Cell viability assay

To determine the number of viable cells in culture we used two different strategies: the CellTiter-Glo (CTG) luminescent assay and the trypan blue exclusion method. The CellTiter-Glo luminescent assay is based on the quantification of the ATP produced by cells, which indicates the existence of metabolically active cells. The addition of the CellTiter-Glo reagent directly to cell culture results in cell lysis and generation of a luminescent signal which is proportional to the amount of ATP present and thus to the number of viable cells. **Figure 3.1** shows the luciferase reaction at the basis of this assay that utilizes a thermostable luciferase (Ultra-Glo$^{TM}$ Recombinant Luciferase) generating a stable luminescent signal.

The trypan blue exclusion test is based on the principle that live cells exclude certain dyes (*i.e.,* trypan blue, eosin and propidium iodide) as they possess intact cell membranes.

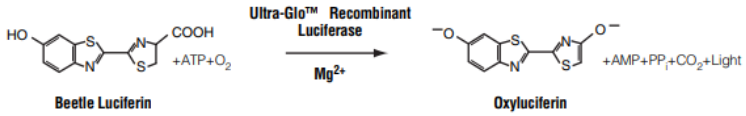


***Figure 3.1: The luciferase reaction***
*Luciferase in the presence of $Mg^{2+}$, ATP and molecular oxygen catalysed the mono-oxygenation of luciferin. Figure adapted from CellTiter-Glo Luminescent Cell Viability Assay technical bulletin.*

---

### 3.3.1 First high-throughput screening

Tecan freedom Evo robot at the IIT screening Unit was used for cell seeding and treatments. Exponentially growing MOLM13 and MV4-11 cells were seeded in 384-well plates (Corning Life Sciences, Acton, MA) at 2500 cells per well in 40 µl of growth medium and allowed to grow for 24 hours at 37°C, 5% $CO_2$, 95% humidity. Compounds were then added at three different final concentrations: 0.05 µM, 0.5 µM and 5 µM. Cells treated with 0.2% of DMSO (the diluent used to resuspend the compounds) were used as a negative control and cells treated with Ara-C (from 0.25 µM to 8 µM) or quizartinib (from 0.25 nM to 8 nM) were used as positive controls **(Figure 3.2)**. Seventy-two hours later, cells were equilibrated at room temperature for 30 minutes, 40 µl of CellTiter-Glo solution was added in each well, incubated for 10 minutes to allow for the reaction to take place and then read on a plate reader (PHERAstar FS, BMG Labtech) according to the manufacturer's instructions. All treatments were done in duplicate. The Z-score was calculated according to Zhang XD.[107]

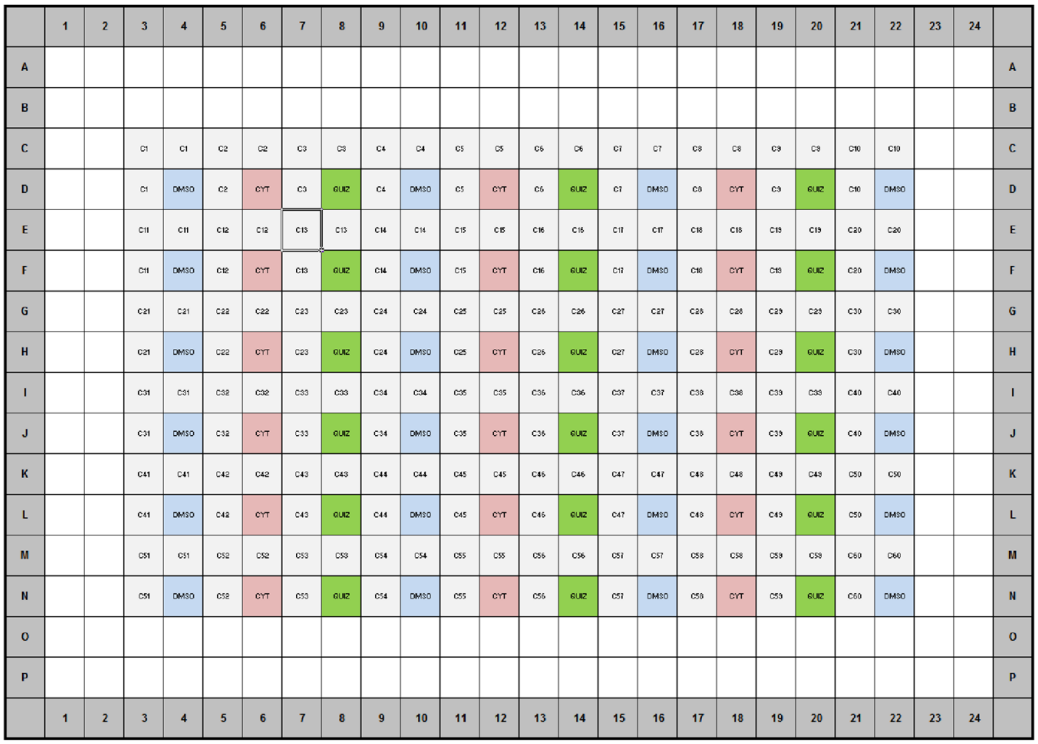


***Figure 3.2: Layout of the 384-well plate used for the first high-throughput screening***
*Cells from each cell line where seeded in a 384-well plate at 2500 cells per well and incubated at 37°C in the humidified atmosphere containing 5% of $CO_2$. Compounds (grey squares), quizartinib (green squares) and Ara-C (pink squares) were added the day after seeding. In each plate, 25 wells without any compound but with DMSO constituted a negative control (light-blue squares). Tested-compounds were added at three different concentrations: 0.05 µM, 0.5 µM and 5 µM. In each plate 60 compounds were tested.*

---

### 3.3.2 Second screening

MOLM13, MV4-11, MONO-MAC-6, THP-1 and OCI-AML2 cell lines were seeded in 96-well plates at $10^4$ cells/well, while PL-21 were seeded at $2x10^4$ cells/well in 100 µl of growth medium and allowed to grow for 24 hours at 37°C, 5% $CO_2$, 95% humidity. Compounds were then added at two different final concentrations: 0.05 µM and 0.5 µM. Cells treated with 0.2% of DMSO were used as a negative control and cells treated with Ara-C (from 16 µM to 0.5 µM) or quizartinib (from 8 nM to 1 nM) were used as positive controls **(Figure 3.3)**. Seventy-two hours later, cells were equilibrated at room temperature for 30 minutes, 100 µl of CellTiter-Glo solution was added in each well, incubated for 10 minutes allow for the reaction to take place and then read on GloMax (Promega) plate

reader according to manufacturer's specifications. All treatments were done in triplicate. Robust Z-score was calculated according to Zhang XD[107] with appropriate adjustments due to the huge bias of the experiment (all compounds within the plate should be active). Thus, in this case the difference between the measurement of a compound and the median of negative controls was divided by the standard deviation of all the negative controls within the plate.

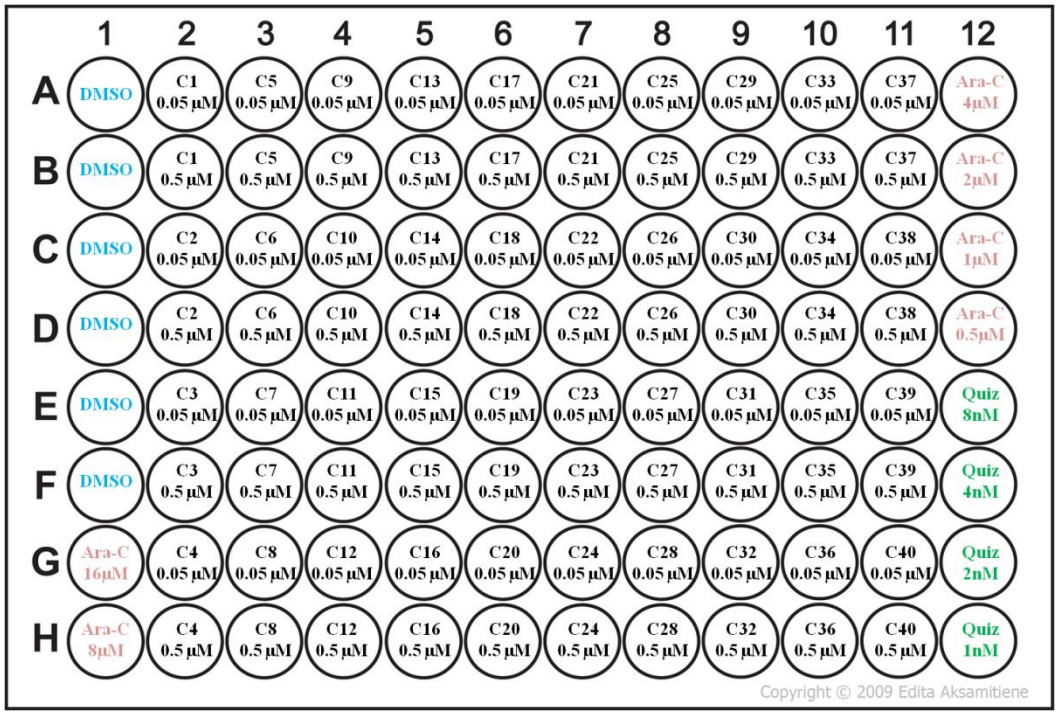


***Figure 3.3: Layout of the 96-well plate used for the second screening***
*Cells from each cell line where seeded in a 96-well plate and incubated at 37°C in the humidified atmosphere containing 5% of $CO_2$. Compounds (C1-C40), quizartinib and Ara-C were added the day after seeding. In each plate, 6 wells without any drug but with DMSO constituted a negative control. Tested-compounds were added at two different concentrations: 0.05 µM and 0.5 µM. In each plate 40 compounds were tested.*

---

### 3.3.3 Dose-response curves

MOLM13, MV4-11, MONO-MAC-6, THP-1 and OCI-AML2 cell lines were seeded in 96-well plates at $10^4$ cells/well while PL-21 were seeded at $2x10^4$ cells/well in 100 µl of growth medium and allowed to grow for 24 hours at 37°C, 5% $CO_2$, 95% humidity. Compounds were then added, as indicated. Seventy-two hours later, cells were equilibrated

at room temperature for 30 minutes, 100 µl of CellTiter-Glo solution was added in each well incubated for 10 minutes to allow for the reaction to take place and then read on GloMax (Promega) plate reader according to the manufacturer's specifications. Cells treated with DMSO (0.2%) were used as a positive control. The half maximal inhibitory concentration ($IC_{50}$) value was calculated in GraphPad (Prism software).

### 3.3.4 *In vitro* proliferation

MOLM13, MV4-11 and OCI-AML2 cells were seeded in duplicate at $10^5$ cells/ml and allowed to grow for 24 hours at 37°C, 5% $CO_2$, 95% humidity. Then cells were treated with concentrations corresponding to the $IC_{50}$ value of auranofin or pyrvinium pamoate or diluents (DMSO, control). After 24, 48 and 72 hours 20 µL of sample was mixed with 20 µL of 0.4% trypan blue by gently pipetting, and then 20 µL of the mix were loaded into the Bürker chamber. Both viable and dead cells were counted under an inverted-light microscope (Leica).

Ba/F3 cells were seeded in duplicate at $10^5$ cells/ml and treated with concentrations of drugs that cause 50% of maximal inhibition of cell proliferation ($GI_{50}$). Thus, cells were treated with auranofin or pyrvinium pamoate or quizartinib or diluents (DMSO, control) in the presence or absence of interleukin-3 (IL-3). After 24, 48 and 72 hours 20 µL of sample was mixed with 20 µL of 0.4% trypan blue by gently pipetting, and then 20 µL of the mix were loaded into the Bürker chamber. Both viable and dead cells were counted under an inverted-light microscope (Leica).

## 3.4 Colony formation

Leukaemic cell lines (MOLM13, MV4-11 and OCI-AML2) were seeded at $10^5$ cells/ml and allowed to grow for 24 hours at 37°C, 5% $CO_2$, 95% humidity. Then cells were treated

with DMSO, auranofin or pyrvinium pamoate at the predetermined $IC_{50}$ concentrations for 72 hours after which cells were resuspended in culture medium with or without auranofin or pyrvinium pamoate. One-hundred viable cells were mixed with Methocult medium (MethoCult SF H4236; StemCell Technologies) and plated into a 6-cm dish. Colonies were counted under an inverted light microscope (Leica) after 14 days.

## 3.5 Combination treatments

MOLM13, MV4-11 and OCI-AML2 cells were seeded at $10^4$ cells/well in 96-well plates and allowed to grow for 24 hours prior to treatment commencement.

Drug concentrations ranged from 3.2 µM to 0.025 µM, from 10 µM to 0.078 µM, from 1 µM to 0.0078 µM, from 80 nM to 0.625 nM, from 3 µM to 0.006 µM, from 1 µM to 0.0078 µM and from 8 nM to 0.0625 nM for Ara-C, auranofin, doxorubicin, methotrexate, midostaurin, pyrvinium pamoate and quizartinib, respectively in the single-drug treatment condition. Treatment effects were then evaluated in a combination setting in which decreasing concentrations of each compound were used **(Figure 3.4)**.

The most common approaches adopted for assessing the effect of a combination are (1) Combination Subthresholding, (2) Highest Single Agent, (3) Response Additivity, and (4) Bliss Independence model. We determined the interaction between two compounds using the Bliss Independence model, which assumes that drugs act independently and have different sites of action, but contribute to common result.

Although it is one of the most popular models, one of the limitations is that drugs could have complex, multiple and unknown mechanisms of action thus this methodology in theory requires an a priori knowledge of detailed mechanisms of action in order to be sure that there is no mechanistic overlap between the agents.

The calculation of the combination index (CI) was calculated as CI = $\frac{E_A + E_B - E_A E_B}{E_{AB}}$. The $E_A$ indicates the effect of compound A, $E_B$ indicates the effect of compound B and $E_{AB}$ the effect of the combination of both compounds. CI<1 indicates synergism; CI=1 indicates an additive effect, and CI>1 indicates antagonism.[185]

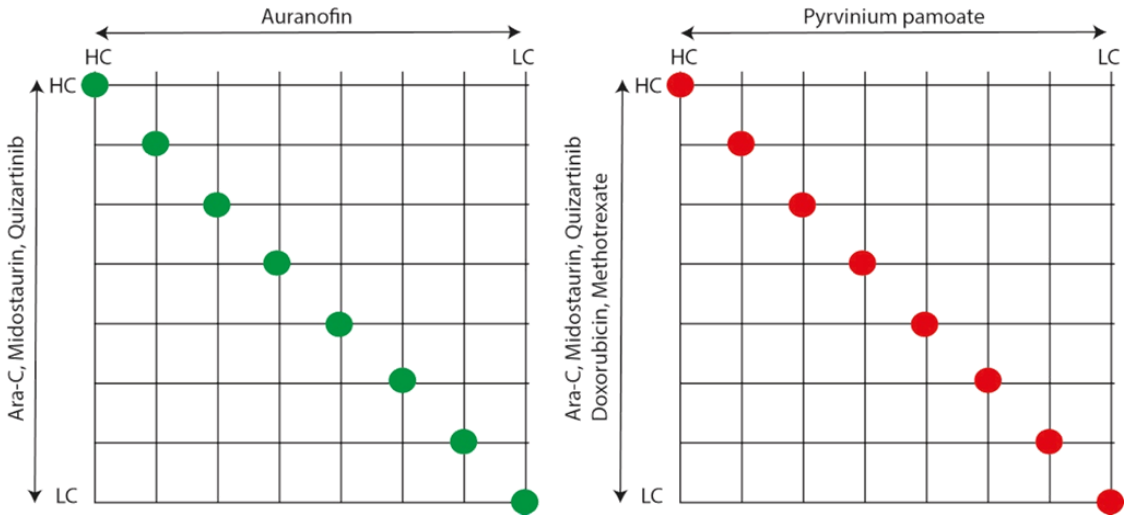


***Figure 3.4: Drug combination setting***
*Cells were exposed to the indicated drugs at decreasing concentration for 72h. Dots on the lines indicate data points used to determine the cytotoxicity effects. HC, highest concentration; LC, lower concentration.*

---

## 3.6 Cell cycle analysis

### 3.6.1 Bromodeoxyuridine (BrdU) staining

The flow cytometric analysis of the immunofluorescent staining of incorporated bromodeoxyuridine (BrdU) is an accurate method for the detection of proliferating cells. The BrdU, an analogue of the DNA precursor thymidine, is incorporated into newly synthesized DNA by cells entering into the S phase (DNA synthesis) of cell cycle. Specific anti-BrdU fluorescent antibodies are used to detect the incorporated chemical, thus indicating cells that are actively replicating their DNA. The incorporation of BrdU is normally coupled with a DNA dye staining such as Propidium Iodide (PI) to perform cell

cycle analysis by flow cytometry. The combination allows for the enumeration and characterization of proliferating cells (BrdU incorporation) in terms of their cell cycle phase (i.e., G0-G1, S, or G2-M phases identified by PI staining).

Ba/F3-WT and -ITD were pulsed with 10 μM of BrdU; $10^6$ cells were kept apart as an unpulsed control. Cells were incubated at 37°C with 5% $CO_2$ for 30 minutes. After 30 minutes of pulse, cells were washed twice with 1X PBS to remove unincorporated BrdU, and then resuspended at $10^5$ cells/ml in fresh medium in the presence or absence of auranofin or pyrvinium pamoate. At each time point (1, 4, 8, and 12 hours after BrdU pulse), $10^6$ cells were harvested, washed with 1X PBS, fixed using BD Cytofix/Cytoperm™ Buffer, washed, and stored at 4ºC. Cells from all time points were simultaneously stained: after fixation, cells were permeabilized with BD Cytoperm Permeabilization Buffer Plus™, incubated with BD Cytofix/Cytoperm™ Buffer, treated with DNAse to expose BrdU epitopes, stained with fluorochrome-conjugated anti-BrdU and with PI (DNA staining solution), resuspended in staining buffer and analysed using flow cytometry (FACSCelesta, FLowJo10 software).

## 3.7 Immunoblotting

Cellular proteins were extracted in 1X Laemmli Buffer (2% SDS, 10% glycerol, 5% 2-mercaptoethanol, 0.002% bromophenol blue and 60 mM Tris HCl, pH. 6.8), and $3\times10^5$ lysed cells were loaded in each lane. Separated proteins were then transferred to Protrane nitrocellulose membrane (GE Healthcare) for antibody probing.

Membranes were blocked by incubation with either 5% non-fat milk or 5% BSA in Tris-buffered saline, 0.1% Tween 20 (TBST) for one hour at room temperature (RT). Next, they were incubated with the primary antibodies diluted in either 5% non-fat milk or 5% BSA in 1X TBST at +4°C overnight, then washed three times with TBST and incubated with a

secondary antibody (anti-mouse, anti-rabbit or anti-goat, according to the primary antibody used) at the dilution of 1:10.000-20.000 in TBST for one hour at RT. The antibody was then visualized using enhanced chemiluminescence (ECL) western blotting detection reagents (Amersham). The signal was acquired using Chemidoc XRS + Imager (Biorad) and analysed with Image Lab software (Biorad).

## 3.8 Thioredoxin reductase assay

Ba/F3-WT and -ITD were treated with predetermined $GI_{50}$ concentration of auranofin for 72 hours and then harvested for detecting thioredoxin reductase (TrxR) activity using Thioredoxin Reductase Assay Kit according to the manufacturer's instructions. In brief, TrxR catalyses the reduction of 5,5'-dithiobios (2-nitrobenzoic) acid (DTNB) with NADPH to 5-thio-2-nitrobenzoic acid ($TNB^{2-}$) that generates a strong yellow color ($\lambda_{max}$ = 412 nm). TrxR-specific inhibitor is employed to determine TrxR specific activity as in biological samples other enzymes (i.e., glutathione reductases and glutathione peroxidase) can also reduce DNTB. Thus, the measurement of the total DNTB reduction by the sample in the presence or absence of TrxR specific inhibitor is performed. The difference between the two results indicates the reduction of DNTB by TrxR.

-Sample preparation

Samples were homogenized in cold assay buffer and supernatant was collected. In each well of a 96-well plate, 25 µl of sample or 10 µl of TrxR positive control were placed and the volume adjusted to 50 µl with assay buffer. Two sets of samples were tested: the first with TrxR inhibitor for testing background enzyme activity, and the second without TrxR inhibitor for testing total DNTB reduction. Accordingly, 10 µl of TrxR inhibitor or assay buffer were added.

-Reaction mix preparation and addition

In each well 40 µl of the reaction mix were added and mixed.

| | | |
|---|---|---|
| Reaction mix: | assay buffer | 30 µl |
| | DNTB solution | 8 µl |
| | NADPH | 2 µl |

-Standard curve preparation

A TNB standard curve was prepared by adding in duplicate in the 96-well plate 0, 2, 4, 6, 8, 10 µl of the TNB standard and adjusting to a final volume of 100 µl with assay buffer for generating 0, 10, 20, 30, 40, 50 nmol/well standards.

-Optical density measurement

The optical density (OD) was read on GloMax (Promega) after 20 and 150 minutes. The OD of the $TNB^{2-}$ generated by TrxR was: $\Delta A_{412} = (A_{2AB}\text{-}A_{2INH}) – (A_{1AB}\text{-}A_{1INH})$; where AB indicates the assay buffer and INH the inhibitor.

-Data analysis

TNB standard curve was plotted and ΔB nmol of TNB get by applying the $\Delta A_{412}$ to the TNB standard curve. TrxR activity was calculated as: $\frac{\Delta B}{(T_2-T_1)\,x\,V}$ x sample dilution factor, where ΔB is the TNB amount from TNB standard curve, $T_1$ is the time of the first reading, $T_2$ is the time of the second reading, V is the pretreated sample volume added into the reaction well.

## 3.9 RNA extraction and reverse transcription

Cells were harvested, washed twice in cold 1X PBS and RNA was extracted using the Quick-RNA™ MiniPrep kit (Zymo Research). RNA was quantified with Nanodrop and 1 µg of template RNA was retrotranscribed into cDNA using random primers and the ImProm-II™ Reverse Transcription System (Promega).

## 3.10 DNA amplification through polymerase chain reaction

The splicing of *Xbp1* mRNA was detected by polymerase chain reaction (PCR), a powerful and sensitive technique for DNA amplification. cDNA was used as template. Amplification of a DNA fragment requires two oligonucleotides flanking the region of interest, working as primers for the DNA polymerase. Primers specific for mouse *Xbp1* detect three possible cDNA products: hybrid, unspliced and spliced isoforms. The former is generated by one strand of unspliced *Xbp1* and one strand of spliced *Xbp1* while the last two isoforms are formed by the annealing of a single strand cDNA with its complementary sequence **(Figure 3.6)**. The 5′ to 3′ sequences of primers used to detect unspliced and spliced *Xbp1* mRNA were adapted from Samali et al, and are as indicated below.[186]

Forward primer: GAACCAGGAGTTAAGAACACG
Reverse primer: AGGCAACAGTGTCAGAGTCC
Size of PCR products: unspliced XBP1 = 205 bp, spliced XBP1 = 179 bp.

*Taq* DNA polymerase enzyme was used for the PCR reaction.

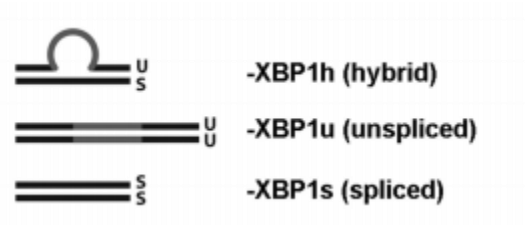


***Figure 3.5: Isoforms of Xbp1***
*Schematic representation of the three possible cDNA products generated by primers flanking Xbp1 spliced intron indicated in grey. Figure adapted from Chalmers et al Wellcome Open Res.2017 Oct 9;2:36.* [187]

| | | |
|---|---|---|
| Reaction mix: | template DNA | 1 µl |
| | reaction buffer | 1X |
| | dNTPs | 200 µM |
| | forward primer | 0.2 µM |

| | |
|---|---|
| reverse primer | 0.2 μM |
| DNA polymerase | 0.625 units |
| $ddH_2O$ | to 25 μl |

DNA amplification was performed on a Mastercycler Nexus thermocycler using the following amplification protocol:

| | | |
|---|---|---|
| 1. heat shock step | 30'' | at 95°C |
| 2. denaturation step | 30'' | at 95°C |
| 3. annealing step | 60'' | at 49°C |
| 4. extension step | 1'/kb | at 68°C |
| 5. repeat 30 times steps from 2 to 4 | | |
| 6. extension step | 5' | at 68°C |
| 7. end | hold | at 4°C |

## 3.11 Agarose gel electrophoresis

Following the addition of 1/6 volume of 6X gel loading dye purple (NEW ENGLAND, BioLabs), DNA samples were loaded on 2% agarose gels along with DNA markers. The agarose powder for gel preparation was melted in 1X Tris-Borate-EDTA (TBE) buffer containing 1X Sybrsafe (Invitrogen) and run at 80-120 volts (V) until the desired separation was achieved. The DNA bands were visualized under a UV lamp (radiation wavelength 260 nm).

## 3.12 Real time PCR

Upon total RNA extraction and reverse transcription 20 ng of the resulting cDNA were used for each real-time PCR reaction together with 0.4 μM primers, 10 μL of SYBR Green Fast Reaction Mix (Applied Biosystems) diluted in a final volume of 20 μL. Accumulation of fluorescent products was monitored by real-time PCR using the 7500 Fast Real-Time

PCR System (Applied Biosystems). All primers were designed using the online Universal Probe Library Assay Design Center by Roche Life Science and listed in **Table 3.1**.

***Table 3.1 Primer used to analysed ER stress/ UPR and Wnt target genes***

| Gene | Forward | Reverse |
|---|---|---|
| ***Atf4*** | ATGATGGCTTGGCCAGTG | CCATTTTCTCCAACATCCAATC |
| ***Atf6*** | TCAAACAAGTCTTTATAATGCAATACC | GTCTTTGTACAGACAGACAACAAAGTT |
| ***Chop*** | GCGACAGAGCCAGAATAACA | GATGCACTTCCTTCTGGAACA |
| ***Dnajb9*** | CACAAAGATGCCTTTTCTACCG | TTAAACTTTTCAGCTTAATGACGTG |
| ***Dnajc3*** | AGACCGTCTTCCAGGAAACTT | CCAGTCTATACCTGGACATACAGC |
| ***Edem1*** | GGTCTTCGAAGCTACGATAAGG | GGGCTGTTTGGAATCAGTTATTA |
| ***Perk*** | CCTTGGTTTCATCTAGCCTCA | ATCCAGGGAGGGGATGAT |
| ***Ire1*** | GAGGCCAAGAGCAAGCTAAC | CCATTGAGGGAGAGGCATAG |
| ***Erp44*** | TGTCCCTCTTGTCCGAGAAA | GAAAAGGCAGTCCTTCTTCTGT |
| ***Herpud1*** | ACCTGAGCCGAGTCTACCC | CAACAGCAGCTTCCCAGAATA |
| ***BiP*** | CTGAGGCGTATTTGGGAAAG | TCATGACATTCAGTCCAGCAA |
| ***Pdia3*** | GTGGCCACTGTAAGAATCTGG | TGACAATATTTGGATCTTTGCTG |
| ***Ppp1r15b*** | TGCTGGAGAAAGATACACCCATA | AATTCTTCCCATGGTCCTTTG |
| ***Axin2*** | GAGAGTGAGCGGCAGAGC | CGGCTGACTCGTTCTCCT |
| ***Tcf4*** | CATATTTGTGGCCATTGAAGG | GTCCCTAAGGCAGCCATTC |
| ***Tbp*** | CTGGAATTGTACCGCAGCTT | TCCTGTGCACACCATTTTTC |

## 3.13 *In vivo* experiments

Mice were maintained accordingly to the guidelines set out in Commission Recommendation 2007/526/EC, 18 June 2007, on guidelines for the accommodation and care of animals used for experimental and other scientific purposes. All experiments were performed in accordance with the Italian Laws (D.L.vo 116/92 and following additions), which enforces EU Directive 86/609 (Council Directive 86/609/EEC of 24 November 1986 on the approximation of laws, regulation, and administrative provisions of the member states regarding the protection of animals used for experimental and other scientific purposes. Experiments involving mice were performed following the approval of the Institutional Review Board and the Italian Ministry of Health (projects 877/15 and 506/18). Animals were bred and housed in the animal facility at the European Institute of Oncology (IEO) and Institute FIRC of Molecular Oncology (IFOM) campus. Animal received ad libitum food and drinking water, and were kept in a regimen of 12-hour light-and-darkness cycle. The animals were controlled twice a week to evaluate the presence of signs of illness and/or altered behaviour such as hunched posture, decreased activity, ears in backward position, laboured breathing and weight loss greater than 10%. Upon signs of acute distress, the animals were immediately euthanized, by inhalation of high concentrations of carbon dioxide. The endpoint of the experiments has never been animal death of the disease. The animals were sacrificed when the level of the blasts in blood reaches 70-80% of the cells.

### 3.13.1 Toxicity study

NOD-scid IL2Rgamma$^{null}$ (NSG) mice aged 6 weeks were injected intraperitoneally (i.p.) with either vehicle (22 % DMSO in PBS) or auranofin (10 mg/Kg/day) or pyrvinium pamoate (0.5 mg/Kg/day, 0.25 mg/Kg/day, 0.126 mg/Kg/day and 0.06 mg/Kg/day), five times weekly for a total duration of three weeks. Mice were injected i.p with Ara-C (60

mg/Kg) for five days. Ara-C was dissolved in water. Mice were weighted once a week both during the treatment and for three weeks after the end of the treatment. The variable measured (weight) is continuous, thus we adopted an ANOVA one-way analysis. In this case, for highlighting differences equal to:

- ➔ Effect size = 0.55
- ➔ Fixing alpha = 0.05

A power of 0.8 was set, when the number of animals per group was equal to 8.
In particular for assessing the impact of pyrvinium pamoate treatment on mice survival, mice were divided as follow: control group (n=5), 0.5 mg/Kg of pyrvinium pamoate (n=4), 0.25 mg/Kg of pyrvinium pamoate (n=4), 0.126 mg/Kg of pyrvinium pamoate (n=4) and 0.06 mg/Kg of pyrvinium pamoate (n=4).
Moreover, for evaluating gender-related toxicity both female and male mice were divided as follow: control group (n=3), 10 mg/Kg of auranofin (n=4) and 0.25 mg/Kg of pyrvinium pamoate (n=3).

Both experiments have to be repeated (biological replicates) to obtain eight mice per group and highlight possible statistical significant differences.

### 3.13.2 *Xenograft* mouse model

NSG mice aged 6 weeks were injected intravenously (i.v.) with $10^6$ of human primary AML cells were obtained following a written informed consent from the patients and approved by the local ethical committee. To monitor leukaemia development, peripheral blood (PB) was drawn periodically (at least 1 per month) from a small incision of the lateral caudal vein. Before the blood sampling, animals were heated up by a red light to dilate the veins. A volume of 100 µl of PB was taken from each animal and was mixed with 20 µl of 0.5 M EDTA in order to prevent it from clotting. PB samples were stained

with PE anti-mouse CD45 and APC anti-human CD45 in the presence of the vitality dye 7AAD for 30 minutes at 4°C. Next, to remove erythrocytes cells were incubated with red cell lysis buffer (150 mM $NH_4Cl$, 9.9 mM $KHCO_3$, 0.083 mM tetrasodium ETDA) for 10 minutes at 4°C. After incubation, cells were centrifuged at 1500 rpm at 4°C for five minutes. Supernatant was discarded and cells were resuspended in lysis buffer for 2 minutes at RT and then centrifuged at 1500 rpm at 4°C for five minutes. Supernatant was discarded and cells resuspended in PBS for flow cytometry analysis. Mice were assigned into treatment and control groups to form cohort characterized by similar average percentage of human CD45 (randomization).

Animals in the treatment group received i.p. administration auranofin (10 mg/Kg, 5mg/Kg and 2.5 mg/Kg) and pyrvinium pamoate (0.5 mg/Kg and 0.25 mg/Kg) daily, five times weekly for three weeks. Ara-C treated group received drug i.p daily at 60 mg/Kg. for five days. The control group were treated with 22% of DMSO in PBS according to the same schedule as the auranofin/pyrvinium pamoate treatment groups. Mice were weighted once a week during the treatment and the development of leukaemia was monitored by PB samples taken every 2-3 weeks after the end of the treatment and analysed by flow cytometry as indicated above. The endpoint of the experiments is never animal death of the disease. Animals were euthanized by $CO_2$ inhalation when signs of suffering and distress were apparent. As mentioned above the variable that we measured (weight and percentage of hCD45) are continuous, thus we adopted an ANOVA one-way analysis. In this case, for highlighting differences equal to:

- ➔ Effect size = 0.55
- ➔ Fixing alpha = 0.05

A power of 0.8 was set, when the number of animals per group is equal to 8.

In the first experiment that we performed mice were divided into five groups: control group (n=3), 10 mg/Kg of auranofin (n=3), 5 mg/Kg of auranofin (n=3), 2.5 mg/Kg of

auranofin (n=3), 0.5 mg/Kg of pyrvinium pamoate (n=3) and 60 mg/Kg of Ara-C (n=5).
In the second experiment, mice were divided as follow: control group (n=6), 10 mg/Kg of auranofin (n=4), 0.25 mg/Kg of pyrvinium pamoate (n=3) and 60 mg/Kg of Ara-C (n=4).

Both experiments have to be repeated (biological replicates) to obtain eight mice per group and highlight possible statistical significant differences.

## 3.14 Statistical analysis

Data from initial and final screenings were normalized using the Normalized Percent Inhibition (NPI) method.[106] The mean (first high-throughput screening) and the median (second high-throughput screening) of the replicates were calculated. Hits in the initial high-throughput screening were called based on two different criteria a Z score > 5SD or a viability < 20%; hits in the final screening were called based on a Robust Z score > 5SD and a viability < 60%. Data collected were expressed as the mean or median ± SD.
Unpaired Student's t test was performed to determine statistic probabilities. GraphPad (Prism software) was used for statistical analysis. $p<0.05$ was considered statistically significant difference.

# 4 Results

## 4.1 First high throughput screening: setting the experimental conditions

With the aim of identifying compounds that inhibit the growth of leukaemic cells, an initial HTS was performed using two different cell lines, MOLM13 and MV4-11, that are cell lines established from AML patients with FLT3-ITD.

The screening was performed on FLT3-ITD cell lines only without including a control of a *wild-type* FLT3 cell line, as initially all agents capable of killing AML cells lines were sought independently of whether they were specific to this type of leukaemia or inhibited the growth of all AMLs.

The seeding density in 384-well plates was the first parameter to be optimized for each cell line, considering that compounds would be added the day after seeding and that viability would be evaluated after further 72h. Cells were plated at three different concentrations in white 384-well plates and the CellTiter-Glo (CTG) luminescence assay was used to determine the number of viable cells. We chose the concentration of cells that results in an exponential growth four days after seeding. Based on the result of this experiment, both cell lines were seeded for the screening at 2500 cells/well and incubated at 37°C **(Figure 4.1)**.

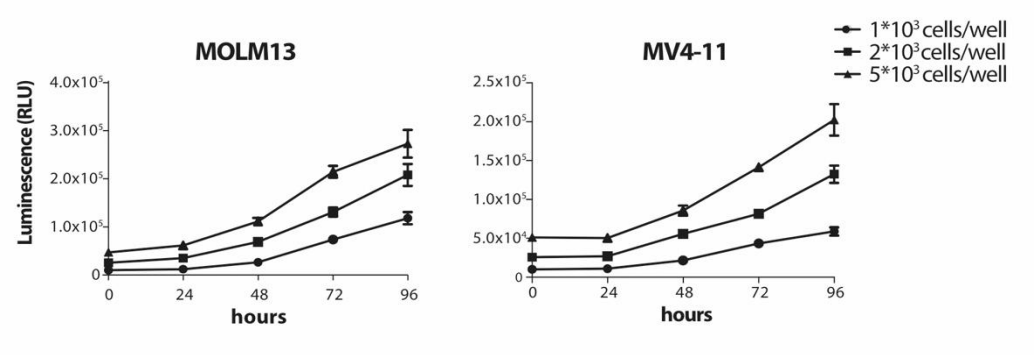


***Figure 4.1: Optimization of seeding density of AML cells for the first HTS***
*Cells were seeded at three different concentrations (1000, 2000 and 5000 cells per well) in a volume of 40µl of appropriate medium in white 384-well plates and incubated at 37°C in the humidified atmosphere containing 5% of $CO_2$. Cell viability was determined by CTG assay. The experiment was repeated twice and data are shown as mean ± SD.*

---

As positive controls for the drug screening we selected cytarabine (Ara-C), an anti-cancer drug used to treat different forms of leukaemia, and quizartinib, a specific FLT3 receptor inhibitor. A dose-response assay for *in vitro* assessment of sensitivity to these positive controls was performed. Both compounds inhibited the growth of MOLM13 and MV4-11 cells in a dose-dependent manner. The half-maximal inhibitory concentrations ($IC_{50}$) for MOLM13 and MV4-11 equalled 1.76 and 0.84 µM for Ara-C treatment, and 1.86 and 0.58 nM for quizartinib treatment, respectively **(Figure 4.2 A and B)**.

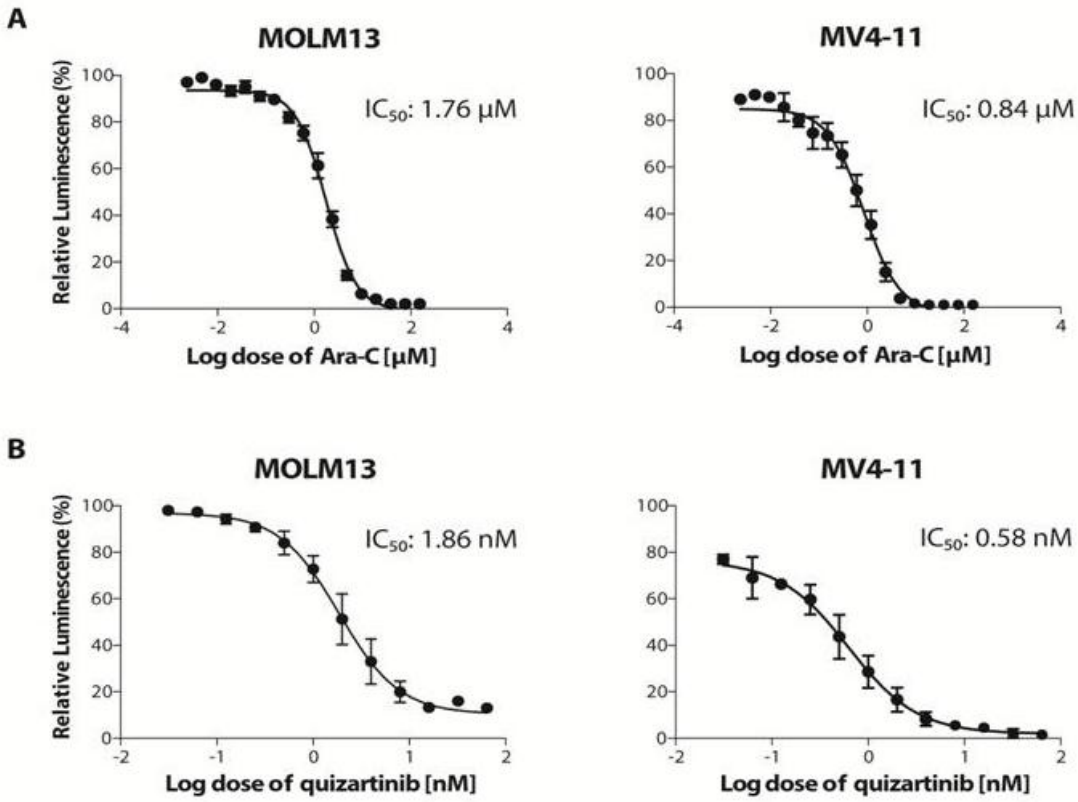


***Figure 4.2: Dose-response curve of MOLM13 and MV4-11 to Ara-C and quizartinib***
*(A) Cells were treated with different concentrations of Ara-C (from 0.002 µM to 153 µM), and (B) quizartinib (from 0.03 nM to 64 nM) for 72h. The viability of cells in all experiments was determined by CTG assay. $IC_{50}$ values are shown for each compound.*
*Experiment was done thrice independently and data are shown as mean ± SEM.*

## 4.2 First high-throughput drug screening to identify compounds that inhibit growth of AML cells expressing FLT3-ITD

A total of 3720 bioactive compounds were tested on MOLM13 and MV4-11 cells in duplicate at three different concentrations (i.e., 0.05 µM, 0.5 µM and 5 µM) for 72h to discover potential novel therapeutic agents against AML cells. Cell viability was evaluated using the CTG luminescence assay. The analysis of results was based on two criteria (Z-score > 5SD or viability < 20%) and led to the identification of 290 hits, namely all of the compounds that were able to inhibit the growth of both cell lines **(Figure 4.3).** Among these, 106 belonged to LOPAC1280 library, 141 to MicroSource Spectrum Collection, and 43 to Selleck Catalogue of New Items.

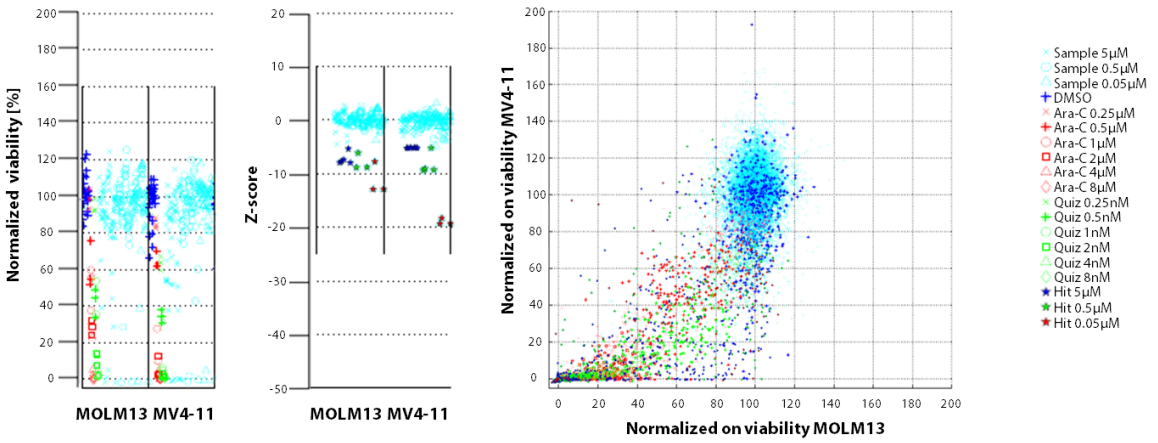


***Figure 4.3: First HTS for the identification of potential novel drugs against AML cells***
*Representative images of screening results showing proliferation-inhibiting compounds (active compounds). The left-hand side panel symbolizes the normalized midpoint value for two plates. MOLM13 and MV4-11 cells were treated with three concentrations of compounds from the LOPAC1280 library (1.280 compounds), MicroSource Spectrum collection (2321 compounds) and Selleck Catalogue of New Items (74 compounds) for 72h; after which, cell viability was assessed by CTG assay. As positive controls, cells were treated with increasing concentration of Ara-C (red symbols) and quizartinib (green symbols), while DMSO treatment (0.2%) represents the negative control (blue symbols). Data were normalized using the NPI method. Light blue symbols indicate tested compounds. Results depicted in the central panel illustrate the calculated Z-score values for all the compounds tested on a plate for both cell lines. The hits were called based on Z-score > 5SD or viability < 20%. Blue, green and red stars indicate compounds active at 5µM, 0.5µM and 0.05µM, respectively. The right-hand side panel points out the percentage of cell viability of MV4-11 plotted against the percentage of cell viability of MOLM13 upon treatment with screened compounds, positive and negative controls.*

Classification of the 290 active compounds identified a wide variety of indications and targets, including anti-infective agents (antibacterial, antibiotics, antifungal, antiprotozoan and antiviral), and compounds regulating cytoskeleton/extracellular matrix, neurotransmission, phosphorylation, apoptosis and DNA/RNA metabolism. Notably, all of the chemotherapeutic drugs currently used for the treatment of AML patients emerged in the screening (amsacrine, cytarabine, daunoribicine, doxorubicin, etoposide, idarubicine, methotrexate, mitoxantrone and topotecan), confirming the reliability of the results.

We decided to disregard all compounds that were active only at the highest concentration (112 drugs) in order to avoid unspecific toxic effects. Moreover, we excluded eight compounds as they were duplicated (present in more than one library) and 13 drugs because they were for topical use (administered externally to body surface). We thus identified 157 bioactive compounds that were re-tested in the secondary screening **(Table 4.1)**.

***Table 4.1 Hits from first HTS***

| Library | Compounds | | | | |
|---|---|---|---|---|---|
| LOPAC 1280 | (R;R)-cis-Diethyl tetrahydro-2;8-chrysenediol | (S)-(+)-Camptothecin | 2;3-Dimethoxy-1;4-naphthoquinone | 5-Bromo-2'-deoxyuridine | 5-Fluorouracil |
| | 7-Cyclopentyl-5-(4-phenoxy) phenyl-7H-pyrrolo [2;3-d]pyrimidin-4-ylamine | A-134974 dihydrochloride hydrate | AC-93253 iodide | Aminopterin | Amsacrine hydrochloride |
| | Auranofin | Bay 11-7082 | Bay 11-7085 | BAY 61-3606 hydrochloride hydrate | Benzamil hydrochloride |
| | BNTX maleate salt hydrate | Brefeldin A from Penicillium brefeldianum | Caffeic acid phenethyl ester | Calcimycin | Calmidazolium chloride |
| | CGP-74514A hydrochloride | Clotrimazole | Cyclosporin A | Dihydrocapsaicin | Dihydroouabain |
| | Diphenyleneiodonium chloride | Ellipticine | Emetine dihydrochloride hydrate | Ganaxolone | IC 261 |
| | Idarubicin | IMS2186 | Indirubin-3'-oxime | L-741;626 | Metrazoline oxalate |
| | JS-K | MRS 2159 | Nocodazole | NSC 95397 | Pentamidine isethionate |
| | Phorbol 12-myristate 13-acetate | R(-)-2;10;11-Trihydroxy-N-propylnoraporphine hydrobromide | Retinoic acid p-hydroxyanilide | Sanguinarine chloride | SKF 96365 |
| | Staurosporine aglycone | SU 4312 | SU 5416 | SU 6656 | Taxol |
| | Tetraethylthiuram disulfide | Thapsigargin | TTNPB | Tyrphostin A9 | Vinblastine sulfate salt |
| MicroSource collection | 10-Hydroxycamptothecin | Alprostadil | Amsacrine | Anthothecol | Antimycin A |
| | Artesunate | Berberine Chloride | Beta-Peltatin | Camptothecin | Clofarabine |
| | Colchicine | Convallatoxin | Cycloheximide | Dactinomycin | Dasatinib |
| | Daunorubicin | Deoxysappanone B 7;3'-Dimethyl Ether Acetate | Deoxysappanone B 7;4'-Dimethyl Ether | Digitoxin | Digoxigenin |
| | Digoxin | Dihydrocelastryl Diacetate | Dihydrorotenone | Disulfiram | Docetaxel |
| | Doxorubicin | Emetine | Epirubicin Hydrochloride | Etoposide | Floxuridine |
| | Fluorouracil | Gentian Violet | Homidium Bromide | Idoxurdine | Irinotecan Hydrochloride |
| | Mercaptopurine | Methotrexate(+/-) | Methylbenzethonium Chloride | Methylene Blue | Mitomycin C |
| | Mitoxantrone Hydrochloride | Mycophenolate Mofetil | Mycophenolic Acid | Ouabain | Paclitaxel |
| | Pararosaniline Pamoate | Paroxetine Hydrochloride | Patulin | Peruvoside | Phenethyl Caffeate (Cape) |
| | Phenylmercuric Acetate | Piplartine | Proscillaridin | Pyrvinium Pamoate | Rotenone |
| | Salinomycin; Sodium | Sanguinarine Sulfate | Sappanone A Dimethyl Ether | Sirolimus | Strophanthidin |
| | Strophanthidinic Acid Lactone Acetate | Tandutinib Teniposide | Thimerosa | Thioguanine | Thioguanosine |
| | Thiotepa | Thiram | Tolonium Chloride | Topotecan Hydrochloride | Valinomycin |
| | Vinblastine Sulfate | Vincristine Sulfate | Vinorelbine | | |
| Selleck Catalogue of New Items | 4SC-202 | Anisomycin | AT13148 | AT7519 HCl | Bardoxolone Methyl |
| | BAY-73-4506 | Belinostat | Cabazitaxel | Cabozantinib malate | Carfilzomib |
| | Cerdulatinib | Combretastatin A4 | Crizotinib | Dasatinib Monohydrate | Defactinib |
| | Dovitinib Lactate | GLPG0634 analogue | Ibrutinib | LDC1267 | Lenvatinib |
| | LY3009120 | MI-773 | Pacritinib | Panobinostat | Picropodophyllin |
| | PND-1186 | Ponatinib | Sunitinib | Trametinib | |

## 4.3 Second screening: setting the experimental condition

We performed a second screening using a larger panel of AML cell lines, with or without FLT3 mutations **(Table 4.2)** to assess FLT3-specificity and to further narrow down the number of hits.

***Table 4.2 Characteristics of patient-derived cell lines***

| Cell line | Gender | Age (years) | Status | Subclass (FAB) | Karyotype | FLT3 status |
|---|---|---|---|---|---|---|
| MOLM13 | M | 20 | Relapse | M5 | Complex including ins(11;9)(q23;p22p23) | FLT3-ITD |
| MV4-11 | M | 10 | De novo | M5 | 48 XY, t(4;11)(q21;q23), +8, +19 | FLT3-ITD |
| PL-21 | M | 24 | De novo | | Complex hyperdiploid | FLT3-ITD |
| MONO-MAC-6 | M | 64 | Relapse | M5 | Complex including t(9;11)(p22;q23) | FLT3-TKD (V592A) |
| THP-1 | M | 1 | De novo | M5 | Near-tetraploid t(9;11)(p22;q23) | FLT3 WT |
| OCI-AML2 | M | 65 | De novo | M4 | Complex hyperdiploid | FLT3 WT |

Prior to carrying out the second screening, we determined the optimal seeding density for each cell line in the 96-well plate format to ensure exponential growth throughout the entire duration of the experiment (96h). Cells were plated at three/four different concentrations in white 96-well plates and cell viability was detected using CTG assay **(Figure 4.4)**. Consequently, MOLM13, MV4-11, MONO-MAC6, THP-1 and OCI-AML2 cells were seeded at $1*10^5$/ml while PL-21 cells were seeded at $2*10^5$/ml for the secondary screening and incubated at 37°C.

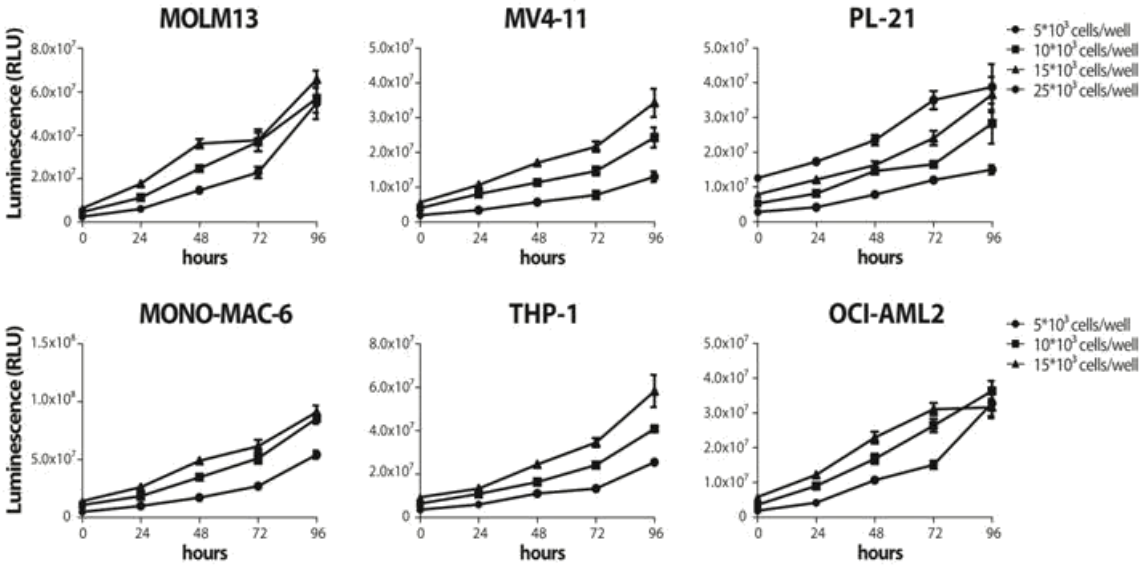


***Figure 4.4: Optimization of seeding density of AML cell lines***
*Cells were seeded at four different concentrations ($5*10^3$, $10*10^3$, $15*10^3$ and $25*10^3$ cells per well) in 100µl of appropriate medium in white 96-well plates and incubated at 37°C in the humidified atmosphere containing 5% of $CO_2$. The viability of cells was determined by using CTG assay. The experiment was repeated twice and data are reported as mean ± SD.*

---

As for the first screening, Ara-C and quizartinib were included as positive controls. We evaluated dose-response to determine the sensitivity of each cell line to these drugs. As expected, all of the AML cell lines responded to Ara-C treatment **(Figure 4.5)**, but only cells bearing FLT3-ITD were responsive to quizartinib treatment. Of note, PL-21 cells did not respond to quizartinib treatment **(Figure 4.6)**; it is possibly due to a mutation in KRAS gene that constitute a potential mechanism of TKI resistance.[188]

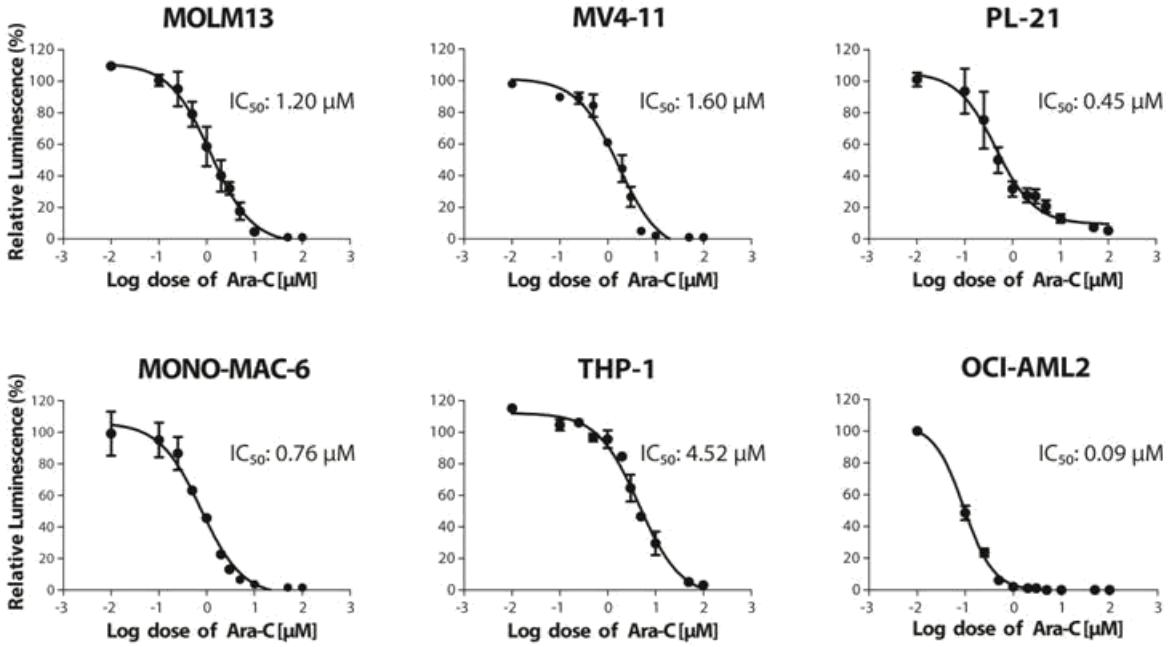


***Figure 4.5: Dose-response curve of the six AML cell lines to Ara-C***
*Cells were treated with growing concentrations of Ara-C (from 0.001 µM to 100 µM) for 72h. The viability of cells was determined by CTG assay. $IC_{50}$ values are shown for each cell line. The results are expressed as percentage luminescence normalized to the luminescence of DMSO treated cells and presented as mean value ± SEM from two independent experiments.*

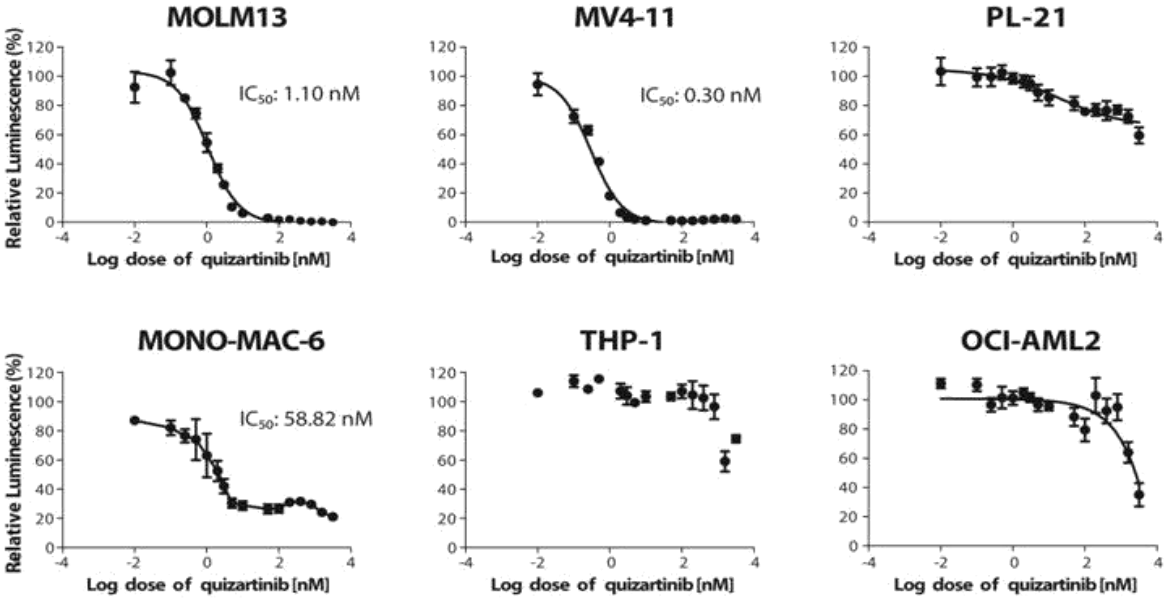


***Figure 4.6: Dose-response curve of the six AML cell lines to quizartinib***
*Cells were treated with increasing concentrations of quizartinib (from 10 pM to 3.2 µM) for 72h. The viability of cells was determined by CTG assay. $IC_{50}$ values are shown for each cell line. The results are expressed as percentage luminescence normalized to the luminescence of DMSO treated cells and presented as mean value ± SEM from three independent experiments.*

## 4.4 Second screening to identify compounds that preferentially inhibit the growth of FLT3 mutated cells

We treated the six AML cell lines in triplicate with compounds identified as hits in the first screening at two different concentrations (0.05 µM and 0.5 µM) at 72 hours. Hits were called based on a robust Z-score > 5SD. Next, we selected those compounds that acted preferentially on FLT3 mutated cell lines based on Z-score value. Thus, we identified 15 compounds: 11 from LOPAC1280 library and four from MicroSource Spectrum collection **(Table 4.3)**.

***Table 4.3 Hits from final screening***

| **Library** | **Compounds** | | |
|---|---|---|---|
| LOPAC 1280 | Auranofin | Bay 11-7085 | BAY 61-3606 Hydrochloride Hydrate |
| | Benzamil Hydrochloride | BNTX Maleate Salt Hydrate | Calmidazolium Chloride |
| | IMS2186 | SKF 96365 | Staurosporine Aglycone |
| | SU 4312 | SU 6656 | |
| MicroSource Spectrum collection | Dasatinib | Deoxysappanone B 7,3'-Dimethyl Ether Acetate | Pyrvinium pamoate |
| | Tandutinib | | |

We discarded dasatinib, as it is already approved for the treatment of CML and is being tested in a number of trials in AML, staurosporine aglycone as it is a precursor of midostaurin, a drug recently approved for the treatment of patients affected by AML bearing FLT3-ITD mutations, and tandutinib because there was an ongoing clinical trial for AML treatment. Moreover, also deoxysappanone b 7,3'-dimethyl ether acetate was rejected as too little information is available on this compound. Five out 11 residual compounds have already been considered as potential anti-cancer drugs as they are tyrosine kinase inhibitors (i.e., Bay 61-3606, SU 4312 and SU 6656) or cell cycle inhibitors (i.e., Bay 11-7085 and IMS2186). Thus, we discarded these compounds as we considered more interesting the repurposing of a non-anticancer drug for the treatment of AML. The

remaining compounds belong to different therapeutic classes: a pain relief drug as auranofin, heart and circulatory drugs (i.e., benzamil hydrochloride, calmidazolium chloride and SKF 96365), opiods such as BNTX maleate salt hydrate and antiinfective agents as pyrvinium pamoate. Then, we looked at the effect of the residual six compounds on cell survival of the six AML cell lines, and decided to select those that reduce the viability by at least 40% in the majority of FLT3-ITD mutated cell lines. Accordingly, auranofin from LOPAC1280 library and pyrvinium pamoate from MicroSourse Spectrum collection were chosen for further studies.

**Name:** auranofin

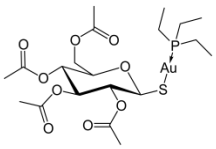

**Alias:** Ridaura

**Primary therapeutic indication:** inflammatory arthritis.

**Side effects:** diarrhea, skin rash, itching, abdominal cramps, nausea, vomiting, and inflammation or sores in the mouth.

**Extremely rare adverse effects:** thrombocytopenia and bone marrow suppression.

**Absorption and excretion:** 85% of the absorbed gold is excreted in the faeces, the remainder in the urine.

**Mechanism of action:** (i) thioredoxin reductase (TrxR) enzyme inhibition inducing mitochondrial oxidative stress and apoptosis (ii) proteasome-associated deubiquitinases (DUBs) inhibition resulting in an accumulation of polyubiquitinated proteins and induction of apoptosis.

**Repurposing attempts:** human ovarian cancer, chronic lymphocytic/myelogenous leukemia, gastrointestinal tumour, non-small cell lung cancer.

**Clinical trials:** 12 clinical trials (clinicaltrial.gov, 2019/08/30). Treatment of different conditions such as HIV, amoebiasis, giardiasis, tuberculosis, pain, rheumatoid arthritis, ovarian and lung cancer, CLL, glioblastoma.

**Name:** pyrvinium pamoate

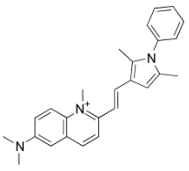

**Alias:** Povan or Vanquin

**Primary therapeutic indication:** pinworms infection.

**Side effects:** skin rash, diarrhea, nausea, vomiting, stomach cramps and increased sensitivity of skin to sunlight.

**Absorption and excretion:** not absorbed from gastrointestinal tract and it is eliminated in faeces.

**Mechanism of action:** (i) inhibition of glucose uptake by pinworms (ii) energy and autophagy reduction (iii) inhibition of Wnt-β-catenin and Akt-related pathways.

**Repurposing attempts:** prostate, lung, breast, colon and blood cancer.

**Clinical trials:** none (clinicaltrial.gov, 2019/08/30).

## 4.5 Auranofin and pyrvinium pamoate cause loss of viability of AML cells

Three arbitrarily-chosen concentrations differing by a factor of 10 were tested in the first screening. They were reduced to the two lowest concentrations in the secondary screening. As these may not, however, be within the therapeutic range for all of compounds, we validated the results for the two chosen drugs by performing a dose-response curve focusing our attention on three representative cell lines: two bearing FLT3-ITD (MV4-11 and MOLM-13) and one with *wild-type* FLT3 (OCI-AML2). Briefly, every cell line was treated with increasing concentrations of each compound at a single time point of 72h and the viability was evaluated through CTG assay. Of these cell lines, MV4-11 cells were the most sensitive to auranofin treatment with an $IC_{50}$ of 0.54 µM followed by MOLM13 and OCI-AML2 with 1.35 µM and 3.93 µM, respectively **(Figure 4.7 A)**. The analysis of pyrvinium pamoate sensitivity showed again that MV4-11 cells were more sensitive than the other two cell lines. The $IC_{50}$ value for MV4-11 cells was 145.6 nM, while it was 218 nM, and 280 nM for OCI-AML2 and MOLM13, respectively **(Figure 4.7 B)**.

These results suggest that both drugs are active in all AML cell lines studied, albeit at different concentrations, and display relatively little selective activity on FLT3-ITD expressing cells, more so in the case of auranofin.

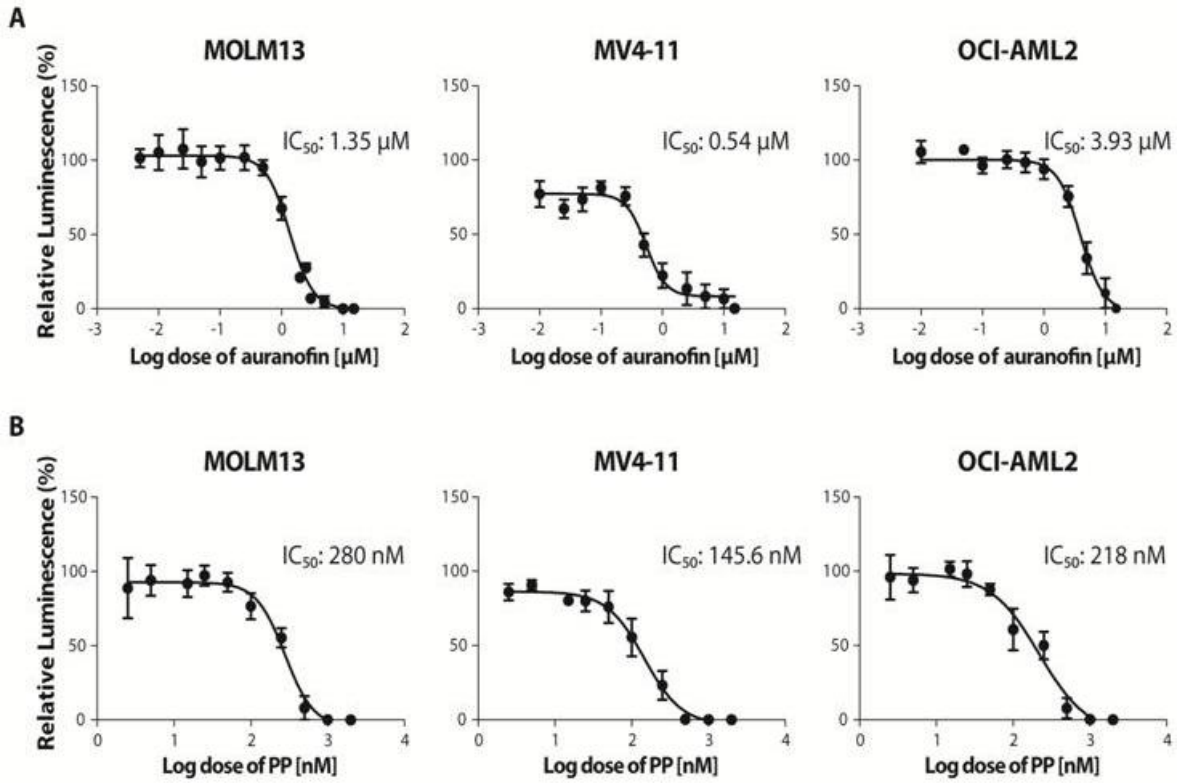


***Figure 4.7: Dose-response curve to auranofin and pyrvinium pamoate of the three indicated AML cell lines***

*Auranofin and pyrvinium pamoate decrease cell proliferation in a dose-dependent manner. (A) Cells were treated with increasing concentration of auranofin (from 0.00025 µM to 15µM) and (B) pyrvinium pamoate (from 0.025 µM to 2 µM). Cell viability was determined 72h after treatment using CTG assay. $IC_{50}$ values are indicated for each cell line. The results are expressed as percentage luminescence normalized to the luminescence of DMSO treated cells and presented as mean value ± SEM from six independent experiments.*

---

For further characterization of drug activity, we next performed the clonogenic colony forming assay on cells pre-treated with the two compounds or with DMSO as a control. Both auranofin and pyrvinium pamoate reduced colony formation capacity for all three cell lines tested **(Figure 4.8)**.

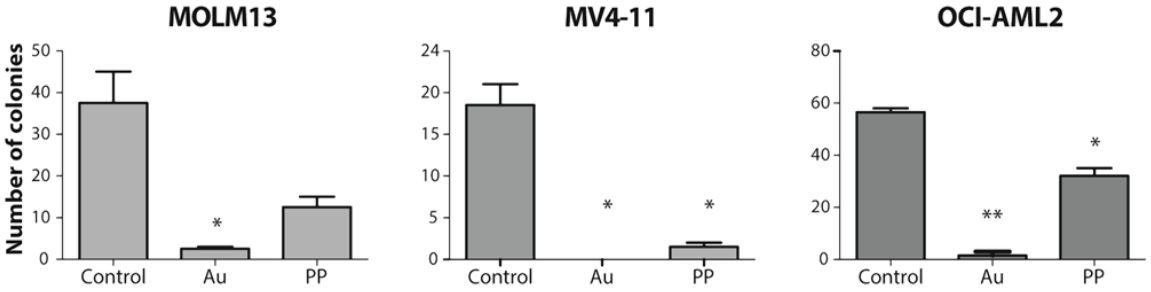


***Figure 4.8: Auranofin and pyrvinium pamoate significantly decrease proliferation of AML cells on methylcellulose***

*Colony formation assay of different AML cell lines in the absence or presence of auranofin and pyrvinium pamoate. The dose of auranofin and pyrvinium pamoate used for MOLM13, MV4-11 and OCI-AML2 corresponded to their $IC_{50}$ values. Data are reported as means ± SD of two independent experiments. *p<0.05, **p<0.01. Au, auranofin; PP, pyrvinium pamoate.*

---

The CTG assay used in the experiments described above is a homogeneous method for estimating the quantity of viable cells based on the measurement of ATP concentration, an indicator of metabolically active cells. The assay cannot be used for determining whether auranofin or pyrvinium pamoate elicit a cytostatic or a cytotoxic effect on treated cell lines. We, therefore, characterized in detail the effects of drug treatment on cell growth. MOLM13, MV4-11 and OCI-AML2 were treated with $IC_{50}$ of auranofin or pyrvinium pamoate for 24h, 48h and 72h or with DMSO as a control. Based on daily counts of live and dead cells, growth curves and bar graphs were plotted, respectively **(Figure 4.9 A and B)**. The results showed that auranofin caused cell death whereas pyrvinium pamoate exerted a cytostatic action.

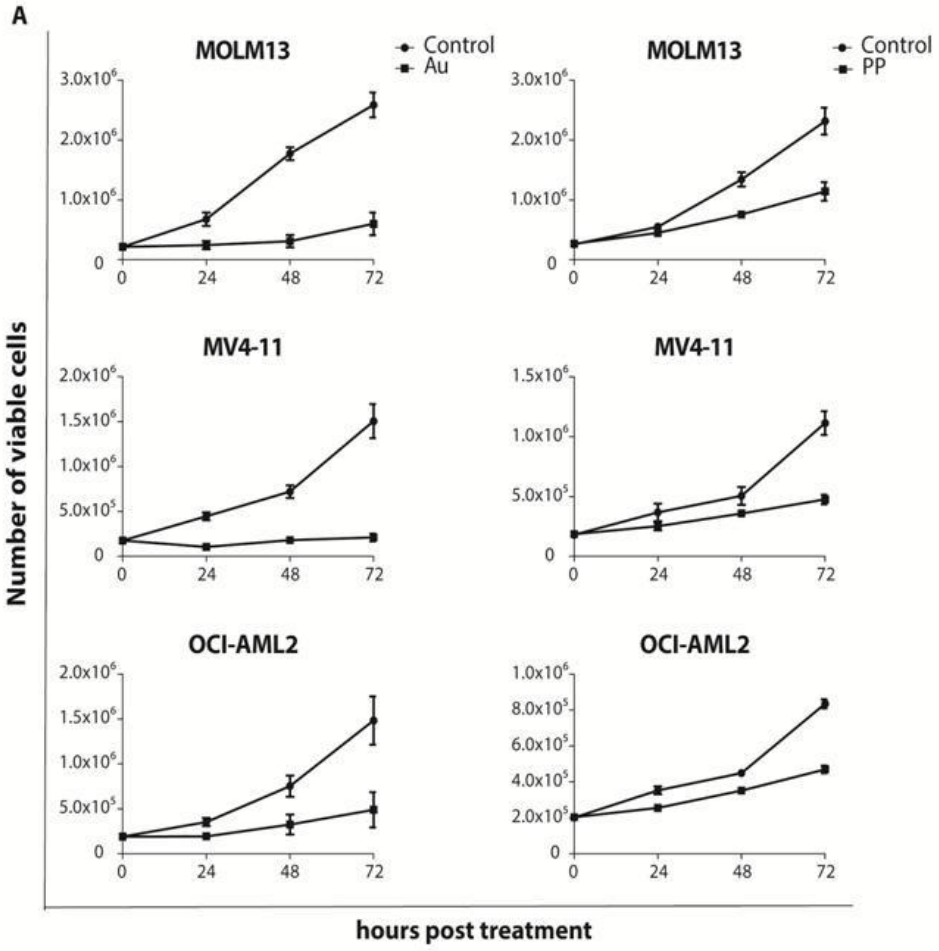
A
MOLM13
Control
Au
MOLM13
Control
PP
MV4-11
MV4-11
OCI-AML2
OCI-AML2
Number of viable cells
hours post treatment

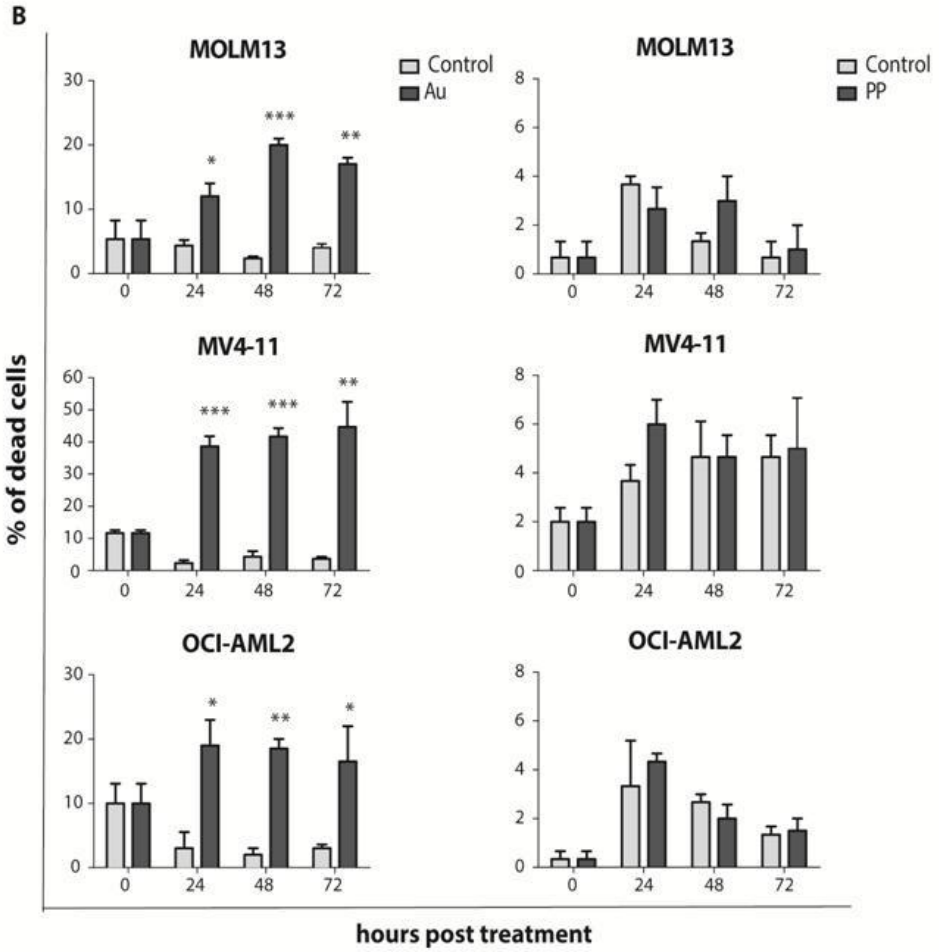
B
MOLM13
Control
Au
MOLM13
Control
PP
MV4-11
MV4-11
OCI-AML2
OCI-AML2
% of dead cells
hours post treatment

***Figure 4.9: Cytotoxic and cytostatic effect of auranofin and pyrvinium pamoate***
*(A) Effect of auranofin and pyrvinium treatment on AML cells growth. Cells were treated with their $IC_{50}$ of auranofin (left-hand side panel) and pyrvinium pamoate (right-hand side panel). Cell viability was determined 24h, 48h and 72h after treatment using trypan blue staining and manual count. The results are presented as mean value ± SEM from two independent experiments. (B) Cell death induction by auranofin and pyrvinium pamoate. Cells were treated with their $IC_{50}$ of auranofin (left-hand side panel) and pyrvinium pamoate (right-hand side panel). Dead cells were detected by trypan blue staining 24h, 48h and 72h after treatment and manual count. The results are presented as mean value ± SEM from two independent experiments. *p<0.05, **p<0.01, ***p< 0.001. Au, auranofin; PP, pyrvinium pamoate*

---

## 4.6 The efficacy of treatment with selected-drugs combined with agents used in standard AML therapy

Combination therapy allows dose reduction thus decreasing the incidence and severity of side effects, and prevents the development of resistance. To assess whether combination therapy would provide a significant advantage over single agents, we treated AML cells with the selected compounds together with different widely used anticancer drugs (i.e., Ara-C, doxorubicin, methotrexate) or with well-known FLT3 inhibitor i.e., quizartinib.

Ara-C is one of the drugs used as the frontline treatment of AML. We investigated whether co-treatment with Ara-C + auranofin or pyrvinium pamoate resulted in synergy, additivity or antagonism. Cells were exposed to auranofin or pyrvinium pamoate and Ara-C at varying stoichiometry. Based on combination index (CI) calculation, a synergistic effect was observed for Ara-C + auranofin in all AML cells (**Figure 4.10 left-hand side panel)**, while only a possible additive effect was uncovered for Ara-C + pyrvinium pamoate in MV4-11 and OCI-AML2 cells (**Figure 4.10 right-hand side panel)**.

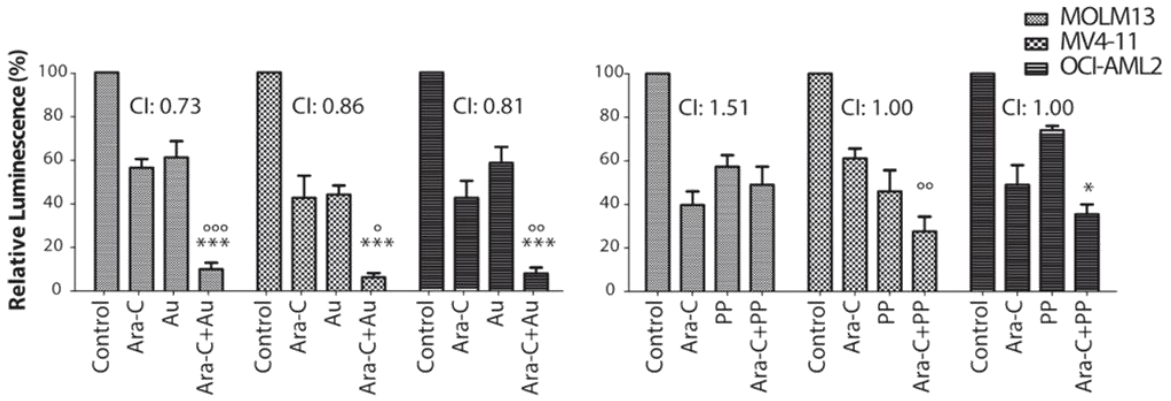


***Figure 4.10: Combination treatment with Ara-C + auranofin or pyrvinium pamoate***
*The indicated cell lines were treated for 72h with single compounds, their combination, or DMSO alone as control. CTG assay was used to assess the effect of each treatment on the cell culture viability. Left-hand side panel, Ara-C/auranofin; right-hand side panel, Ara-C/pyrvinium pamoate combination. The bar graph represents the effect of one of the eight concentrations tested. CI values are shown for each combination. The results are presented as mean value ± SEM from three independent experiments. In all panels, symbols (°) indicate significance versus Ara-C; asterisks (*) indicate significance versus auranofin or pyrvinium pamoate; one symbol, p<0.05; two symbols, p<0.01, three symbols, p<0.001, four symbols, p<0.0001. Au, auranofin; PP, pyrvinium pamoate, CI, combination index.*

---

Recently, midostaurin, a non-specific tyrosine kinase inhibitor, received FDA approval for the treatment of AML with FLT3-ITD mutations. Indeed, midostaurin significantly prolongs survival of FLT3-mutated AML patients when combined with conventional induction and consolidation therapies.[65] We confirmed the cytotoxic effect of midostaurin on AML cell lines. Briefly, the cells were treated with increasing concentrations of midostaurin at a single time point of 72h and the viability was evaluated through CTG assay (**Figure 4.11)**. We established that midostaurin suppresses AML cell growth in a dose-dependent manner. Next, we studied the effect of combining midostaurin and auranofin or pyrvinium pamoate. We treated cells, as described above for Ara-C, with midostaurin and auranofin **(Figure 4.12 left-hand side panel)** or pyrvinium pamoate **(Figure 4.12 right-hand side panel)** at varying stoichiometry but failed to detect any synergistic effect on AML cell lines. A nearly additive effect was observed in MOLM13 cells upon combination of auranofin or pyrvinium pamoate with midostaurin.

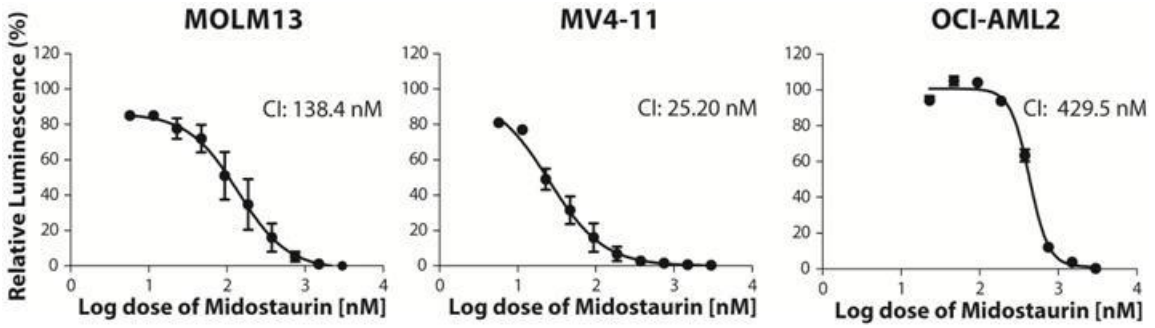


***Figure 4.11: Midostaurin suppresses the growth of AML cells***
*Dose-response curve. Cells were treated with different concentrations of midostaurin (from 3 µM to 5 nM) for 72h. The viability of cells was determined by CTG assay. Results are expressed as percentage of luminescence normalized to the luminescence of DMSO treated cells and presented as mean value ± SEM. from four independent experiments. $IC_{50}$ values are shown for each cell line.*

---

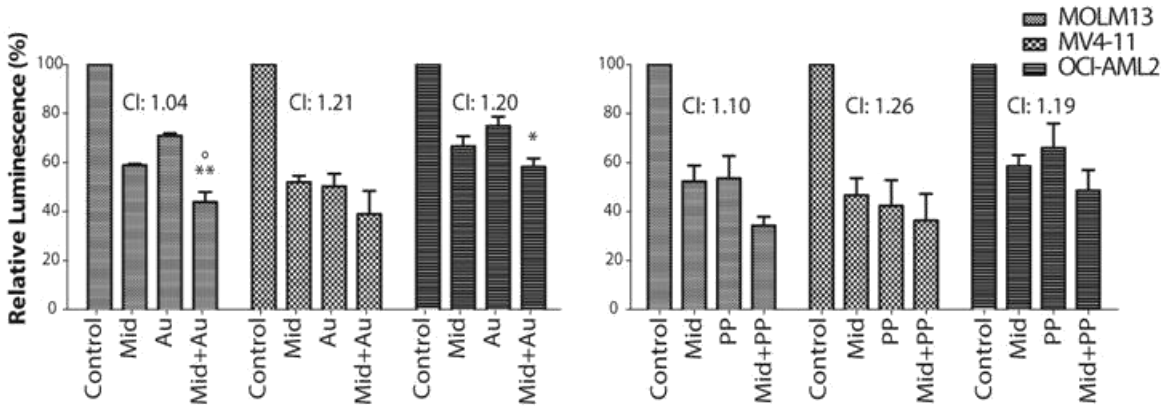


***Figure 4.12: Combination treatment with midostaurin and auranofin or pyrvinium pamoate***
*The indicated cell lines were treated for 72h with single compounds, their combination, or DMSO alone as control. CTG assay was used to assess the effect of each treatment on the cell viability. Left-hand side panel, midostaurin/auranofin; right-hand side panel, midostaurin/pyrvinium pamoate combination. The bar graph represents the effect of one of the eight concentrations tested. CI values are shown for each combination. The results are presented as mean value ± SEM from three independent experiments. In all panels, symbols (°) indicate significance versus midostaurin; asterisks (*) indicate significance versus auranofin or pyrvinium pamoate; one symbol, $p<0.05$; two symbols, $p<0.01$. Au, auranofin; Mid, midostaurin; PP, pyrvinium pamoate, CI, combination index.*

---

Quizartinib is a potent FLT3 inhibitor currently under investigation in childhood AML and other myeloid malignancies. It has a favourable bioavailability and pharmacokinetics. We detected a nearly additive effect in MOLM13 and MV4-11 upon combination of quizartinib with auranofin **(Figure 4.13 left-hand side panel)** whereas a moderate

synergism and a nearly additive effect were observed upon combination of quizartinib with pyrvinium pamoate in MOLM13 and MV4-11 cells, respectively. **(Figure 4.13 right-hand side panel)**.

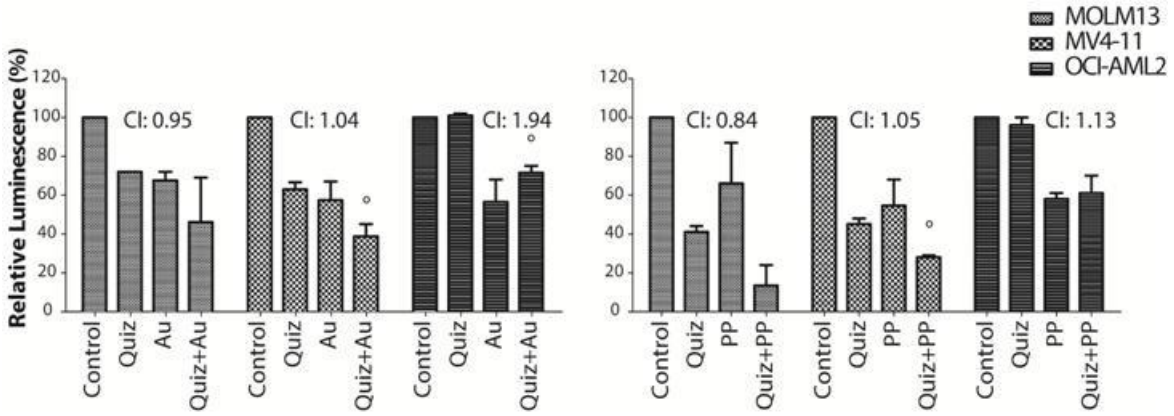


***Figure 4.13: Combination treatment with quizartinib and auranofin or pyrvinium pamoate***
*The indicated cell lines were treated for 72h in the presence of compounds as single agents or in combination, or DMSO alone as control. CTG assay was used to assess the effect of each treatment on the cell culture viability. Left-hand side panel, quizartinib/auranofin; right-hand side panel quizartinib/pyrvinium pamoate combination. The bar graph represents the effect of one of the eight concentrations tested. CI values are shown for each combination. The results are presented as mean value ± SEM from two independent experiments. Symbols (°) indicate significance versus quizartinib; p<0.05. Au, auranofin; PP, pyrvinium pamoate; Quiz, quizartinib; CI, combination index.*

---

Given that pyrvinium pamoate did not synergise with any of the agents tested so-far, we considered combining it with other anti-cancer drugs, i.e.,doxorubicin and methotrexate. Doxorubicin is an anthracycline antibiotic adopted against disseminated neoplastic conditions including ALL, AML, malignant lymphoma, breast, ovarian, thyroid, bladder and stomach cancers. Methotrexate, instead, is an antimetabolite widely used for the treatment of various types of cancers as well as leukaemia, lymphoma, osteosarcoma, breast and lung cancers. CTG assay to determine sensitivity and dose-response profile of the studied cell lines to these known anti-cancer drugs was performed. Both compounds decreased cell viability in a dose-dependent manner (**Figure 4.14 A and B)**. Subsequently, we treated cells with increasing concentrations of doxorubicin or methotrexate and pyrvinium pamoate for 72h. A nearly additive effect was established in all AML cells upon combination of doxorubicin with pyrvinium pamoate (**Figure 4.15 left-hand side panel)**. No synergy or additivity was observed for methotrexate + pyrvinium pamoate combination

(**Figure 4.15 right-hand side panel)**.

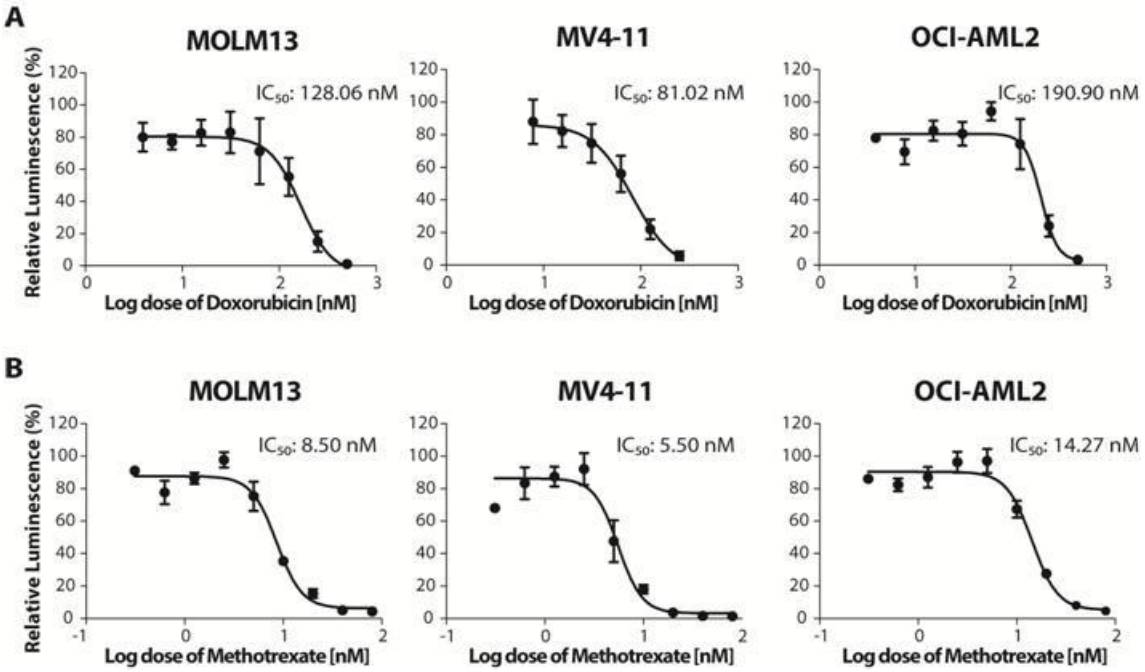


***Figure 4.14: Dose-response curve of the indicated AML cell lines to doxorubicin and methotrexate***
*(A) Cells were treated with different concentrations of doxorubicin (from 0.004 µM to 1µM) and (B) methotrexate (from 0.30 nM to 80 nM) for 72h. The viability of cells was determined by CTG assay. $IC_{50}$ values are shown for each cell line. Results are expressed as percentage luminescence normalized to the luminescence of DMSO treated cells and presented as mean value ± SEM from three independent experiments.*

---

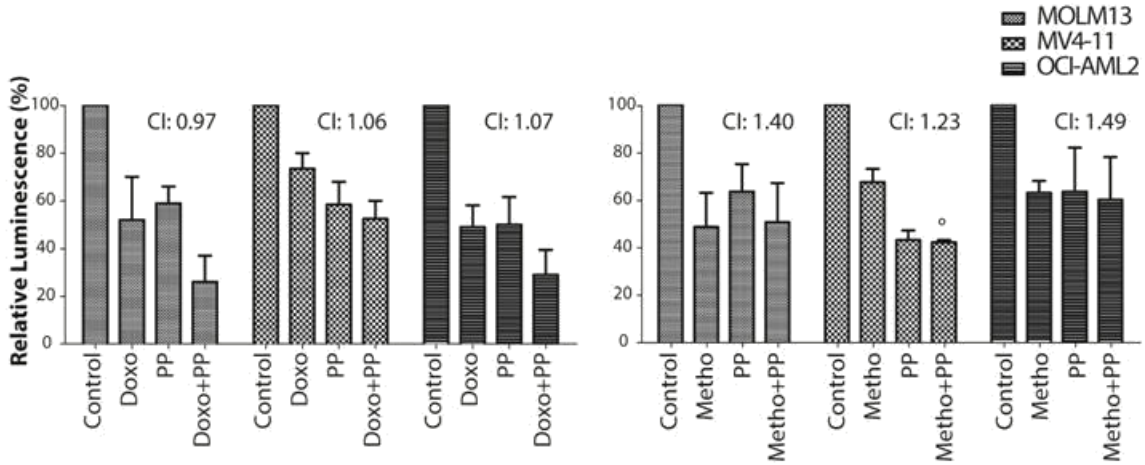


***Figure 4.15: Combination treatment of doxorubicin or methotrexate with pyrvinium pamoate***
*The indicated cell lines were treated for 72h with a single compound, their combination, or DMSO alone as control. CTG assay was used to assess the effect of each treatment on the cell viability. Left-hand side panel doxorubicin/pyrvinium pamoate; right-hand side panel, methotrexate/pyrvinium pamoate combination. The bar graph represents the effect of one of the eight concentrations tested. CI values are shown for each combination. The results are presented as mean value ± SEM from three independent experiments. Symbols (°) indicate significance versus*

*methotrexate; Au, auranofin; Doxo, doxorubicin; Metho, methotrexate; PP, pyrvinium pamoate, CI, combination index.*

## 4.7 The effect of auranofin and pyrvinium pamoate in *xenograft* mouse model

Given that the *in vitro* experiments have shown promising anti-cancer activity of both auranofin and pyrvinium pamoate, we next investigated the *in vivo* effect of the selected-compounds using NOD-scid IL2rg$^{null}$ (NSG) *xenograft* mouse model. We injected $10^6$ of primary human AML cells with *wild-type* NPM and FLT3-ITD mutation in the caudal vein of 20 NSG mice by intravenous injection. The engraftment was assessed in the peripheral blood (PB) by measuring the percentages of the human CD45 (hCD45) positive cells by FACS. Once the hCD45 positive cells reached maximum 1% in the PB, approximately one month post-transplant, mice were randomized into six groups and treated with solvent (22% of DMSO in PBS), auranofin at three different concentrations (10 mg/Kg, 5 mg/Kg, 2.5 mg/Kg), or pyrvinium pamoate 0.5 mg/Kg or Ara-C 60 mg/Kg. All compounds, with the exception of Ara-C, were given daily by i.p. injection five times a week for three weeks. Ara-C was given intraperitoneally for five consecutive days starting on the same day as the other groups. The concentration of all agents was established based on the data reported in the literature.[189–193] Results showed that the concentration of pyrvinium pamoate may be toxic as all of the mice in the PP group died two or three days after the treatment commencement. Surprisingly, the week after the end of the treatment mice of both control and 5 mg/Kg auranofin group died **(Figure 4.16)**. After three weeks of treatment the level of hCD45 in the PB was measured and ascertained to be low (maximum 1.6%) by FACS **(Figure 4.17)**. Thus, we assumed that the death was not attributable to the

development of leukaemia.

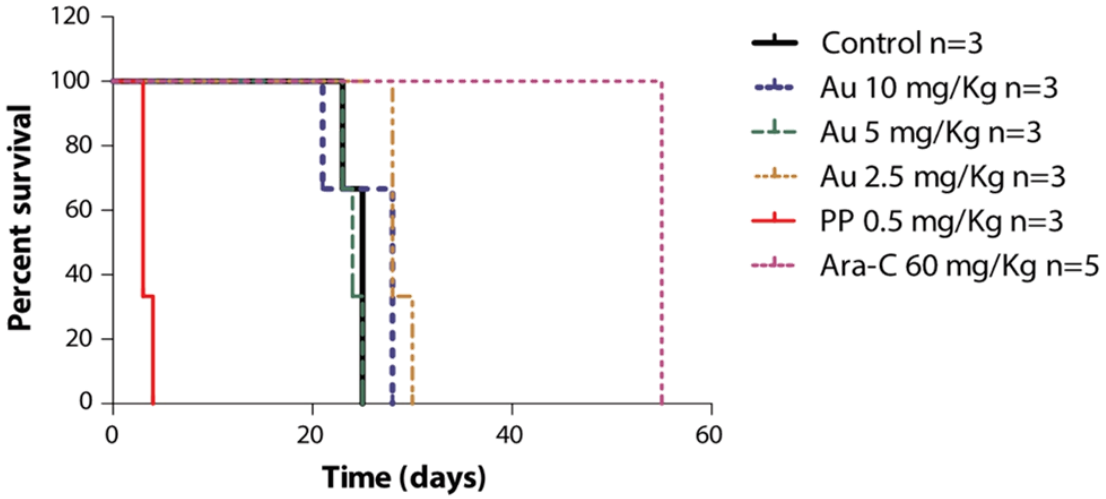


***Figure 4.16: Impact of auranofin and pyrvinium pamoate treatment on mice survival***
*Kaplan-Meier survival plot of xenograft NSG mice treated with auranofin, pyrvinium pamoate or Ara-C compared to the untreated mice (control). Au, auranofin; PP, pyrvinium pamoate.*

---

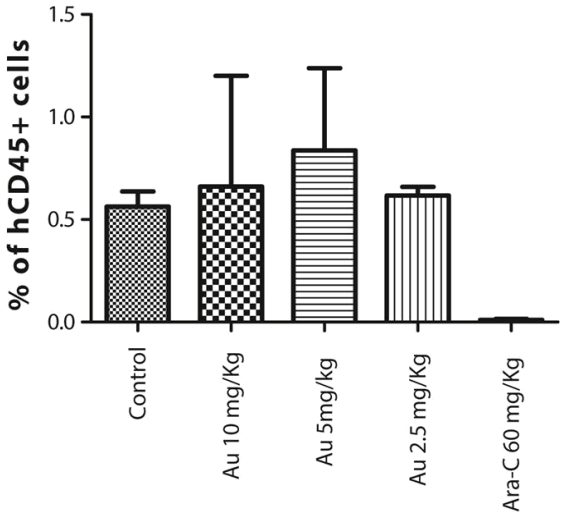


***Figure 4.17: Leukaemia cell burden evaluation upon compounds treatment***
*Xenograft NSG mice were treated with auranofin, Ara-C or DMSO as control. The percentage of hCD45 positive cells in the PB was evaluated by flow cytometry. Mean ± SEM are reported. Au, auranofin.*

---

Mice treated with Ara-C survived for five weeks following treatment and were sacrificed when the level of hCD45 in the PB was 70%.

To assess the possible toxicity of pyrvinium pamoate, male NSG mice were treated by i.p. injection with four different concentrations of pyrvinium pamoate: 0.5mg/Kg. 0.25 mg/Kg, 0.125 mg/Kg and 0.06 mg/Kg following the experimental design described above. We proved that the highest concentration was toxic as all mice treated with 0.5 mg/Kg of PP died within the second week of treatment. However, the other concentrations seemed to be well tolerated as no mice died during the three weeks of treatment and up to three weeks post-treatment **(Figure 4.18)**. Moreover, the body weight remained relatively stable during and after the treatment and no signs of pain/distress were noticed **(Figure 4.19)**.

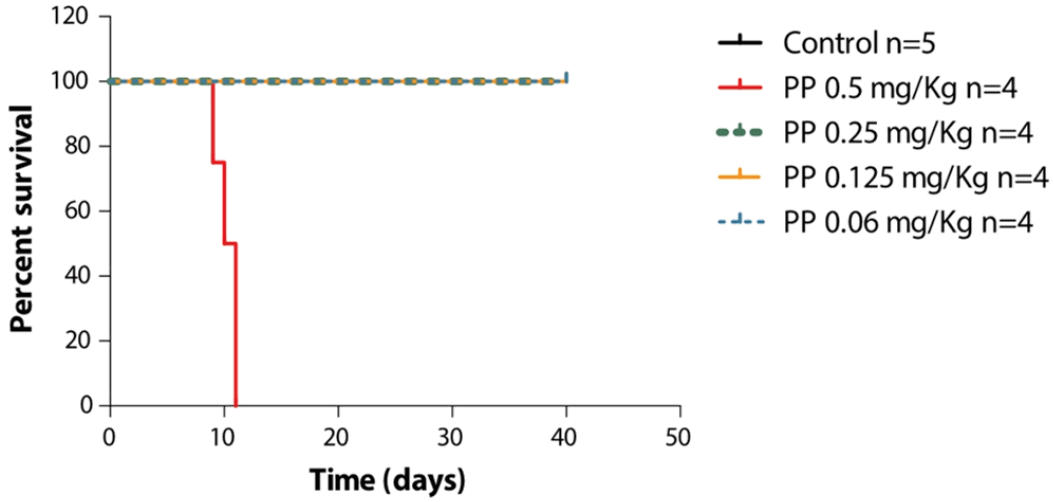


***Figure 4.18: Impact of pyrvinium pamoate treatment on mice survival***
*Kaplan-Meier survival plot of NSG mice treated with indicated concentration of pyrvinium pamoate (five times a week for three weeks) compared to the untreated mice (control). PP, pyrvinium pamoate.*

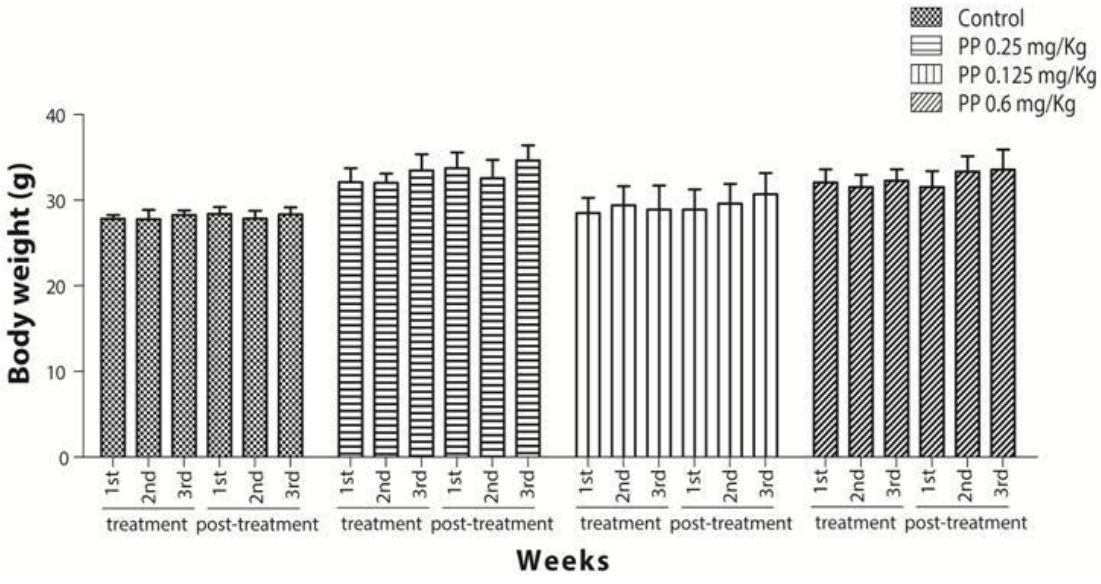

***Figure 4.19: Effect of pyrvinium pamoate treatment on mice body weight***
*Body weight was recorded every week. Mean ± SD are reported. PP, pyrvinium pamoate.*

Thus, we chose 0.25 mg/Kg as the concentration of PP to be used in further investigations. Next, to determine if gender-related toxicity of the compounds at the chosen concentrations i.e., 10 mg/Kg for auranofin and 0.25 mg/Kg for PP exists, we treated both female and male NSG mice with the experimental procedure explain above. No mice died during the treatment and up to three weeks post-treatment. Furthermore, no variation in body weight was observed either in female or male mice **(Figure 4.20A and B)**. We concluded that both drugs are well tolerated regardless mouse's sex.

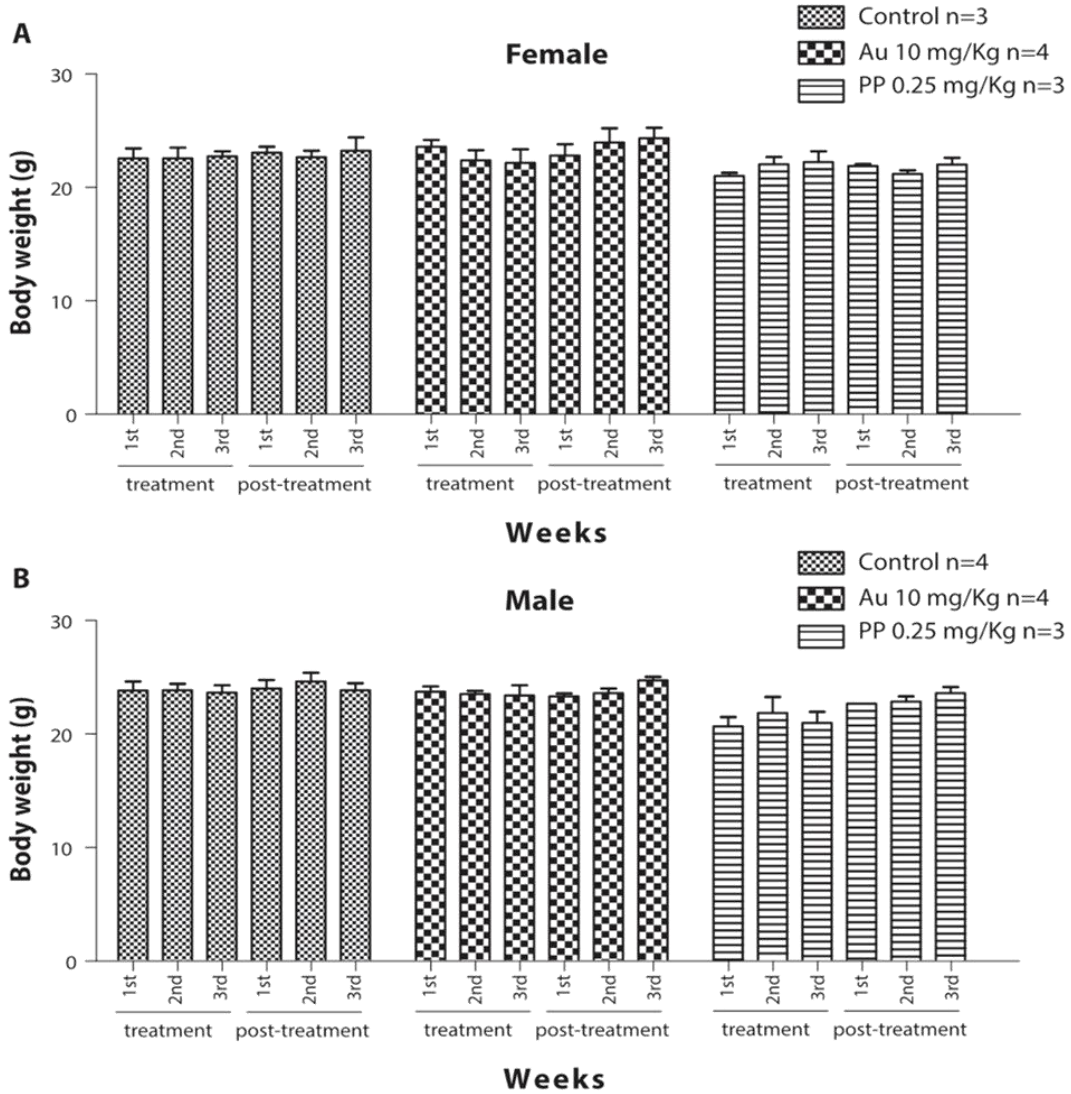


***Figure 4.20: Effect of auranofin and pyrvinium pamoate treatment on mice body weight***
*Body weight was recorded every week both for (A) female and (B) male mice. Mean ± SD are reported. Au, auranofin; PP, pyrvinium pamoate.*

Upon the completion of the toxicity tests, we inoculated $10^6$ of primary human AML cells (NPM *wild-type* and FLT3-ITD) by i.v. injection into 24 female NSG mice. The engraftment was assessed in the PB by measuring the percentages of hCD45 positive cells by FACS. As in the first experiment, once the hCD45 reached maximum 1% in the PB, mice were randomized into four groups and treated with solvent (22% of DMSO in PBS), 10 mg/Kg of auranofin, 0.25 mg/Kg of pyrvinium pamoate or 60 mg/Kg of Ara-C. Unexpectedly, all mice in the control, auranofin and pyrvinium pamoate groups died or were sacrificed due to apparent suffering within the second week of treatment **(Figure 4.21)**. Of note, mice from Ara-C group were sacrificed when all mice belonging to the control, auranofin or pyrvinium pamoate cohort died or were sacrificed to compare the level of hCD45 cells among the groups. We discovered an incongruence between the percentage of hCD45 positive cells in the PB and in the hemopoietic organs such as spleen and bone marrow (BM) **(Figure 4.22)**. In fact, although the percentage of hCD45 in the PB remained very low, an infiltration level of 70% was detected by FACS in the BM. Thus, one possible explanation of the failure of both experiments aiming at assessing the efficacy of the compounds is that mice were already compromised prior to the beginning of the treatment due to the development of the leukaemia. Ara-C treatment reduced the burden of leukaemia compared to the other compounds **(Figure 4.22)**, confirming its efficacy in the treatment of AML.

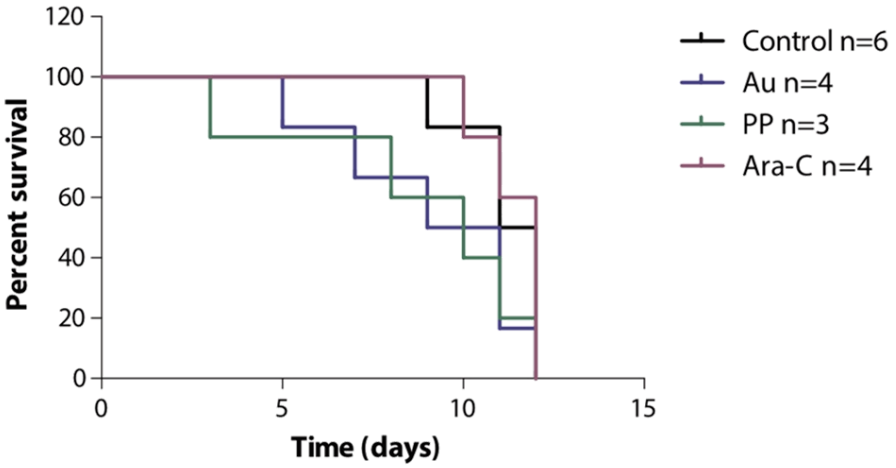


***Figure 4.21: Impact of auranofin and pyrvinium pamoate on xenograft mice survival***
*Kaplan-Meier survival plot of xenograft NSG mice treated with indicated concentration of pyrvinium pamoate and auranofin (five times a week for three weeks) compared to the untreated mice (control). Ara-C treated group was used as positive control. Au, auranofin; PP, pyrvinium pamoate.*

---

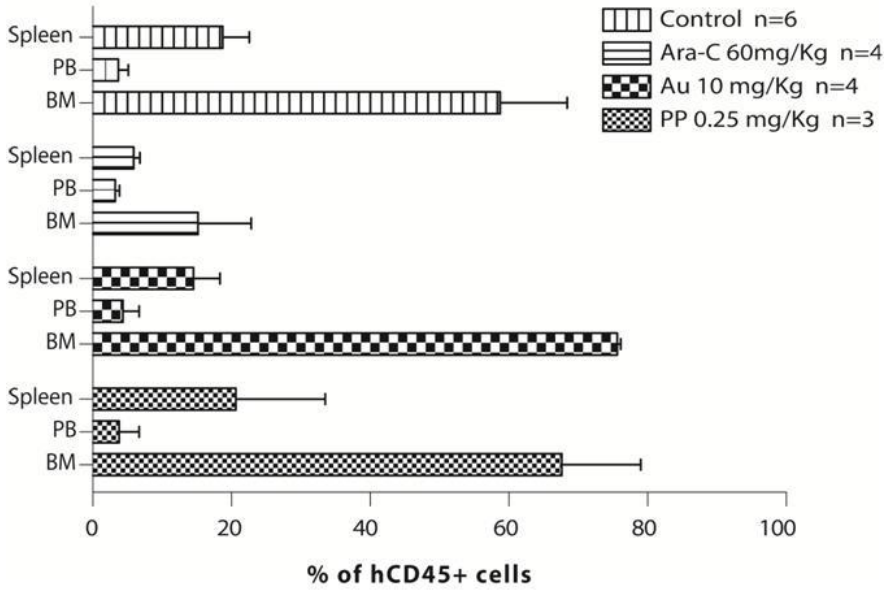


***Figure 4.22: Leukaemia cell burden evaluation upon compounds treatment***
*Xenograft NSG mice were treated with auranofin, pyrvinium pamoate or Ara-C and compared to the untreated mice (control). The percentage of hCD45 positive cells in the BM, spleen and PB was evaluated by flow cytometry. Mean ± SEM are reported. Au, auranofin; BM, bone marrow; PB, peripheral blood; PP, pyrvinium pamoate.*

---

## 4.8 Auranofin and pyrvinium pamoate induce a delay in cell cycle progression

Patient-derived cell lines are inappropriate to study the molecular mechanism of action of therapeutic agents since they contain numerous additional mutations and corresponding normal control cells lack. We therefore used the Ba/F3 cell line, a murine interleukin-3 (IL-3) dependent pro-B cell line, frequently adopted for drug screenings and for assessing both the potency and downstream signalling of oncogenes kinases.[194] An *in vitro* dose-response assay to determine their sensitivity to the selected-compounds was performed. Briefly, Ba/F3 cells transduced with FLT3-WT or FLT3-ITD (from here on referred to as Ba/F3-WT and Ba/F3-ITD) were treated with three different concentrations of auranofin and pyrvinium pamoate for 72h. The number of viable cells was determined by trypan blue staining and the concentration for 50% of maximal inhibition of cell proliferation (growth inhibition 50, $GI_{50}$) was established **(Figure 4.23 A and B)**. The auranofin concentration resulting in $GI_{50}$ for both Ba/F3 WT and ITD cells was 1.5 µM, while it was 30 nM and 15 nM for pyrvinium pamoate in Ba/F3-WT and -ITD, respectively. We did not observe cell death after by trypan blue staining, thus we assumed that the treatment of cells with both compounds had a cytostatic effect.

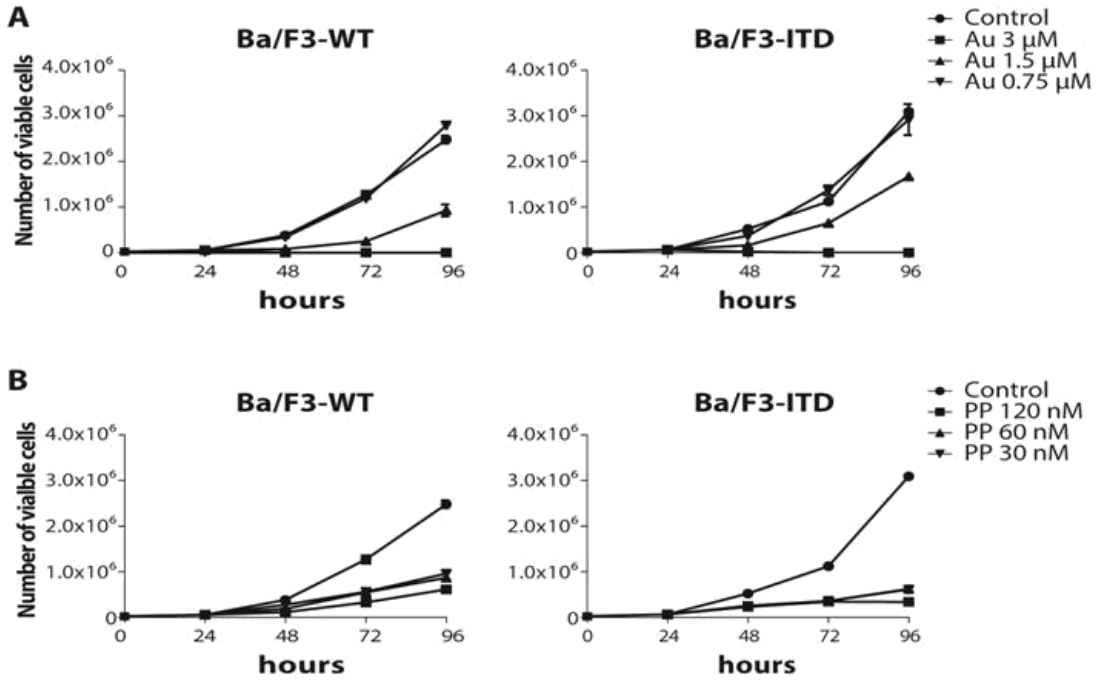


***Figure 4.23: Auranofin and pyrvinium pamoate suppress the growth of Ba/F3 cells***
*Growth curve. Cells were treated with three different concentrations of (A) auranofin and (B) pyrvinium pamoate for 72h. The viability of cells in all experiments was determined by trypan blue staining. Experiment was done twice independently and data are shown as mean ± SD*

---

Next, we investigated how auranofin and pyrvinium pamoate treatment impacted cell cycle. A BrdU pulse-chase time course and subsequently a flow-cytometric DNA content analysis were performed. Briefly, Ba/F3-WT and Ba/F3-ITD cells were pulsed with 10 µM BrdU for 30 minutes, washed with PBS and then treated with $GI_{50}$ auranofin in BrdU free-medium. The BrdU-labeled population changes were characterized over time as the distribution transitions through the phases of the cell cycle by BD FACSCelesta system. Initially, we analysed cell cycle progression of the untreated Ba/F3-WT cells. As shown in **Figure 4.24 A**, one hour after the BrdU pulse, 65% of untreated Ba/F3-WT cells were in S phase. Analysing the labelled cell cohorts over time, we observed the emergence of the first-generation progeny (G1*), which was initially in S phase as well as a transition to late S and G2 phases at four hours (S/G2*). These results indicate that S phase BrdU positive cells transitioned to G2 phase (S/G2*) and after undergoing mitosis (G2/M*), entered the G1* phase. Interestingly, upon auranofin treatment Ba/F3-WT cells transitioned to late S

and G2 phases four hours later than the untreated cells. The results suggested that auranofin-treated cells in early S phase at the onset cycled more slowly as compared to the untreated cells and almost all BrdU labelled cells were still in S phase after four hours from the treatment beginning **(Figure 4.24 B)**. Similar effect was obtained for Ba/F3-ITD cells **(Figure 4.25 A and B)** confirming that auranofin impaired cell cycle progression.

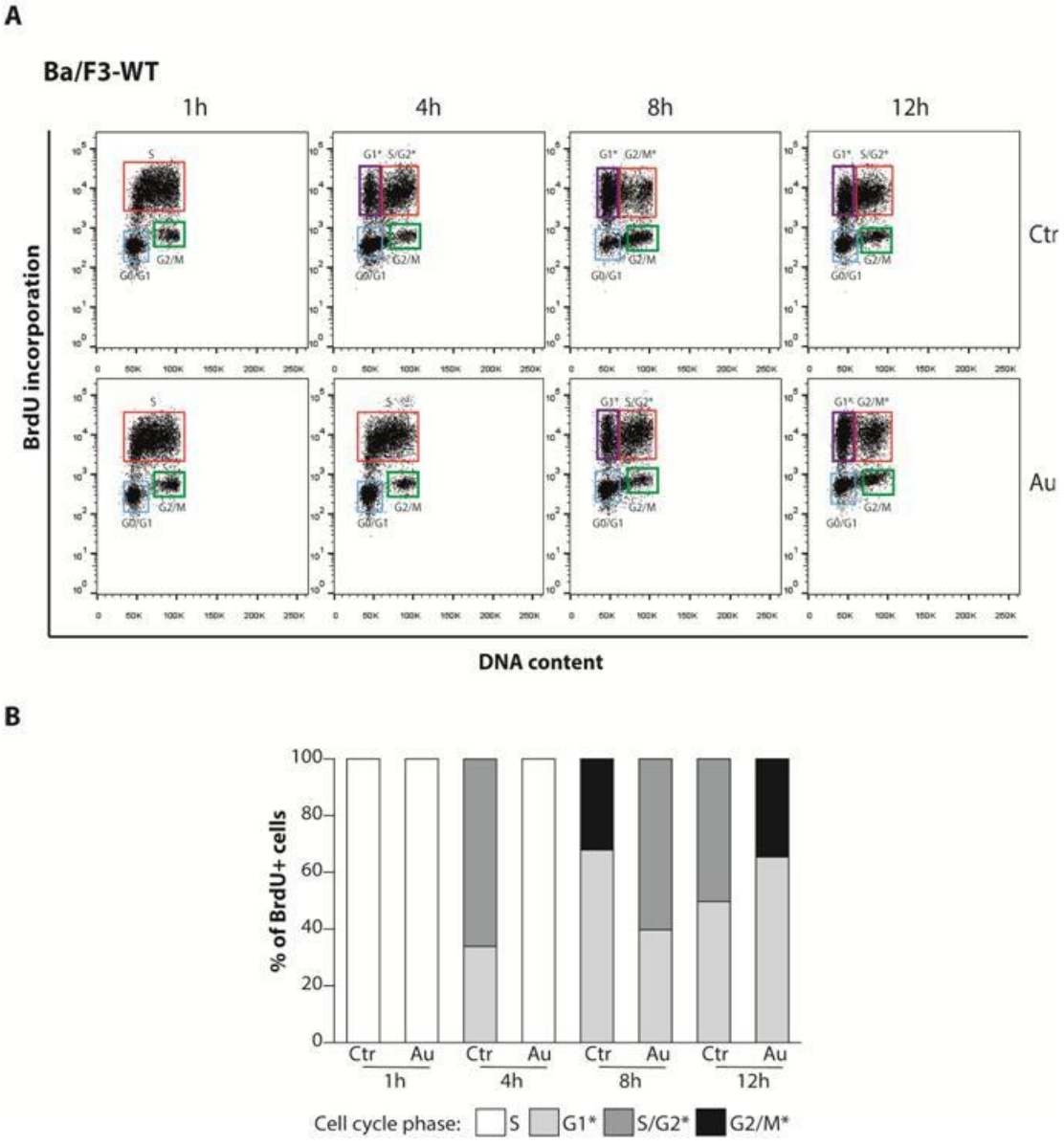


***Figure 4.24: Progression of actively dividing BrdU-pulsed Ba/F3-WT cells over 12 hour-time course of auranofin treatment***

*BrdU pulse-chase time course. (A) Representative dot plot of Ba/F3-WT BrdU-labelled cells stained for DNA-content (X-axis) and BrdU (Y-axis). Cells were pulsed with BrdU for 30 minutes. The indicated times are the hours after BrdU pulse. For all time points, unique gates displaying the following population were drawn: G0/G1, S and G2/M. For 4, 8, and 12h BrdU labelled G1*, S/G2* and G2/M population are show. (B) Representative histogram graph showing BrdU+ cells distribution in four different cell cycle phases indicated as diverse shades of grey. Au, auranofin; Ctr, control.*

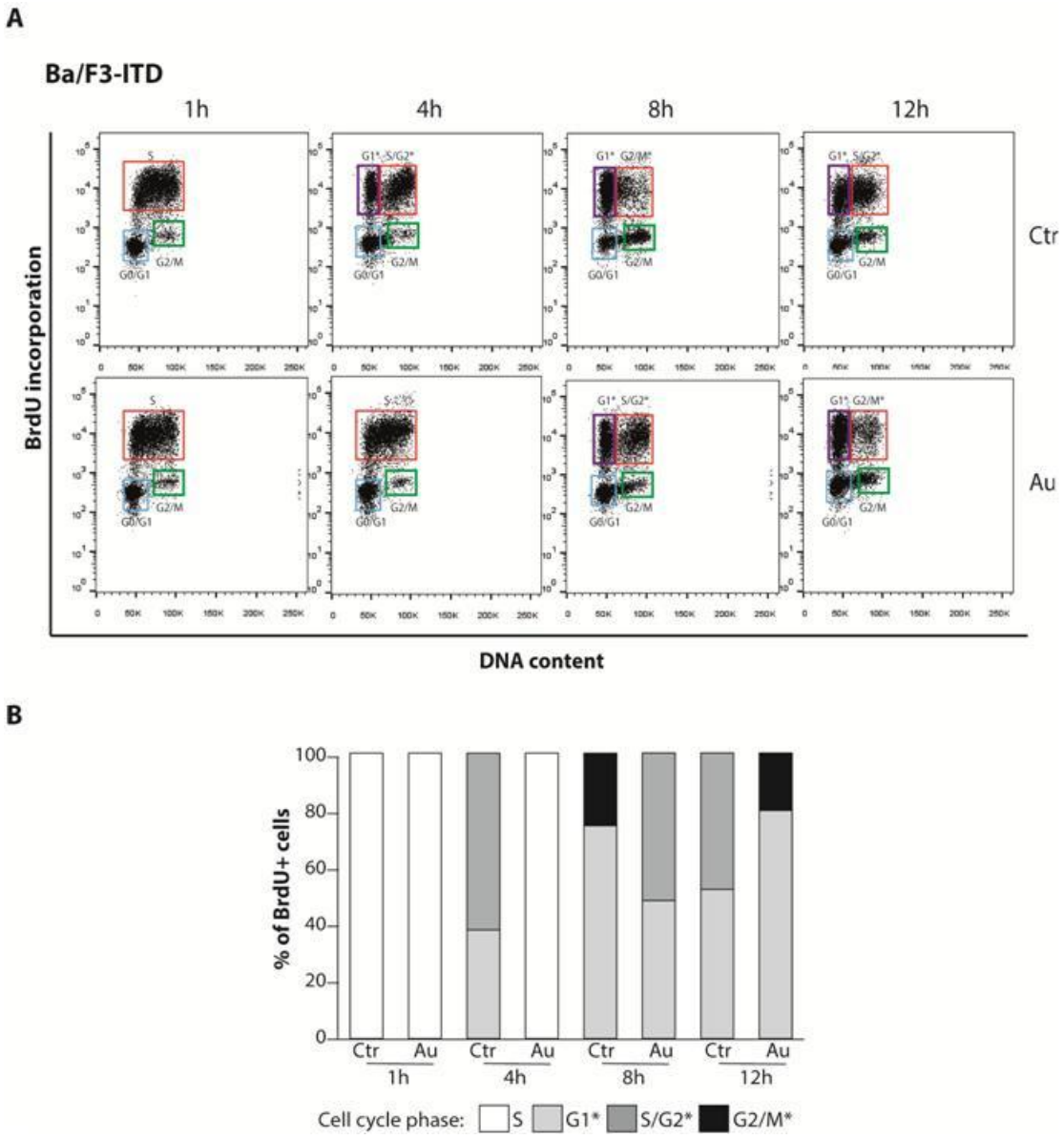


***Figure 4.25: Progression of actively dividing BrdU-pulsed Ba/F3-ITD cells over 12 hour-time course of auranofin treatment***

*BrdU pulse-chase time course. (A) Representative dot plot of Ba/F3-ITD BrdU-labelled cells stained for DNA-content (X-axis) and BrdU (Y-axis). Cells were pulsed with BrdU for 30 minutes. The indicated times are the hours after BrdU pulse. For all time points, unique gates displaying the following population were drawn: G0/G1, S and G2/M. For 4, 8, and 12h BrdU labelled G1*, S/G2* and G2/M population are show. (B) A representative histogram graph showing BrdU+ cells distribution in four different cell cycle phases indicated as diverse shades of grey. Au, auranofin; Ctr, control.*

---

Next, we repeated the same experiment for both Ba/F3-WT and -ITD cells upon pyrvinium pamoate treatment. We noticed a slight cell cycle delay following PP treatment. Indeed, after four and eight hours, the percentage of cells belonging to the first-generation progeny

was higher in the control group compared to the treated group, suggesting that the untreated cells proliferate faster than PP-treated cells **(Figure 4.26)**.

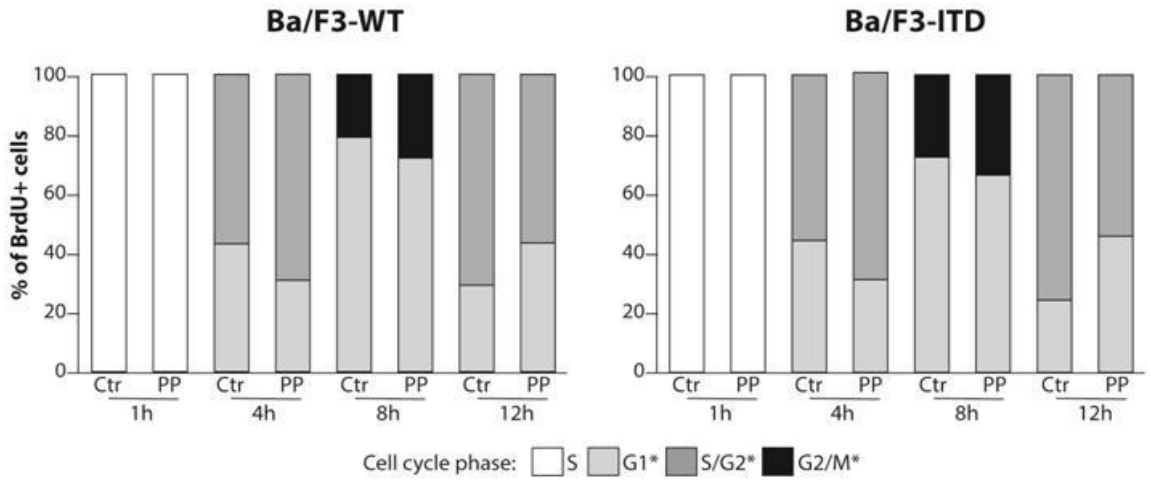


***Figure 4.26: Progression of actively dividing BrdU-pulsed Ba/F3 cells over 12 hour-time course of pyrvinium pamoate treatment***
*Representative histogram graphs showing BrdU+ cells distribution in four different cell cycle phases indicated as diverse shades of grey. Cells were pulsed with BrdU for 30 minutes. The indicated times are the hours after BrdU pulse. Ctr, control; PP, pyrvinium pamoate*

---

## 4.9 Auranofin and pyrvinium pamoate: confirming known mechanism of action

We next investigated the reported mechanism(s) of action of the selected compounds. The most common mechanism by which auranofin acts is the inhibition of the TrxR. TrxR is a ubiquitous enzyme and a component of the thioredoxin (Trx) system that includes NADPH and Trx. The Trx system promotes cell growth and survival and it is also crucial for maintaining the intracellular levels of reactive oxygen species (ROS). TrxRs are selenoproteins with disulfide reductase activity that cause the reduction of Trx leading to the generation of reduced disulfide bond in cells. Electrons are taken from NADPH via TrxR and are transferred to the active site of Trx, which goes on to reduce protein

disulfides or other substrates.[195] Auranofin interacts with selenocysteine residue of mitochondrial TrxR blocking its activity and inducing mitochondrial oxidative stress that ultimately causes apoptosis.

To corroborate auranofin's inhibitory activity on TrxR, we treated Ba/F3-WT and Ba/F3-ITD cells with auranofin for 72h and performed an *in vitro* colorimetric TrxR assay according to the manufacturer's instructions. Our results demonstrated that TrxR activity was significantly reduced by auranofin treatment. In particular, the endogenous TrxR activity was reduced by 85% in Ba/F3-WT and 100% in Ba/F3-ITD, suggesting that Ba/F3-ITD cells are more sensitive to auranofin treatment than Ba/F3-WT cells (**Figure 4.27).**

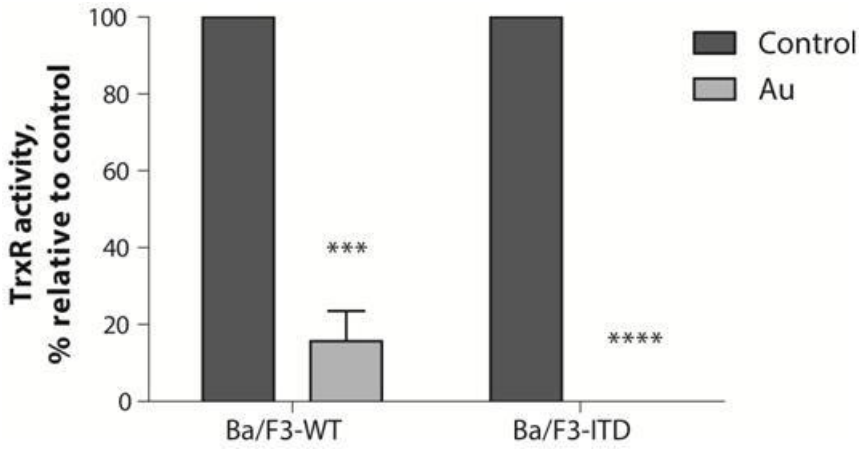


***Figure 4.27: Auranofin reduces the TrxR activity***
*Activity of endogenous TrxR in the indicated cell lysates following incubation with DMSO as a control or the concentration of auranofin resulting in $GI_{50}$ for 72h. The numbers indicate the percentage activity of TrxR compared to control. Experiment was done thrice independently and data are shown as mean ± SEM. Asterisks indicate significance versus control; ***p<0.001,****p<0.0001. Au, auranofin.*

---

Pyrvinium pamoate was originally used for the treatment of pinworm infections and it acts by interfering glucose uptake by pinworms. Recently, a wide variety of new mechanisms of action of pyrvinium pamoate has been proposed (i.e., inhibition of mitochondrial electron-transport chain under aerobic or anaerobic conditions, inhibition of Wnt signalling and inhibition of androgen receptor).[196]

The Wnt-β-catenin pathways support cell proliferation and survival. Constitutive activation of Wnt signalling occurs in diverse human diseases such as cancer. β-catenin has a central role in the Wnt signalling pathway. In the absence of Wnt ligand, β-catenin is degraded through the ubiquitin proteasome system upon association with the destruction complex. The destruction complex includes glycogen synthase kinase 3 (GSK3), casein kinase 1α (CK1α), adenomatous polyposis coli (APC) and Axin. The phosphorylation on Ser45 by CK1 primes β-catenin for subsequent phosphorylation on Ser33, 37 and Thr41 by GSK3β that destabilizes β-catenin triggers to its degradation mediated by ubiquitin/proteasomes. Upon Wnt activation, cytoplasmic β-catenin is stabilized and then translocated to the nucleus, where it binds to co-regulators as LEF-1/TCF to activate the transcription of targets genes such as *Axin2, Tcf, c-Myc and cyclin D1*.[197]

We tested the effect of pyrvinium pamoate on Wnt signalling as it plays a crucial role in the initiation and propagation/acceleration of AML.[198] For this purpose, Ba/F3-WT and Ba/F3-ITD cells were treated with pyrvinium pamoate for 24, 48 and 72 hours and levels of total β-catenin, total GSK3β, phosphorylated β-catenin (S33/37/T41) and phosphorylated GSK3β (S9) were examined by western blotting. Pyrvinium pamoate treatment completely abrogated the expression of pGSK3β (S9 phosphorylation) compared to DMSO treated samples resulting in the activation of GSK3β. Surprisingly, we did not observe either a clear increase in the expression of pβ-catenin or a decrease of total β-catenin expression levels upon pyrvinium pamoate treatment **(Figure 4.28)**.

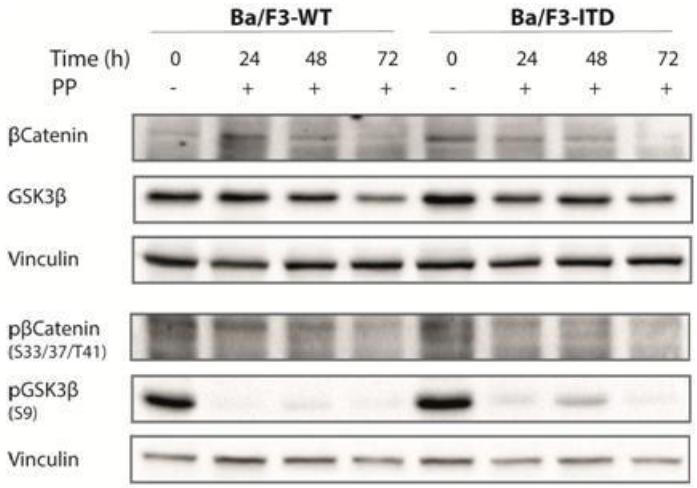


***Figure 4.28: Pyrvinium pamoate attenuates Wnt signalling***
*Representative immunoblot analysis of Wnt signalling pathway. Ba/F3-WT and -ITD cells were treated with $GI_{50}$ of pyrvinium pamoate for the indicated time duration. The expression of pβ-catenin (S33/37/T41), pGSK3β (S9), total β-catenin and GSK3β was analysed by SDS-PAGE and western blotting. Vinculin levels were used as a loading control.*

---

To further validate the effect of pyrvinium pamoate on Wnt signalling pathway, well-known β-catenin target genes, *Tcf4* and *Axin*2, were analysed by real-time PCR. After eight hours of treatment we detected a decrease of *Axin2* and *Tcf4* mRNA expression levels both in Ba/F3-WT and Ba/F3-ITD, suggesting that PP may act through the modulation of Wnt signalling **(Figure 4.29)**

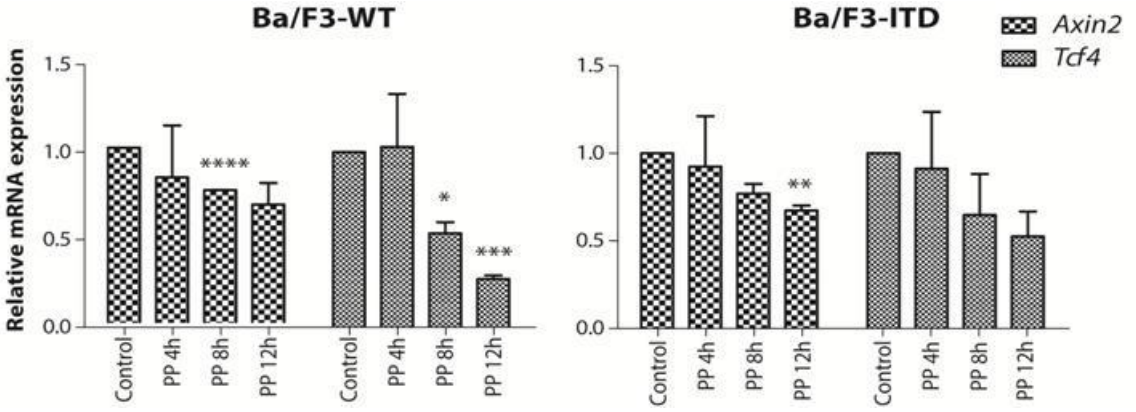


***Figure 4.29: Pyrvinium pamoate inhibits Wnt target genes***
*Relative mRNA expression of Axin 2 and Tcf4 in Ba/F3 cells treated with $GI_{50}$ of pyrvinium pamoate for the indicated time compared with untreated control cells. Experiment was done twice independently and data are shown as mean ± SEM. Asterisks (*) indicate significance versus control; * p<0.05, ** p<0.01, *** p<0.001, **** p<0.0001.*

---

## 4.10 FLT3 receptor is not inhibited by auranofin and pyrvinium pamoate treatment

Protein kinases are often constitutively active in cancer cells as a result of genomic rearrangements, point mutations in the regulatory region or, as is the case of FLT3 receptor, due to an alteration in the juxtamembrane region. They have become an attractive target for cancer therapy as most of them have been implicated in tumour development and progression. In fact, FLT3-ITD is a common mutation that confers poor prognosis in AML patients. Thus, we raised the question of whether treatment with auranofin or pyrvinium pamoate interfered with FLT3 or FLT3-ITD signalling taking advantage of Ba/F3 cell proprieties. Indeed, Ba/F3 cells depend on IL-3 for their growth, however, when expressing a constitutively active tyrosine kinase, they gain independence from IL-3. Accordingly, Ba/F3 cells expressing FLT3-ITD receptor are able to proliferate in the absence of IL-3 whereas Ba/F3-WT cells are not.[194] The inhibition of a constitutively active tyrosine kinase results in growth arrest and apoptosis because cells depend on it for their proliferation. The addition of IL-3 to the growth media can rescue cell survival. We, therefore, performed an experiment treating Ba/F3-ITD cells with the two compounds in the presence or absence of IL-3. The supplementation of culture media with the supernatant of WEHI cells, as a source of IL-3, did not change the number of growing cells, suggesting that both auranofin and pyrvinium pamoate did not selectively target FLT3-ITD receptor **(Figure 4.30 A)**. As positive control we used quizartinib, a potent FLT3-ITD inhibitor **(Figure 4.30 B)** Upon IL-3 supplementation, the growth of quizartinib-treated cells was comparable to the untreated ones confirming the specificity of this second generation FLT3 inhibitor.

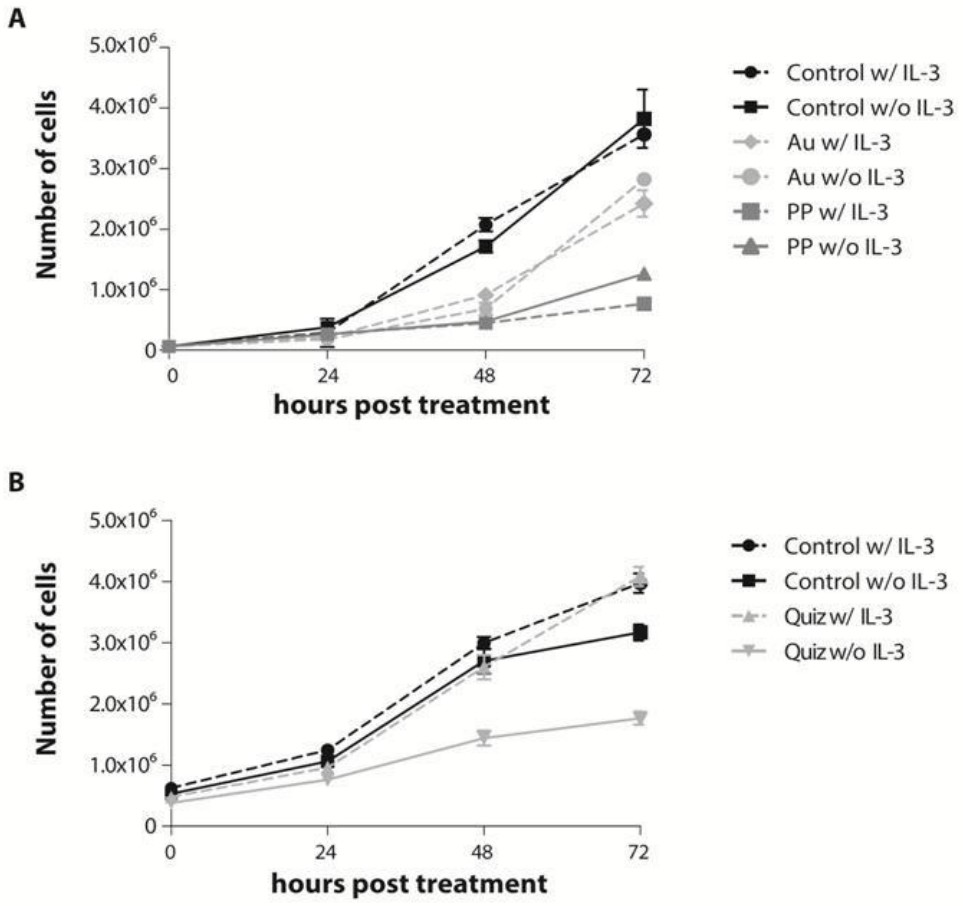


***Figure 4.30: Influence of auranofin and pyrvinium pamoate treatment on FLT3 receptor signalling***
*Growth curve. Cells were treated with (A) auranofin or pyrvinium pamoate and (B) quizartinib for 72h in the presence or absence of IL-3. Cells were counted at the indicated time point by trypan blue staining. The experiment was repeated twice and data are shown as mean ± SEM. Au, auranofin; PP, pyrvinium pamoate; Quiz, quizartinib.*

---

## 4.11 Auranofin and pyrvinium pamoate modulate ER stress and UPR

Recently, Prof. Pier Giuseppe Pelicci's group demonstrated that Ba/F3-ITD cells are characterised by elevated levels of ER stress markers in basal conditions compared to Ba/F3-WT cells. If proven, the activation of the UPR process upon ER stress may constitute a potential therapeutic target for AML patients bearing FLT3-ITD mutation.

We established a collaboration to investigate if the chosen drugs may perhaps trigger ER stress and UPR response. We treated Ba/F3 cells with auranofin or pyrvinium pamoate and then analysed by western blotting the expression levels of UPR proteins. We observed that auranofin caused a strong induction of ATF4 protein after four hours from treatment commencement in both Ba/F3-WT and Ba/F3-ITD cells. On the contrary, CHOP protein levels seemed to increase after eight hours and only in Ba/F3-WT cells **(Figure 4.31 A)**. Upon pyrvinium pamoate treatment, we noticed an induction of ATF4 and CHOP protein after 24h and 48h, respectively **(Figure 4.31 B)**. Data suggested that both auranofin and pyrvinium pamoate treatment led to the activation of the UPR and, in particular, of the PERK branch.

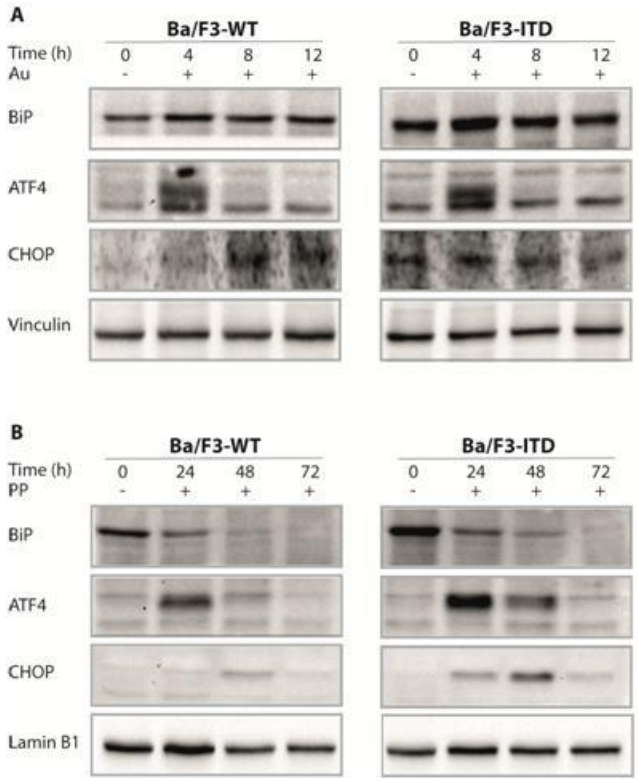


***Figure 4.31: Auranofin and pyrvinium pamoate activate PERK branch of the UPR***
*Ba/F3-WT and Ba/F3-ITD cells were treated with (A) 1.5 μM of auranofin and (B) 30 and 15 nM of pyrvinium pamoate, respectively, for the indicated time duration. The expression of BiP, ATF4 and CHOP were analysed by SDS-PAGE electrophoresis followed by Western blotting. Vinculin and Lamin B1 levels were used as loading controls. Au, auranofin; PP, pyrvinium pamoate.*

---

Next, we analysed by semiquantitative RT-PCR the splicing of the XBP1 transcription factor that occurs upon activation of the IRE1α and ATF6 branches. We used primers

specific for *XBP1*, which detect both unspliced and spliced isoforms formed by the annealing of single stranded cDNA to its complementary strand. A third cDNA product formed from one strand of unspliced *XBP1* and one strand of spliced *XBP1* was also seen (hybrid).[187]

The induction of both XBP1 and ATF4 is considered to be the second wave of events in the ER stress UPR process. Thus, based on previous western blotting results, Ba/F3 cells were treated with auranofin and pyrvinium pamoate up to 24 and 72 hours, respectively.

Results indicated that neither auranofin nor pyrvinium pamoate caused the activation of IRE1α or ATF6 branches. In order to generate a positive control, cells were exposed to thapsigargin, a well-known ER inducer **(Figure 4.32 A and B)**.

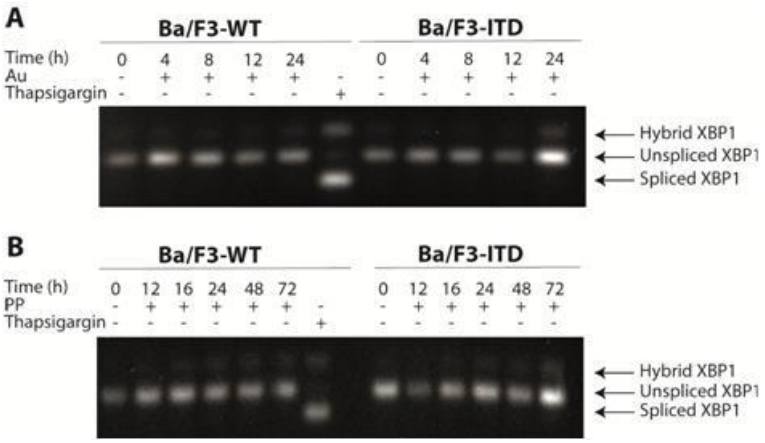


***Figure 4.32: Detection of XBP1 splice variants***
*Modulation of XBP1 splicing. Total RNA was isolated from Ba/F3-WT and Ba/F3-ITD cells treated with (A) 1.5 µM of auranofin and (B) 30 and 15 nM of pyrvinium pamoate, respectively, for the indicated time duration. Thapsigargin treated cells were used as a positive control. RT-PCR analysis of total RNA was performed to detect both spliced and unspliced XBP1 mRNA. Au, auranofin; PP, pyrvinium pamoate.*

---

Finally, the induction of UPR target genes at the mRNA level was analysed in Ba/F3 cells using real-time PCR. The panel of UPR target genes included genes encoding Heat Shock Proteins (HSP) such as *BiP* and *DNAJC3*, proteins involved in the folding process such as *ERP44* and *DNAJB9*, ERAD proteins as *EDEM1* and *HERPUD1*, transcription factors

such as *ATF4*, *ATF6* and *IRE1*, and proteins that are involved in the induction of apoptosis such as *PERK*, *CHOP*, *PDIA3* and *Ppp1R15B.*

To determine the quality of the primers, Ba/F3-ITD cells were treated with 1 mM dithiothreitol (DTT), an ER inducing agent, for three hours. Total RNA was isolated and reverse transcription was carried out. Relative expression was evaluated using the ΔΔCT method **(Figure 4.33)**. We observed an increase in the amount of the majority of UPR target genes at the mRNA level. In particular, a 4-fold increase of *BiP* levels, the first sensor of ER stress; a 7-fold increase of *Chop* levels and a 8-fold increase of *Herpud* gene one of the most inducible genes during UPR was seen. A decrease of *Ppp1r15b* expression, the protein that promotes the dephosphorylation of *eif2α* regulating the translation during ER stress was also detected.

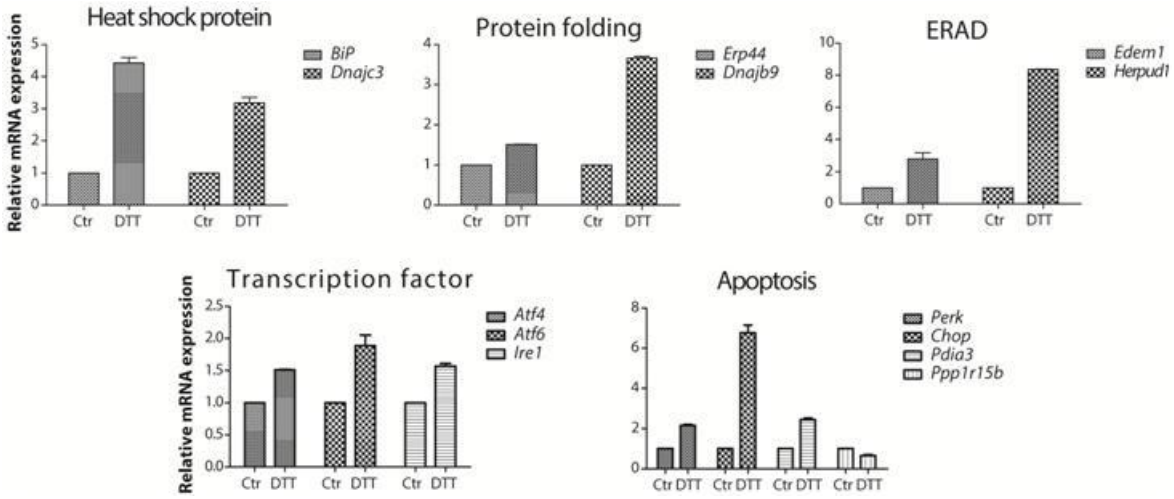


***Figure 4.33: DTT (UPR inducer) increased the amount of ER and UPR target genes***
*Ba/F3 cells were treated with 1mM of DTT for three hours. The relative mRNA levels of UPR target genes were quantified by real-time RT-PCR. All values were normalized using TBP as internal control. Values are presented as mean ± SEM. Ctr, control; DTT, dithiothreitol.*

---

We treated Ba/F3 cells with auranofin or pyrvinium pamoate and analysed the expression of UPR target genes **(Figure 4.34 A-E)**. We noticed that auranofin treatment induced the expression of HSP genes as well as genes encoding proteins that support folding and ERAD processes after four hours of treatment in Ba/F3 cells. Moreover, the induction of *Atf4* and *Chop* genes occurred after four hours in both Ba/F3-WT and Ba/F3-ITD cells

while it seemed that the induction of *Perk* gene happened later. Furthermore, *Atf6* levels were higher in Ba/F3-ITD cells after 8 hours form the treatment compared to the Ba/F3-WT cells. Pyrvinium pamoate treatment led to an increase of the expression of *Herpud* gene after 24 hours especially in Ba/F3-ITD cells as well as *Atf4* and *Atf6*. Furthermore, a 5-fold increase of *Chop* gene was detected after 24 hours of treatment. These results suggest that auranofin and pyrvinium pamoate modulate ER stress by inducing different UPR target genes.

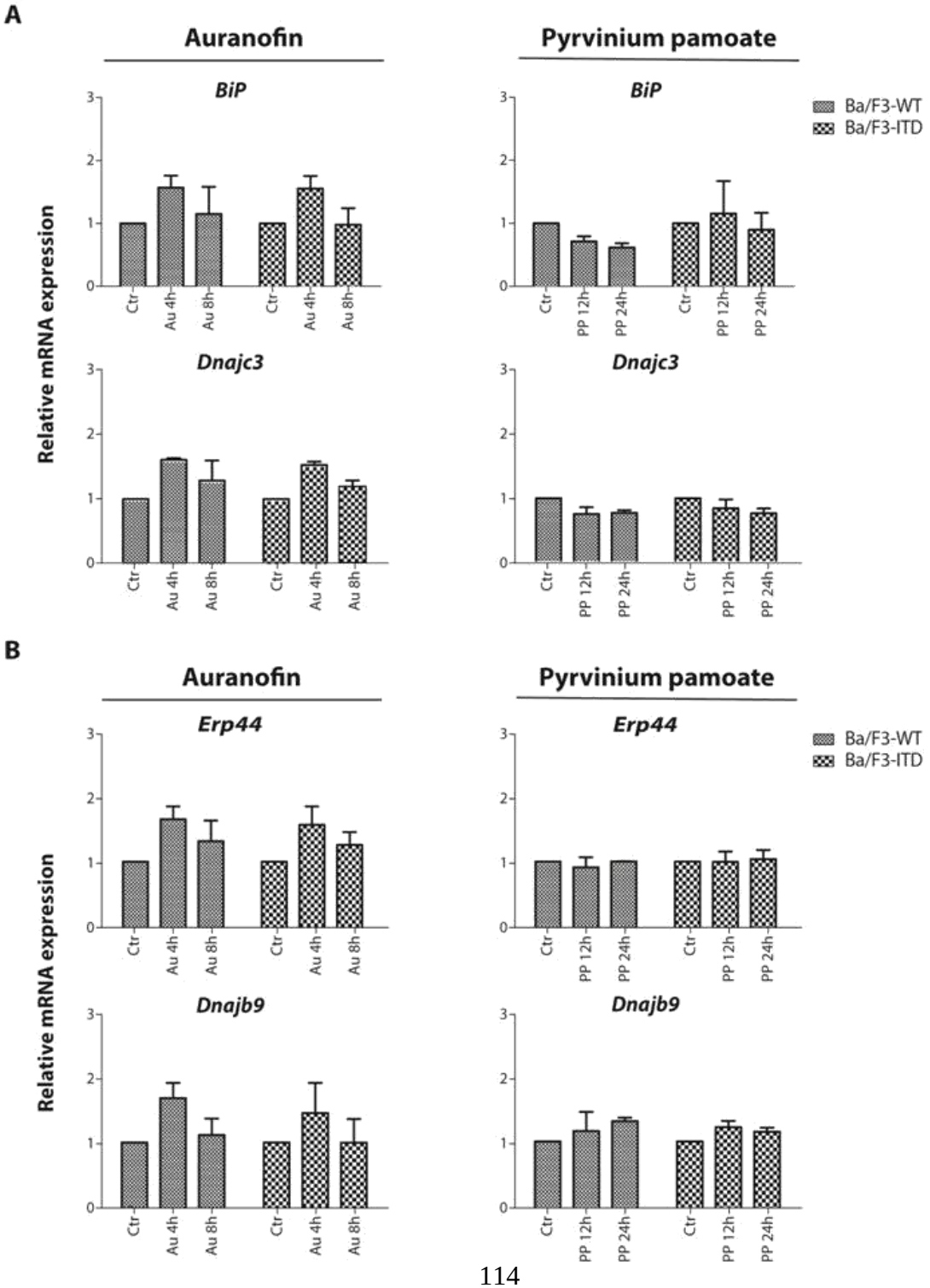

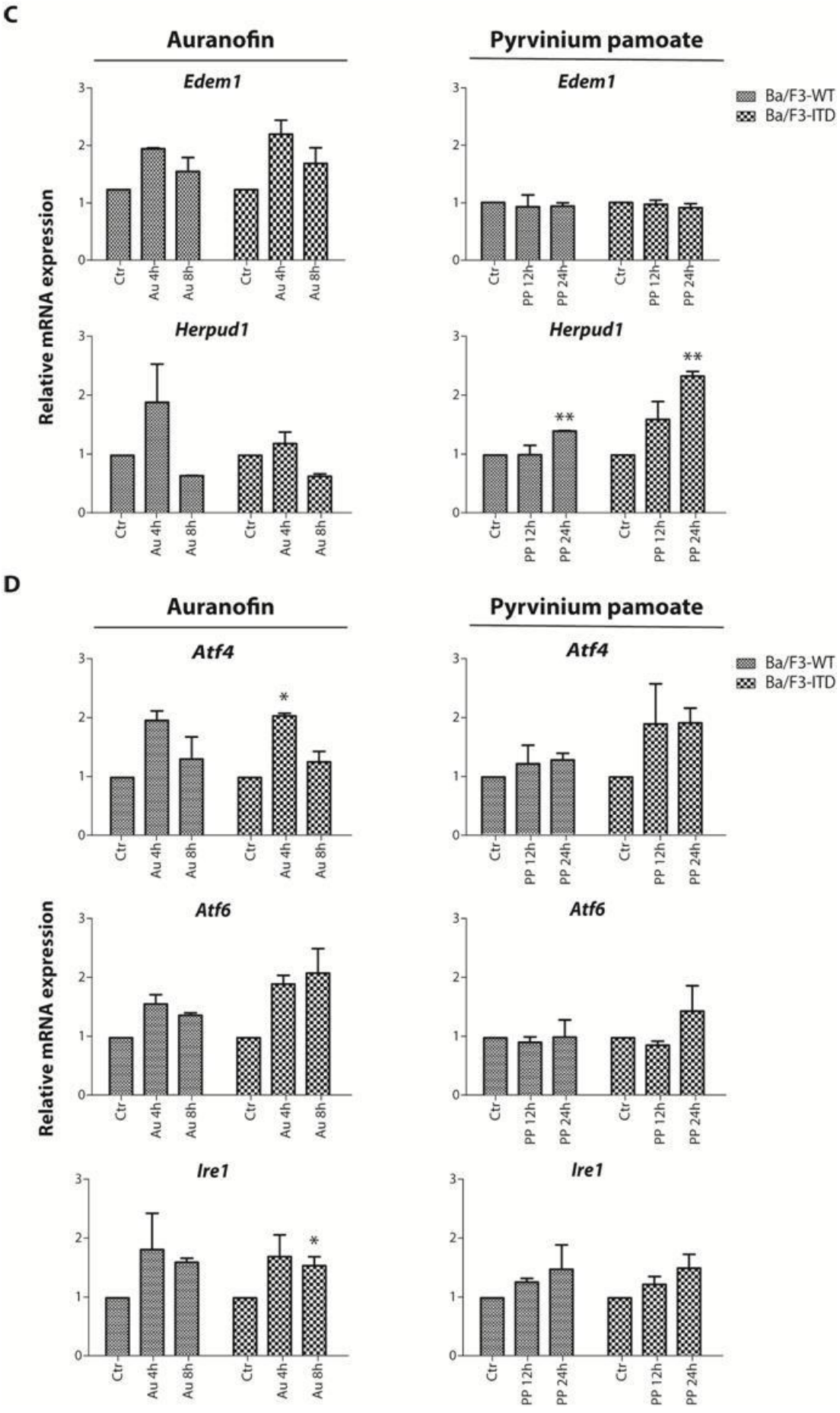
C
Auranofin
Pyrvinium pamoate
Edem1
Herpud1
Relative mRNA expression
Ba/F3-WT
Ba/F3-ITD
Ctr
Au 4h
Au 8h
PP 12h
PP 24h
**
D
Atf4
Atf6
Ire1
*

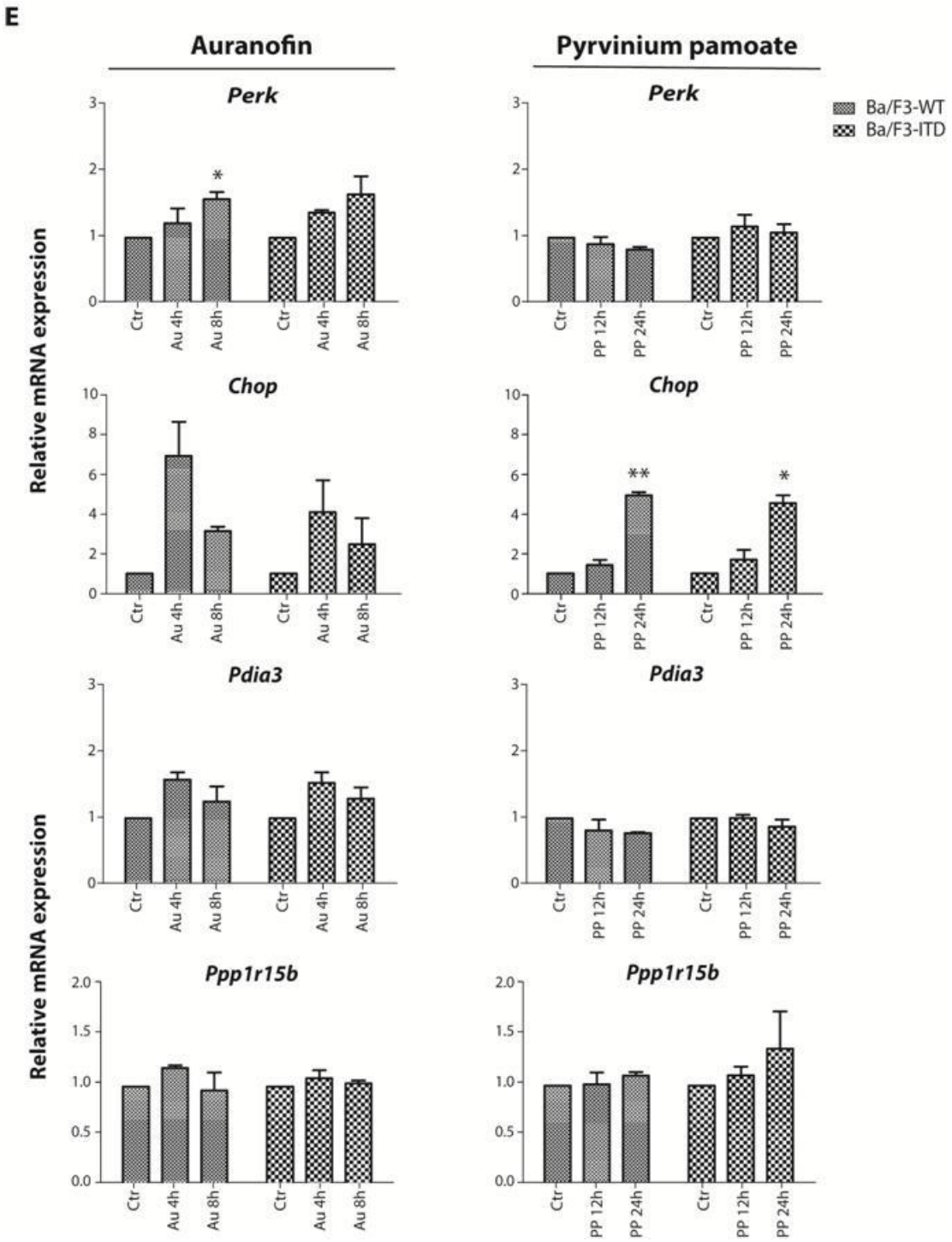


***Figure 4.34: Auranofin and pyrvinium pamoate induce UPR target genes expression***
*Ba/F3 cells were treated with $GI_{50}$ of auranofin and pyrvinium pamoate. The relative mRNA levels of genes encoding (A) Heat Shock Proteins; (B) folding proteins; (C) ERAD components; (D) transcription factors; (E) apoptosis effector UPR target genes were quantified by real-time RT-PCR. All values were normalized using TBP as internal control. Values are presented as mean ± SEM. * $p<0.05$, ** $p<0.01$.*

# 5 Discussion and future directions

For decades the therapeutic landscape in AML has remained relatively unchanged with the gold standard of treatment being the "7+3" regimen consisting of seven days of cytarabine and three of anthracycline. Recently, six new drugs received the FDA approval for AML treatment: midostaurin, CPX-351, enasidenib, gemtuzumab ozogamicin, venetoclax and daurismo.[199,200] Of these, only midostaurin, a non-specific tyrosine kinase inhibitor, was shown in the RATIFY study to significantly prolong the OS of patients suffering from FLT3-ITD AML.[65] FLT3 status is, thus, routinely determined at diagnosis in order to incorporate midostaurin when appropriate. Midostaurin treatment is also offered to elderly patients eligible for intensive chemotherapy independently of the mutational FLT3 status.[199] Still, the treatment of elderly or frail patients requires further refinement and improvement as efficient therapeutic options for them lack. As AML is predominantly a disease of the elderly, the quest for efficient therapies is still ongoing.

Drug repurposing is a possible strategy to identify active compounds that hugely accelerates the discovery by reusing an old drug in a new therapeutic context.[86] Since 2011, a large number of drug repurposing screens has been recorded, as attested to by the number of published papers. Such a surge in popularity is probably due to the availability of drug collections and the improvement of screening technologies.

We performed two rounds of screening using three different collections of FDA-approved agents or compounds in advanced phase clinical trials, and identified two promising compounds. Thus, auranofin and pyrvinium pamoate, an anti-rheumatic and an anthelmintic agent, respectively, were chosen as the top candidates to be repurposed. Both compounds inhibited the growth of AML cells. Moreover, the MV4-11 cells were the most sensitive to auranofin treatment whereas OCI-AML2 cells – the least responsive, as they require seven times greater concentration of auranofin to achieve the same percentage of

proliferation inhibition. The different response rates to auranofin treatment may reflect the FLT3 status as MV4-11 and MOLM13 cells have a homozygous and heterozygous FLT3-ITD mutation, respectively, while the *wild-type* receptor is expressed by OCI-AML2 cells. Finally, we proved that auranofin induced apoptosis in all of the cell lines tested. For pyrvinium pamoate, we demonstrated that the $IC_{50}$ concentration for MOLM13 cells was 2-times higher than for the MV4-11 cell line underscoring the greater sensitivity of the MV4-11 cells compared to MOLM13 cell line. The response of OCI-AML2 cells to pyrvinium pamoate treatment was similar to that of MOLM13. Thus, there was no specificity of pyrvinium pamoate towards FLT3-ITD-bearing cell lines and the inhibition of cell growth was due to a cytostatic effect.

Although the speed and overall simplicity of the experiment constitute the strong points of the repurposing strategy, some weaknesses have to be mentioned. Strict timeline and concentration range have to be used. A possibility exists that some compounds require less or more incubation time in order to optimally detect their activity and the same can be said for the concentration range. The inclusion of three different concentrations differing by a factor of 10 should have provided a wide enough range for almost all compounds.

A second problem during the screening phase is represented by the edge-effect that is caused by temperature differences across the plate, by which the inner wells reach 37°C more slowly than the outermost wells. This leads to a consistent evaporation of medium at the edges of the plate, a factor very relevant to 96- and 384-well plates given how small the overall volume per well is. We have minimized the edge-related bias by leaving empty the first and the last column of the plate whenever possible, and by filling the spaces between wells with water to diminish medium evaporation by creating a humidified atmosphere. In addition, there are bioinformatic tools for edge-effect normalisation during the analysis phase and they have been applied to the results of the primary screening. Moreover, DMSO is generally used for the preparation of all the compounds within the library. Even though, DMSO is a potent solvent, in which the majority of organic compounds are

soluble, is possible that some compounds were missed due to a solubility problem. Whether or not some compounds were missed due to a solubility problem is difficult to predict, but having worked with such large numbers, the issue should be negligible. Finally, coloured agents may alter the luminescence reading; however, when identified as hits (e.g., pyrvinium pamoate) their activity is validated through methods that do not require the use of plate readers.

The identification of compounds with weak potency, i.e., an $IC_{50}$ value higher than the plasma concentration considered safe for humans, is often a bottleneck that comes into light in the validation phase of a repurposing project, and hampers the implementation of any given molecule.[201] Toxicology data shows that auranofin (gold particles) is safe up to the plasma concentration of 1.5 µg/ml (corresponding to the concentration of ~2.21 µM),[202] while no safe plasma concentration value is available for pyrvinium pamoate given that it is not absorbed from the gastrointestinal tract. It is said to be safe in humans up to the concentration of 35 mg/Kg of patient's body mass when administered orally.[203] The results obtained for auranofin show that $IC_{50}$ concentration of auranofin for OCI-AML2 cells (equal to 3.93 µM) is higher compare to the plasma concentration reported to be safe, but it should not be a problem as if validated further, auranofin could be specifically repurposed against FLT3-ITD AML. Big pharmaceutical companies deal with the dose-related toxicity problem by modifying the structure of the molecule to render it more potent, an approach that requires specific know-how and financial investments. Otherwise, one way of reducing the doses is that of using a combination of drugs rather than single agents. In fact, the combination of two or more compounds may result in a synergistic or additive effect at lower doses. Moreover, combination therapy significantly reduces the development of drug resistance, a common problem in cancer patients, as tumour is less likely to become resistant to multiple compounds simultaneously. We observed a clear synergistic effect in AML cell lines when treating with the combination of auranofin and cytarabine. The combination of quizartinib with auranofin, instead, produced an additive

effect in FLT3-ITD expressing cells. We looked for possible synergistic effect of pyrvinium pamoate in combination with standard therapeutic agents or known FLT3 inhibitors hoping to see a cytotoxic rather than cytostatic effect. Pyrvinium pamoate showed neither synergy nor additivity with cytarabine and performed barely better in combination with quizartinib. It showed an additive effect in combination with doxorubicine in the three cell lines tested.

The *in vivo* validation of chosen compounds was initiated but has not been completed in the timeframe of the PhD studentship. To date, we established the maximal tolerated doses of auranofin and pyrvinium pamoate and discovered that the *xenograft* model used in this project was not straightforward: the disease could not be monitored on the basis of the hCD45+ cell level in peripheral blood as it did not correspond to the disease advancement. Thus, we decided to change the *xenograft* mouse model by choosing a different AML-patient derived *xenograft* leukemias through the collaboration with Dr F. Bertolini. Moreover, we will evaluate the effect of the selected agents in transgenic mouse model (NPMc+ and FLT3-ITD) thus in mice with intact immune system.

*In vivo* imaging techniques may be adopted to monitor the development and subsequent progression/regression of the disease circumventing the problems encountered in the initial experiments. In order to take advantage of the *in vivo* imaging techniques, leukemic cells will be transduced with the pGL4 Luciferase Reporter Vector (Promega). Luciferase-expressing cryopreserved splenocytes from primary murine leukaemias and from xenografted animals will be thawed and injected intravenously into appropriate hosts (C57BL/6 or NSG mice, respectively). Upon detection of the insurgence of leukaemia, mice will be treated with selected drugs, initially as single agents and later in combination with standard therapeutic agents, such as cytarabine, or with FLT3 inhibitor *i.e.* quizartinib.

Some attempts at repurposing both auranofin and pyrvinium pamoate have been made in a

number of clinical settings. Analogously to the results obtained by us, preclinical studies demonstrated that treatment with auranofin decreased cell viability and induced apoptosis in human CLL/CML, ovarian, gastrointestinal and non-small cell lung cancer warranting the conduction of clinical trials.[204] To date, 12 clinical trials have been initiated to assess the utility and efficacy of auranofin for the treatment of a wide range of disparate conditions, such as HIV, amoebiasis, giardiasis, tuberculosis, pain, rheumatoid arthritis, ovarian and lung cancer, CLL or glioblastoma. Some evidence supports the efficacy of auranofin against haematological malignancies. For example, in CLL auranofin made it into Phase I and IIa clinical trials, however, its repurposing program was subsequently stopped not because auranofin did not work, but because new agents to treat CLL became available questioning the need to pursue additional research (NCT01419691).[205]

Literature reports cytotoxic activity of pyrvinium pamoate against a range of cancer cell lines (i.e., colorectal cancer, breast cancer, prostate tumour, myeloma, lymphoma and chronic myeloid leukaemia);[206] however, no clinical trials of pyrvinium pamoate are to date registered on the ClinicalTrials.gov database. Thus, the absence of pre-clinical data or clinical trials of both auranofin and pyrvinium pamoate for the treatment of AML confirms the novelty of our candidates.

So why should an anti-rheumatic or an anthelmintic agent work against leukemic cells? Cancer cells are characterised by uncontrolled growth, insensitivity to growth-inhibitory signals, evasion of programmed cell death and limitless replication potential.[207] Many of the evolutionary-conserved pathways, such as Wnt, Notch or Hedgehog signalling, become reactivated. High metabolic rate generates elevated levels of ROS, while high requirement of protein production clogs the entire system of transcription, translation and protein folding. Accordingly, cancer cells upregulate the antioxidant system, such as the TrxR enzyme, to maintain the balance between generation and elimination of ROS, as well as systems to remove misfolded proteins. Hence, also UPR is frequently upregulated. By

chance, auranofin, our main candidate for repurposing in AML, was shown to induce ROS production in *Escherichia histolytica trophozoites* and CML, and to inhibit TrxR.[189,208] The overexpression of TrxR has been linked to enhanced proliferation, resistance to apoptosis, angiogenesis and chemoresistance.[195] It stands to reason that targeting a redox enzyme such as the TrxR, may constitute a successful therapeutic strategy. Indeed, we showed that auranofin kills AML cell lines and confirmed that it inhibits TrxR in Ba/F3 cells possibly causing ROS accumulation. It may be hypothesised that the auranofin-induced apoptosis observed by us in AML cell lines is, at least in part, the consequence of lethal oxidative stress. Thus, we would like to perform a FACS analysis to demonstrate that auranofin causes ROS accumulation using a probe for measuring cellular oxidative stress. The cell-permeant dye exhibits bright fluorescence only upon oxidation by ROS. For further evaluating the possible link between ROS accumulation and cell death induction we plan to treat AML cells with N-acetylcysteine (NAC), an antioxidant able to minimize oxidative stress. If the co-treatment results in an equal percentage of apoptotic cells as for the single treatment, it would mean that the effect of auranofin on cell survival does not depend on TrxR inhibition. In such case, we will analyse how auranofin treatment interferes with the deubiquitination process through Western blot analysis, as another mechanism of action of auranofin is its ability to inhibit deubiquitinase proteins leading to the accumulation of polyubiquitinated proteins and induction of apoptosis.

The results of this PhD thesis also show that auranofin concomitantly induces ER stress with the subsequent molecular response to it as detected by the increase of the major UPR target genes at the mRNA level and of ATF4 and CHOP UPR effectors at the protein level. Sustained CHOP expression results in apoptosis, especially due to the induction of pro-apoptotic proteins such as BIM, along with the inhibition of pro-survival proteins e.g., BCL2 and MCL1. Further investigation is necessary to ascertain if auranofin-induced ER stress may be a secondary effect in the wake of auranofin-induced ROS accumulation and whether these two events cooperate in inducing cell death.

To determine the existence of a link between ROS accumulation and ER stress induction in provoking cell death we will adopt two different strategies: a shRNA against *CHOP* and the analysis of mRNA and protein levels of ATF4, CHOP and its target genes upon co-treatment with auranofin and NAC. Supposing that CHOP protein cooperates with ROS accumulation in cell death induction, shRNA treatment should result in a lower number of apoptotic cells. If not, the two effects observed upon auranofin treatment are unrelated. Then, a repression of ATF4 and CHOP proteins in the co-treatment experiments would confirm the correlation between TrxR inhibition and ER stress induction. Moreover, it remains to be determined if the induction of ATF4 and CHOP depends on PERK activation or if it occurs in response to the activity of other kinases, such as GCN2 and PKR, as they have been reported to phosphorylate eIF2α inducing ATF4 expression.[209] To do so, western blot analysis and RT-qPCR will be performed.

The activity of pyrvinium pamoate in cancer is not casual either, as it inhibits the canonical Wnt signalling pathway. Wnt signalling is relevant to the pathogenesis of AML and upregulated by most AML-specific mutations, including FLT3-ITD.[29] We showed that pyrvinium pamoate interferes with Wnt-β-catenin pathway as attested to by the complete abrogation of GSK3β phosphorylation on serine 9 in Ba/F3 cells that causes β-catenin degradation. Moreover, we further confirmed Wnt signalling inhibition by showing that mRNA levels of two major Wnt target genes, *Tcf4* and *Axin2*, are decreased after pyrvinium pamoate treatment in both Ba/F3-WT and Ba/F3-ITD cells. We are planning to evaluate the effect of pyrvinium pamoate both at mRNA and protein levels of a larger panel of β-catenin targets by performing RT-PCR and Western blotting, respectively. Moreover, it would be interesting to assess the accumulation nuclear translocation of β-catenin following pyrvinium pamoate treatment through immunofluorescence analysis.

Recently, Costa et al. demonstrated that impairment of mitochondrial ATP production downregulates Wnt signalling via ER stress induction.[210] Our data shows that pyrvinium pamoate treatment induces the expression of ATF4 and CHOP proteins after 24 and 48

hours of treatment, respectively. Thus, it is possible that pyrvinium pamoate treatment reduces the synthesis of mitochondrial ATP as reported by Harada et al.,[211] which then decreases the level of $Ca^{2+}$ in the ER resulting in the induction of ER stress thorough the phosphorylation of eIF2α and activation of its effectors such as ATF4 and CHOP. We will detect cytoplasmic and mitochondrial $Ca^{2+}$ using specific fluorochromes.

Several published reports connect the inhibition of the Wnt-β-catenin pathway with CHOP protein.[212,213] However, the exact mechanism that links these events requires further clarification. A shRNA against *CHOP* will allow us to assess the effect of CHOP on Wnt signalling. The lack of β-catenin target genes inhibition upon shRNA treatment will confirm the correlation between CHOP and Wnt-β-catenin pathway.

In summary, we identified and selected two compounds, auranofin and pyrvinium pamoate, capable of killing leukaemic cells through two rounds of drug repurposing screening. Their activity was validated in *in vitro* experiments and is being tested *in vivo*. Known and novel mechanisms of action have been confirmed and proposed. Taken together, the results of this project corroborate the potential of auranofin as a therapeutic option for AML patients, should its *in vivo* efficacy be proven. On the contrary, given the lack of cytotoxicity and modest results of combination treatment, as well as inexistent toxicity data when injected into an organism, the utility of repurposing pyrvinium pamoate is much less convincing, although clearly, the *in vivo* part of the project requires further work for both compounds.

It is also important to point out that the screening yielded many more candidates and its results constitute a resource that one can tap into for further validation projects.

# References


1. Döhner, H., Weisdorf, D. J. & Bloomfield, C. D. Acute Myeloid Leukemia. *N. Engl. J. Med.* **373,** 1136–1152 (2015).
2. Bennett, J. M. *et al.* PROPOSALS FOR CLASSIFICATION OF ACUTE LEUKEMIAS. *Br. J. Haematol.* **33,** 451- (1976).
3. Arber, D. A. *et al.* The 2016 revision to the World Health Organization classification of myeloid neoplasms and acute leukemia. *Blood* **127,** 2391–2405 (2016).
4. Vardiman, J. W. *et al.* The 2008 revision of the World Health Organization (WHO) classification of myeloid neoplasms and acute leukemia: rationale and important changes. *Blood* **114,** 937–951 (2009).
5. Meyer, S. C. & Levine, R. L. Translational implications of somatic genomics in acute myeloid leukaemia. *Lancet Oncol.* **15,** e382–e394 (2014).
6. Gruszka, A. M., Valli, D. & Alcalay, M. Understanding the molecular basis of acute myeloid leukemias: where are we now? *Int. J. Hematol. Oncol.* **6,** 43–53 (2017).
7. Gary Gilliland, D. & Griffin, J. D. The roles of FLT3 in hematopoiesis and leukemia. *Blood* **100,** 1532–1542 (2002).
8. Ley, T. J. *et al.* Genomic and epigenomic landscapes of adult de novo acute myeloid leukemia. *N. Engl. J. Med.* **368,** 2059–2074 (2013).
9. Anderson, K. *et al.* Genetic variegation of clonal architecture and propagating cells in leukaemia. *Nature* **469,** 356–361 (2011).
10. Kim, T. *et al.* Clonal dynamics in a single AML case tracked for 9 years reveals the complexity of leukemia progression. *Leukemia* **30,** 295–302 (2016).
11. Klco, J. M. *et al.* Functional heterogeneity of genetically defined subclones in acute myeloid leukemia. *Cancer Cell* **25,** 379–392 (2014).
12. Rosnet, O. *et al.* Human FLT3/FLK2 gene: cDNA cloning and expression in hematopoietic cells. *Blood* **82,** 1110–1119 (1993).
13. Rosnet, O. FLT3 (FMS-like tyrosine kinase 3). *Atlas Genet. Cytogenet. Oncol. Haematol.* (2011). doi:10.4267/2042/37508
14. Rosnet, O. *et al.* Human FLT3/FLK2 receptor tyrosine kinase is expressed at the surface of normal and malignant hematopoietic cells. *Leukemia* **10,** 238–248 (1996).
15. Griffith, J. *et al.* The Structural Basis for Autoinhibition of FLT3 by the Juxtamembrane Domain. *Mol. Cell* **13,** 169–178 (2004).
16. Agnès, F. *et al.* Genomic structure of the downstream part of the human FLT3 gene: exon/intron structure conservation among genes encoding receptor tyrosine kinases (RTK) of subclass III. *Gene* **145,** 283–288 (1994).
17. Martelli, A. M., Evangelisti, C., Chiarini, F. & McCubrey, J. A. The phosphatidylinositol 3-kinase/Akt/mTOR signaling network as a therapeutic target in acute myelogenous leukemia patients. *Oncotarget* **1,** 89–103 (2010).
18. Kim, K. T., Levis, M. & Small, D. Constitutively activated FLT3 phosphorylates BAD partially through Pim-1. *Br. J. Haematol.* **134,** 500–509 (2006).
19. Yang, J. Y. & Hung, M. C. A new fork for clinical application: Targeting forkhead transcription factors in cancer. *Clinical Cancer Research* **15,** 752–757 (2009).
20. Scholl, C., Gilliland, D. G. & Fröhling, S. Deregulation of Signaling Pathways in Acute Myeloid Leukemia. *Semin. Oncol.* **35,** 336–345 (2008).
21. Nakao, M. *et al.* Internal tandem duplication of the flt3 gene found in acute myeloid leukemia. *Leukemia* **10,** 1911–1918 (1996).
22. Breitenbuecher, F. *et al.* Identification of a novel type of ITD mutations located in nonjuxtamembrane domains of the FLT3 tyrosine kinase receptor. *Blood* **113,** 4074–4077 (2009).
23. Reindl, C. *et al.* Point mutations in the juxtamembrane domain of FLT3 define a new class of activating mutations in AML. *Blood* **107,** 3700–3707 (2006).
24. Schmidt-Arras, D.-E. *et al.* Tyrosine phosphorylation regulates maturation of receptor tyrosine kinases. *Mol. Cell. Biol.* **25,** 3690–703 (2005).
25. Yamamoto, Y. *et al.* Activating mutation of D835 within the activation loop of FLT3 in human hematologic malignancies. *Blood* **97,** 2434–2439 (2001).

26. Scholl, S. *et al.* Specific detection of Flt3 point mutations by highly sensitive real-time polymerase chain reaction in acute myeloid leukemia. *J. Lab. Clin. Med.* **145,** 295–304 (2005).
27. Zheng, R. *et al.* Internal tandem duplication mutation of FLT3 blocks myeloid differentiation through suppression of C/EBPα expression. *Blood* **103,** 1883–1890 (2004).
28. Hayakawa, F. *et al.* Tandem-duplicated Flt3 constitutively activates STAT5 and MAP kinase and introduces autonomous cell growth in IL-3-dependent cell lines. *Oncogene* **19,** 624–631 (2000).
29. Tickenbrock, L. *et al.* Flt3 tandem duplication mutations cooperate with Wnt signaling in leukemic signal transduction. *Blood* **105,** 3699–3706 (2005).
30. Welch, J. S. *et al.* The origin and evolution of mutations in acute myeloid leukemia. *Cell* **150,** 264–278 (2012).
31. Thiede, C. *et al.* Analysis of FLT3-activating mutations in 979 patients with acute myelogenous leukemia: Association with FAB subtypes and identification of subgroups with poor prognosis. *Blood* **99,** 4326–4335 (2002).
32. Schnittger, S. *et al.* Analysis of FLT3 length mutations in 1003 patients with acute myeloid leukemia: Correlation to cytogenetics, FAB subtype, and prognosis in the AMLCG study and usefulness as a marker for the detection of minimal residual disease. *Blood* **100,** 59–66 (2002).
33. Dicker, F. *et al.* Mutation analysis for RUNX1, MLL-PTD, FLT3-ITD, NPM1 and NRAS in 269 patients with MDS or secondary AML. *Leukemia* **24,** 1528–1532 (2010).
34. Fröhling, S. *et al.* Prognostic significance of activating FLT3 mutations in younger adults (16 to 60 years) with acute myeloid leukemia and normal cytogenetics: A study of the AML study group Ulm. *Blood* **100,** 4372–4380 (2002).
35. Meshinchi, S. *et al.* Prevalence and prognostic significance of Flt3 internal tandem duplication in pediatric acute myeloid leukemia. *Blood* **97,** 89–94 (2001).
36. Iwai, T. *et al.* Internal tandem duplication of the FLT3 gene and clinical evaluation in childhood acute myeloid leukemia. *Leukemia* **13,** 38–43 (1999).
37. Stirewalt, D. L. *et al.* FLT3, RAS, and TP53 mutations in elderly patients with acute myeloid leukemia. *Blood* **97,** 3589–3595 (2001).
38. Xu, F. *et al.* Tandem duplication of the FLT3 gene is found in acute lymphoblastic leukaemia as well as acute myeloid leukaemia but not in myelodysplastic syndrome or juvenile chronic myelogenous leukaemia in children. *Br. J. Haematol.* **105,** 155–162 (1999).
39. Yokota, S. *et al.* Internal tandem duplication of the FLT3 gene is preferentially seen in acute myeloid leukemia and myelodysplastic syndrome among various hematological malignancies. A study on a large series of patients and cell lines. *Leukemia* **11,** 1605–1609 (1997).
40. Baldwin, B. R., Zheng, R. & Small, D. FLT3 is not frequently mutated in solid tumors. *Blood* **98,** 156b–157b (2001).
41. Ishii, E., Zaitsu, M., Ihara, K., Hara, T. & Miyazaki, S. High expression but no internal tandem duplication of FLT3 in normal hematopoietic cells. *Pediatr. Hematol. Oncol.* **16,** 437–441 (1999).
42. Stirewalt, D. L. & Radich, J. P. The role of FLT3 in haematopoietic malignancies. *Nature Reviews Cancer* **3,** 650–665 (2003).
43. Kottaridis, P. D., Gale, R. E. & Linch, D. C. FLT3 mutations and leukaemia. *British Journal of Haematology* **122,** 523–538 (2003).
44. Whitman, S. P. *et al.* Absence of the wild-type allele predicts poor prognosis in adult de novo acute myeloid leukemia with normal cytogenetics and the internal tandem duplication of FLT3: A cancer and leukemia group B study. *Cancer Res.* **61,** 7233–7239 (2001).
45. Linch, D. C., Hills, R. K., Burnett, A. K., Khwaja, A. & Gale, R. E. Impact of FLT3ITD mutant allele level on relapse risk in intermediate-risk acute myeloid leukemia. *Blood* **124,** 273–276 (2014).
46. Stirewalt, D. L. *et al.* Size of FLT3 internal tandem duplication has prognostic significance in patients with acute myeloid leukemia. *Blood* **107,** 3724–3726 (2006).
47. Au, W. Y. *et al.* FLT-3 aberrations in acute promyelocytic leukaemia: Clinicopathological associations and prognostic impact. *Br. J. Haematol.* **125,** 463–469 (2004).
48. Schnittger, S. *et al.* Prognostic impact of FLT3-ITD load in NPM1 mutated acute myeloid leukemia. *Leukemia* **25,** 1297–1304 (2011).

49. Su, L. The Impact of DNMT3A/FLT3-ITD/NPM1 on Patients with Acute Myeloid Leukemia after Allogeneic Hematopoietic Stem Cell Transplantation. *Turkish journal of haematology : official journal of Turkish Society of Haematology* **36,** 64–66 (2019).
50. Murphy, K. M. *et al.* Detection of FLT3 internal tandem duplication and D835 mutations by a multiplex polymerase chain reaction and capillary electrophoresis assay. *J. Mol. Diagnostics* **5,** 96–102 (2003).
51. De Kouchkovsky, I. & Abdul-Hay, M. 'Acute myeloid leukemia: A comprehensive review and 2016 update'. *Blood Cancer Journal* **6,** (2016).
52. Dombret, H. & Gardin, C. An update of current treatments for adult acute myeloid leukemia. *Blood* **127,** 53–61 (2016).
53. Medinger, M., Lengerke, C. & Passweg, J. Novel therapeutic options in Acute Myeloid Leukemia. *Leukemia Research Reports* **6,** 39–49 (2016).
54. Thol, F., Schlenk, R. F., Heuser, M. & Ganser, A. How I treat refractory and early relapsed acute myeloid leukemia. *Blood* **126,** 319–327 (2015).
55. Larrosa-Garcia, M. & Baer, M. R. FLT3 Inhibitors in acute myeloid leukemia: Current status & future directions. *Molecular Cancer Therapeutics* **16,** 991–1001 (2017).
56. O'Farrell, A. M. *et al.* An Innovative Phase I Clinical Study Demonstrates Inhibition of FLT3 Phosphorylation by SU11248 in Acute Myeloid Leukemia Patients. *Clin. Cancer Res.* **9,** 5465–5476 (2003).
57. Fiedler, W. *et al.* A phase 1 study of SU11248 in the treatment of patients with refractory or resistant acute myeloid leukemia (AML) or not amenable to conventional therapy for the disease. *Blood* **105,** 986–993 (2005).
58. Fiedler, W. *et al.* A phase I/II study of sunitinib and intensive chemotherapy in patients over 60 years of age with acute myeloid leukaemia and activating FLT3 mutations. *Br. J. Haematol.* **169,** 694–700 (2015).
59. Borthakur, G. *et al.* Phase I study of sorafenib in patients with refractory or relapsed acute leukemias. *Haematologica* **96,** 62–68 (2011).
60. Ravandi, F. *et al.* Phase 2 study of azacytidine plus sorafenib in patients with acute myeloid leukemia and FLT-3 internal tandem duplication mutation. *Blood* **121,** 4655–4662 (2013).
61. Ravandi, F. *et al.* Phase I/II study of combination therapy with sorafenib, idarubicin, and cytarabine in younger patients with acute myeloid leukemia. *J. Clin. Oncol.* **28,** 1856–1862 (2010).
62. Al-Kali, A. *et al.* Patterns of molecular response to and relapse after combination of sorafenib, idarubicin, and cytarabine in patients with FLT3 mutant acute myeloid leukemia. *Clin. Lymphoma, Myeloma Leuk.* **11,** 361–366 (2011).
63. Levis, M. *et al.* Results from a randomized trial of salvage chemotherapy followed by lestaurtinib for patients with FLT3 mutant AML in first relapse. *Blood* **117,** 3294–3301 (2011).
64. Knapper, S. *et al.* A randomized assessment of adding the kinase inhibitor lestaurtinib to first-line chemotherapy for FLT3-mutated AML. *Blood* **129,** 1143–1154 (2017).
65. Stone, R. M. *et al.* Midostaurin plus chemotherapy for acute myeloid leukemia with a FLT3 Mutation. *N. Engl. J. Med.* **377,** 454–464 (2017).
66. Schiller, G. J. *et al.* Final results of a randomized phase 2 study showing the clinical benefit of quizartinib (AC220) in patients with FLT3-ITD positive relapsed or refractory acute myeloid leukemia. *J. Clin. Oncol.* **32,** 7100–7100 (2014).
67. Cortes, J. E. *et al.* Results of a phase 2 randomized, open-label, study of lower doses of quizartinib (AC220; ASP2689) in subjects with FLT3-ITD positive relapsed or refractory Acute Myeloid Leukemia (AML). *Blood* **122,** (2013).
68. Cortes, J. E. *et al.* Phase I study of quizartinib administered daily to patients with relapsed or refractory acute myeloid leukemia irrespective of FMS-like tyrosine kinase 3-internal tandem duplication status. in *Journal of Clinical Oncology* **31,** 3681–3867 (2013).
69. Swaminathan, M. *et al.* The Combination of Quizartinib with Azacitidine or Low Dose Cytarabine is Highly Active in Patients (Pts) with FLT3-ITD Mutated Myeloid Leukemias: Interim Report of a Phase I/II Trial. *Clin. Lymphoma Myeloma Leuk.* **17,** S3 (2017).
70. Alvarado, Y. *et al.* Treatment with FLT3 inhibitor in patients with FLT3-mutated acute myeloid leukemia is associated with development of secondary FLT3-tyrosine kinase domain mutations. *Cancer* **120,** 2142–2149 (2014).
71. Perl, A. E. *et al.* A phase 3, open-label, randomized study of the FLT3 inhibitor gilteritinib

versus salvage chemotherapy in adults with first relapse or primary refractory FLT3 mutation-positive acute myeloid leukemia. *J. Clin. Oncol.* **34,** TPS7072-TPS7072 (2016).
72. Altman, J. K. *et al.* Antileukemic Activity and Tolerability of ASP2215 80mg and Greater in FLT3 Mutation-Positive Subjects with Relapsed or Refractory Acute Myeloid Leukemia: Results from a Phase 1/2, Open-Label, Dose-Escalation/Dose-Response Study. *Blood* **126,** 321 (2015).
73. J.E., C. *et al.* Crenolanib besylate, a type I pan-FLT3 inhibitor, to demonstrate clinical activity in multiply relapsed FLT3-ITD and D835 AML. *J. Clin. Oncol.* **34,** (2016).
74. Randhawa, J. K. *et al.* Results of a Phase II Study of Crenolanib in Relapsed/Refractory Acute Myeloid Leukemia Patients (Pts) with Activating FLT3 Mutations. *Blood* **124,** 389 (2014).
75. Sato, T. *et al.* FLT3 ligand impedes the efficacy of FLT3 inhibitors in vitro and in vivo. *Blood* **117,** 3286–3293 (2011).
76. Brunner, A. M. *et al.* Haematopoietic cell transplantation with and without sorafenib maintenance for patients with FLT3-ITD acute myeloid leukaemia in first complete remission. *Br. J. Haematol.* **175,** 496–504 (2016).
77. Antar, A., Kharfan-Dabaja, M. A., Mahfouz, R. & Bazarbachi, A. Sorafenib maintenance appears safe and improves clinical outcomes in FLT3-ITD acute myeloid leukemia after allogeneic hematopoietic cell transplantation. *Clin. Lymphoma, Myeloma Leuk.* **15,** 298–302 (2015).
78. Sammons, S. L., Pratz, K. W., Smith, B. D., Karp, J. E. & Emadi, A. Sorafenib is tolerable and improves clinical outcomes in patients with FLT3-ITD acute myeloid leukemia prior to stem cell transplant and after relapse post-transplant. *American Journal of Hematology* **89,** 936–938 (2014).
79. Sandmaier, B. M. *et al.* Results of a phase 1 study of quizartinib as maintenance therapy in subjects with acute myeloid leukemia in remission following allogeneic hematopoietic stem cell transplant. *Am. J. Hematol.* **93,** 222–231 (2018).
80. Li, G. X., Wang, L., Yaghmour, B., Ramsingh, G. & Yaghmour, G. The role of FLT3 inhibitors as maintenance therapy following hematopoietic stem cell transplant. *Leukemia Research Reports* **10,** 26–36 (2018).
81. Pantziarka, P., Bouche, G., Meheus, L., Sukhatme, V. & Sukhatme, V. P. The Repurposing Drugs in Oncology (ReDO) Project. *ecancermedicalscience* **8,** (2014).
82. Sleire, L. *et al.* Drug repurposing in cancer. *Pharmacological Research* **124,** 74–91 (2017).
83. Pantziarka, P., Bouche, G., Meheus, L., Sukhatme, V. & Sukhatme, V. P. Repurposing drugs in your medicine cabinet: Untapped opportunities for cancer therapy? *Future Oncology* **11,** 181–184 (2015).
84. Gupta, S. C., Sung, B., Prasad, S., Webb, L. J. & Aggarwal, B. B. Cancer drug discovery by repurposing: Teaching new tricks to old dogs. *Trends in Pharmacological Sciences* **34,** 508–517 (2013).
85. Sukhai, M. A. *et al.* New sources of drugs for hematologic malignancies. *Blood* **117,** 6747–6755 (2011).
86. Nosengo, N. Can you teach old drugs new tricks? *Nature* **534,** 314–316 (2016).
87. Research, C. for D. E. and. Information for Consumers (Drugs) - The FDA's Drug Review Process: Ensuring Drugs Are Safe and Effective. *Food Drug Adm.* (2017).
88. Beaver, J. A. *et al.* A 25-Year Experience of US Food and Drug Administration Accelerated Approval of Malignant Hematology and Oncology Drugs and Biologics: A Review. *JAMA Oncol.* **4,** 849–856 (2018).
89. Gurova, K. New hopes from old drugs: Revisiting DNA-binding small molecules as anticancer agents. *Future Oncology* **5,** 1685–1704 (2009).
90. Li, F., Zhao, C. & Wang, L. Molecular-targeted agents combination therapy for cancer: Developments and potentials. *International Journal of Cancer* **134,** 1257–1269 (2014).
91. Pushpakom, S. *et al.* Drug repurposing: Progress, challenges and recommendations. *Nature Reviews Drug Discovery* **18,** 41–58 (2018).
92. Pantziarka, P., Pirmohamed, M. & Mirza, N. New uses for old drugs. *BMJ* **361,** k2701 (2018).
93. Diggle, G. E. Thalidomide: 40 years on. *Int. J. Clin. Pract.* **55,** 627–31 (2001).
94. Pfizer's Expiring Viagra Patent Adversely Affects Other Drugmakers Too. Available at: https://www.forbes.com/sites/investor/2013/12/20/pfizers-expiring-viagra-patent-adversely-

affects-other-drugmakers-too/#23d9f7d168d4. (Accessed: 29th October 2019)
95. Bertolini, F., Sukhatme, V. P. & Bouche, G. Drug repurposing in oncology—patient and health systems opportunities. *Nat. Publ. Gr.* **12,** (2015).
96. Lamb, J. *et al.* The Connectivity Small Molecules , Map : Genes , Using to Connect and Disease Signatures. *Adv. Sci.* **313,** 1929–1936 (2012).
97. Iorio, F. *et al.* A semi-supervised approach for refining transcriptional signatures of drug response and repositioning predictions. *PLoS One* **10,** (2015).
98. Oprea, T. I., Tropsha, A., Faulon, J. L. & Rintoul, M. D. Systems chemical biology. *Nature Chemical Biology* **3,** 447–450 (2007).
99. Yang, L. & Agarwal, P. Systematic drug repositioning based on clinical side-effects. *PLoS One* **6,** (2011).
100. Campillos, M., Kuhn, M., Gavin, A. C., Jensen, L. J. & Bork, P. Drug target identification using side-effect similarity. *Science (80-. ).* **321,** 263–266 (2008).
101. Kitchen, D. B., Decornez, H., Furr, J. R. & Bajorath, J. Docking and scoring in virtual screening for drug discovery: methods and applications. *Nat. Rev. Drug Discov.* **3,** 935–949 (2004).
102. Sanseau, P. *et al.* Use of genome-wide association studies for drug repositioning. *Nature Biotechnology* **30,** 317–320 (2012).
103. Jensen, P. B., Jensen, L. J. & Brunak, S. Mining electronic health records: Towards better research applications and clinical care. *Nature Reviews Genetics* **13,** 395–405 (2012).
104. Swinney, D. C. & Anthony, J. How were new medicines discovered? *Nat. Rev. Drug Discov.* **10,** 507–519 (2011).
105. Shukla, A. A. High Throughput Screening of Small Molecule Library: Procedure, Challenges and Future. *J. Cancer Prev. Curr. Res.* **5,** (2016).
106. Malo, N., Hanley, J. A., Cerquozzi, S., Pelletier, J. & Nadon, R. Statistical practice in high-throughput screening data analysis. *Nature Biotechnology* **24,** 167–175 (2006).
107. Zhang, X. D. Illustration of SSMD, z score, SSMD*, z* score, and t statistic for hit selection in RNAi high-throughput screens. *J. Biomol. Screen.* **16,** 775–785 (2011).
108. Birmingham, A. *et al.* Statistical methods for analysis of high-throughput RNA interference screens. *Nature Methods* **6,** 569–575 (2009).
109. Pantziarka, P., Bouche, G. & André, N. 'Hard' drug repurposing for precision oncology: The missing link? *Frontiers in Pharmacology* **9,** (2018).
110. Ho, K. V., Solimando, D. A. & Waddell, J. A. Clofarabine and Cytarabine Regimen for Acute Myeloid Leukemia. *Hosp. Pharm.* **50,** 969–974 (2015).
111. ReDO project.
112. Pantziarka, P. *et al.* Redo_DB: The repurposing drugs in oncology database. *Ecancermedicalscience* **12,** (2018).
113. Pantziarka, P. *et al.* Repurposing non-cancer Drugs in Oncology — How many drugs are out there? *bioRxiv* **1,** (2017).
114. Matchett, K. B. *et al.* High-Throughput Screen Identification of Albendazole As a Novel Repurposed Drug in Acute Myeloid Leukaemia. *Blood* **130,** 5062 LP-5062 (2017).
115. Spagnuolo, P. A. *et al.* The antihelmintic flubendazole inhibits microtubule function through a mechanism distinct from Vinca alkaloids and displays preclinical activity in leukemia and myeloma. *Blood* **115,** 4824–4833 (2010).
116. Matchett, K. B. *et al.* Mebendazole: A candidate FDA approved drug for repurposing in leukaemia. (2016).
117. Lara-Castillo, M. C. *et al.* Repositioning of bromocriptine for treatment of acute myeloid leukemia. *J. Transl. Med.* **14,** (2016).
118. Wang, F. *et al.* Metformin synergistically sensitizes FLT3-ITD-positive acute myeloid leukemia to sorafenib by promoting mTOR-mediated apoptosis and autophagy. *Leuk. Res.* **39,** 1421–1427 (2015).
119. Sabnis, H. S. *et al.* Synergistic cell death in FLT3-ITD positive acute myeloid leukemia by combined treatment with metformin and 6-benzylthioinosine. *Leuk. Res.* **50,** 132–140 (2016).
120. Shadman, M. *et al.* Idarubicin, cytarabine, and pravastatin as induction therapy for untreated acute myeloid leukemia and high-risk myelodysplastic syndrome. *Am. J. Hematol.* **90,** 483–486 (2015).
121. Advani, A. S. *et al.* SWOG0919: A Phase 2 study of idarubicin and cytarabine in

combination with pravastatin for relapsed acute myeloid leukaemia. *Br. J. Haematol.* **167,** 233–237 (2014).
122. Eriksson, A. *et al.* Drug screen in patient cells suggests quinacrine to be repositioned for treatment of acute myeloid leukemia. *Blood Cancer J.* **5,** e307 (2015).
123. Sharma, A. *et al.* Pyrimethamine as a Potent and Selective Inhibitor of Acute Myeloid Leukemia Identified by High-throughput Drug Screening. *Curr. Cancer Drug Targets* **16,** 818–828 (2016).
124. Borden, K. L. B. & Culjkovic-Kraljacic, B. Ribavirin as an anti-cancer therapy: Acute myeloid leukemia and beyond? *Leukemia and Lymphoma* **51,** 1805–1815 (2010).
125. Tickenbrock, L. *et al.* Increased HDAC1 deposition at hematopoietic promoters in AML and its association with patient survival. *Leuk. Res.* **35,** 620–625 (2011).
126. Blaheta, R., Nau, H., Michaelis, M. & Cinatl.Jr, J. Valproate and Valproate-Analogues: Potent Tools to Fight Against Cancer. *Curr. Med. Chem.* **9,** 1417–1433 (2012).
127. Göttlicher, M. *et al.* Valproic acid defines a novel class of HDAC inhibitors inducing differentiation of transformed cells. *EMBO J.* **20,** 6969–6978 (2001).
128. Hetz, C. The unfolded protein response: Controlling cell fate decisions under ER stress and beyond. *Nature Reviews Molecular Cell Biology* **13,** 89–102 (2012).
129. Marcu, M. G. *et al.* Heat Shock Protein 90 Modulates the Unfolded Protein Response by Stabilizing IRE1 . *Mol. Cell. Biol.* **22,** 8506–8513 (2002).
130. Corazzari, M., Gagliardi, M., Fimia, G. M. & Piacentini, M. Endoplasmic reticulum stress, unfolded protein response, and cancer cell fate. *Front. Oncol.* **7,** (2017).
131. Yoshida, H., Matsui, T., Yamamoto, A., Okada, T. & Mori, K. XBP1 mRNA is induced by ATF6 and spliced by IRE1 in response to ER stress to produce a highly active transcription factor. *Cell* **107,** 881–891 (2001).
132. Lee, K. *et al.* IRE1-mediated unconventional mRNA splicing and S2P-mediated ATF6 cleavage merge to regulate XBP1 in signaling the unfolded protein response. *Genes Dev.* **16,** 452–466 (2002).
133. Calfon, M. *et al.* IRE1 couples endoplasmic reticulum load to secretory capacity by processing the XBP-1 mRNA. *Nature* **415,** 92–96 (2002).
134. Acosta-Alvear, D. *et al.* XBP1 Controls Diverse Cell Type- and Condition-Specific Transcriptional Regulatory Networks. *Mol. Cell* **27,** 53–66 (2007).
135. Lee, A.-H., Iwakoshi, N. N. & Glimcher, L. H. XBP-1 Regulates a Subset of Endoplasmic Reticulum Resident Chaperone Genes in the Unfolded Protein Response. *Mol. Cell. Biol.* **23,** 7448–7459 (2003).
136. Ron, D. & Hubbard, S. R. How IRE1 Reacts to ER Stress. *Cell* **132,** 24–26 (2008).
137. Chen, Y. & Brandizzi, F. IRE1: ER stress sensor and cell fate executor. *Trends in Cell Biology* **23,** 547–555 (2013).
138. Ameri, K. & Harris, A. L. Activating transcription factor 4. *International Journal of Biochemistry and Cell Biology* **40,** 14–21 (2008).
139. Schröder, M. & Kaufman, R. J. THE MAMMALIAN UNFOLDED PROTEIN RESPONSE. *Annu. Rev. Biochem.* **74,** 739–789 (2005).
140. Song, B., Scheuner, D., Ron, D., Pennathur, S. & Kaufman, R. J. Chop deletion reduces oxidative stress, improves β cell function, and promotes cell survival in multiple mouse models of diabetes. *J. Clin. Invest.* **118,** 3378–3389 (2008).
141. Marciniak, S. J. *et al.* CHOP induces death by promoting protein synthesis and oxidation in the stressed endoplasmic reticulum. *Genes Dev.* **18,** 3066–3077 (2004).
142. Woo, C. W., Kutzler, L., Kimball, S. R. & Tabas, I. Toll-like receptor activation suppresses ER stress factor CHOP and translation inhibition through activation of eIF2B. *Nat. Cell Biol.* **14,** 192–200 (2012).
143. Chitnis, N. S. *et al.* MiR-211 Is a Prosurvival MicroRNA that Regulates chop Expression in a PERK-Dependent Manner. *Mol. Cell* **48,** 353–364 (2012).
144. Guo, F.-J. *et al.* XBP1S protects cells from ER stress-induced apoptosis through Erk1/2 signaling pathway involving CHOP. *Histochem. Cell Biol.* **138,** 447–460 (2012).
145. Haze, K., Yoshida, H., Yanagi, H., Yura, T. & Mori, K. Mammalian transcription factor ATF6 is synthesized as a transmembrane protein and activated by proteolysis in response to endoplasmic reticulum stress. *Mol. Biol. Cell* **10,** 3787–3799 (1999).
146. Yamamoto, K. *et al.* Transcriptional Induction of Mammalian ER Quality Control Proteins Is Mediated by Single or Combined Action of ATF6α and XBP1. *Dev. Cell* **13,** 365–376

(2007).
147. Szegezdi, E., Logue, S. E., Gorman, A. M. & Samali, A. Mediators of endoplasmic reticulum stress-induced apoptosis. *EMBO Reports* **7,** 880–885 (2006).
148. Szegezdi, E., MacDonald, D. C., Chonghaile, T. N., Gupta, S. & Samali, A. Bcl-2 family on guard at the ER. *American Journal of Physiology - Cell Physiology* **296,** (2009).
149. Westphal, D., Dewson, G., Czabotar, P. E. & Kluck, R. M. Molecular biology of Bax and Bak activation and action. *Biochimica et Biophysica Acta - Molecular Cell Research* **1813,** 521–531 (2011).
150. Samali, A., Zhivotovsky, B., Jones, D., Nagata, S. & Orrenius, S. Apoptosis: Cell death defined by caspase activation [1]. *Cell Death and Differentiation* **6,** 495–496 (1999).
151. Cazanave, S. C. *et al.* CHOP and AP-1 cooperatively mediate PUMA expression during lipoapoptosis. *Am. J. Physiol. - Gastrointest. Liver Physiol.* **299,** (2010).
152. Ghosh, A. P., Klocke, B. J., Ballestas, M. E. & Roth, K. A. CHOP potentially co-operates with FOXO3a in neuronal cells to regulate PUMA and BIM expression in response to ER stress. *PLoS One* **7,** (2012).
153. McCullough, K. D., Martindale, J. L., Klotz, L.-O., Aw, T.-Y. & Holbrook, N. J. Gadd153 Sensitizes Cells to Endoplasmic Reticulum Stress by Down-Regulating Bcl2 and Perturbing the Cellular Redox State. *Mol. Cell. Biol.* **21,** 1249–1259 (2001).
154. Yoshida, H., Uemura, A. & Mori, K. pXBP1(U), a negative regulator of the unfolded protein response activator pXBP1(S), targets ATF6 but not ATF4 in proteasome-mediated degradation. *Cell Struct. Funct.* **34,** 1–10 (2009).
155. Donovan, N., Becker, E. B. E., Konishi, Y. & Bonni, A. JNK phosphorylation and activation of bad couples the stress-activated signaling pathway to the cell death machinery. *J. Biol. Chem.* **277,** 40944–40949 (2002).
156. Lei, K. & Davis, R. J. JNK phosphorylation of Bim-related members of the Bcl2 family induces Bax-dependent apoptosis. *Proc. Natl. Acad. Sci. U. S. A.* **100,** 2432–2437 (2003).
157. Upton, J.-P., Wang, L., Han, D. & Wang, E. S. IRE1alpha cleaves select microRNAs During ER Stress to derepress translation of proapoptotic Caspase-2. *Nat. Rev. Mol. Cell Biol.* **8,** 519–29 (2007).
158. Wang, Q. *et al.* ERAD inhibitors integrate ER stress with an epigenetic mechanism to activate BH3-only protein NOXA in cancer cells. *Proc. Natl. Acad. Sci. U. S. A.* **106,** 2200–2205 (2009).
159. Lin, W. C. *et al.* Endoplasmic reticulum stress stimulates p53 expression through NF-κB activation. *PLoS One* **7,** (2012).
160. Pagliarini, V. *et al.* Downregulation of E2F1 during ER stress is required to induce apoptosis. *J. Cell Sci.* **128,** 1166–1179 (2015).
161. Ohoka, N., Yoshii, S., Hattori, T., Onozaki, K. & Hayashi, H. TRB3, a novel ER stress-inducible gene, is induced via ATF4-CHOP pathway and is involved in cell death. *EMBO J.* **24,** 1243–1255 (2005).
162. Romero-Ramirez, L. *et al.* XBP1 is essential for survival under hypoxic conditions and is required for tumor growth. *Cancer Res.* **64,** 5943–5947 (2004).
163. Ranganathan, A. C., Adam, A. P., Zhang, L. & Aguirre-Ghiso, J. A. Tumor cell dormancy induced by p38SAPK and ER-stress signaling: An adaptive advantage for metastatic cells? *Cancer Biology and Therapy* **5,** 729–735 (2006).
164. Fels, D. R. & Koumenis, C. The PERK/eIF2α/ATF4 module of the UPR in hypoxia resistance and tumor growth. *Cancer Biology and Therapy* **5,** 723–728 (2006).
165. Ma, X. H. *et al.* Targeting ER stress-induced autophagy overcomes BRAF inhibitor resistance in melanoma. *J. Clin. Invest.* **124,** 1406–1417 (2014).
166. Corazzari, M. *et al.* Oncogenic BRAF induces chronic ER stress condition resulting in increased basal autophagy and apoptotic resistance of cutaneous melanoma. *Cell Death Differ.* **22,** 946–958 (2015).
167. Giglio, P., Fimia, G. M., Lovat, P. E., Piacentini, M. & Corazzari, M. Fateful music from a talented orchestra with a wicked conductor: Connection between oncogenic BRAF, ER stress, and autophagy in human melanoma. *Mol. Cell. Oncol.* **2,** (2015).
168. Carrasco, D. R. *et al.* The Differentiation and Stress Response Factor XBP-1 Drives Multiple Myeloma Pathogenesis. *Cancer Cell* **11,** 349–360 (2007).
169. Garg, A. D., Maes, H., van Vliet, A. R. & Agostinis, P. Targeting the hallmarks of cancer with therapy-induced endoplasmic reticulum (ER) stress. *Molecular and Cellular Oncology*

**2,** (2015).
170. Chen, X. *et al.* XBP1 promotes triple-negative breast cancer by controlling the HIF1α pathway. *Nature* **508,** 103–107 (2014).
171. Davies, M. P. A. *et al.* Expression and splicing of the unfolded protein response gene XBP-1 are significantly associated with clinical outcome of endocrine-treated breast cancer. *Int. J. Cancer* **123,** 85–88 (2008).
172. Kharabi Masouleh, B. *et al.* Drugging the unfolded protein response in acute leukemias. *Journal of Hematology and Oncology* **8,** (2015).
173. Dudek, J. *et al.* Functions and pathologies of BiP and its interaction partners. *Cellular and Molecular Life Sciences* **66,** 1556–1569 (2009).
174. Zhang, Y., Liu, R., Ni, M., Gill, P. & Lee, A. S. Cell surface relocalization of the endoplasmic reticulum chaperone and unfolded protein response regulator GRP78/BiP. *J. Biol. Chem.* **285,** 15065–15075 (2010).
175. Lee, A. S. GRP78 induction in cancer: Therapeutic and prognostic implications. *Cancer Research* **67,** 3496–3499 (2007).
176. Pyrko, P., Schöntha, A. H., Hofman, F. M., Chen, T. C. & Lee, A. S. The unfolded protein response regulator GRP78/BiP as a novel target for increasing chemosensitivity in malignant gliomas. *Cancer Res.* **67,** 9809–9816 (2007).
177. Dong, D. *et al.* Critical role of the stress chaperone GRP78/BiP in tumor proliferation, survival, and tumor angiogenesis in transgene-induced mammary tumor development. *Cancer Res.* **68,** 498–505 (2008).
178. Jamora, C., Dennert, G. & Lee, A. S. Inhibition of tumor progression by suppression of stress protein GRP78/BiP induction in fibrosarcoma B/C10ME. *Proc. Natl. Acad. Sci. U. S. A.* **93,** 7690–7694 (1996).
179. Wang, M. & Kaufman, R. J. The impact of the endoplasmic reticulum protein-folding environment on cancer development. *Nature Reviews Cancer* **14,** 581–597 (2014).
180. Hart, L. S. *et al.* ER stress-mediated autophagy promotes Myc-dependent transformation and tumor growth. *J. Clin. Invest.* **122,** 4621–4634 (2012).
181. Bobrovnikova-Marjon, E. *et al.* PERK promotes cancer cell proliferation and tumor growth by limiting oxidative DNA damage. *Oncogene* **29,** 3881–3895 (2010).
182. Huber, A. L. *et al.* P58 IPK -Mediated Attenuation of the Proapoptotic PERK-CHOP Pathway Allows Malignant Progression upon Low Glucose. *Mol. Cell* **49,** 1049–1059 (2013).
183. Nakagawa, H. *et al.* ER Stress Cooperates with Hypernutrition to Trigger TNF-Dependent Spontaneous HCC Development. *Cancer Cell* **26,** 331–343 (2014).
184. Khan, M. M. *et al.* The Fusion Oncoprotein PML-RARα Induces Endoplasmic Reticulum (ER)-associated Degradation of N-CoR and ER Stress. *J. Biol. Chem.* **279,** 11814–11824 (2004).
185. Foucquier, J. & Guedj, M. Analysis of drug combinations: current methodological landscape. *Pharmacology Research and Perspectives* **3,** (2015).
186. Gupta, S., Samali, A., Fitzgerald, U. & Deegan, S. Methods for monitoring endoplasmic reticulum stress and the unfolded protein response. *International Journal of Cell Biology* (2010). doi:10.1155/2010/830307
187. Chalmers, F., Sweeney, B., Cain, K. & Bulleid, N. J. Inhibition of IRE1α-mediated XBP1 mRNA cleavage by XBP1 reveals a novel regulatory process during the unfolded protein response. *Wellcome Open Research* **2,** (2017).
188. Reiter, K. *et al.* Tyrosine kinase inhibition increases the cell surface localization of FLT3-ITD and enhances FLT3-directed immunotherapy of acute myeloid leukemia. *Leukemia* **32,** 313–322 (2018).
189. Fiskus, W. *et al.* Auranofin induces lethal oxidative and endoplasmic reticulum stress and exerts potent preclinical activity against chronic lymphocytic leukemia. *Cancer Res.* **74,** 2520–2532 (2014).
190. Liu, N. *et al.* Clinically used antirheumatic agent auranofin is a proteasomal deubiquitinase inhibitor and inhibits tumor growth. *Oncotarget* **5,** 5453–5471 (2014).
191. Huang, H. *et al.* Two clinical drugs deubiquitinase inhibitor auranofin and aldehyde dehydrogenase inhibitor disulfiram trigger synergistic anti-tumor effects in vitro and in vivo. *Oncotarget* **7,** 2796–808 (2016).
192. Xiang, W. *et al.* Pyrvinium selectively targets blast phase-chronic myeloid leukemia

through inhibition of mitochondrial respiration. *Oncotarget* **6,** 33769–33780 (2015).
193. Aroua, N. *et al.* <em>In Vivo</em> Response to Cytarabine Chemotherapy Uncovers the Role of the Oxidative and Energetic Metabolism in the Chemoresistance of Human Primary AML Stem Cells. *Blood* **126,** 4269 LP-4269 (2015).
194. Warmuth, M., Kim, S., Gu, X. J., Xia, G. & Adrián, F. Ba/F3 cells and their use in kinase drug discovery. *Current Opinion in Oncology* **19,** 55–60 (2007).
195. Zhang, J., Li, X., Han, X., Liu, R. & Fang, J. Targeting the Thioredoxin System for Cancer Therapy. *Trends in Pharmacological Sciences* **38,** 794–808 (2017).
196. Ishii, I., Harada, Y. & Kasahara, T. Reprofiling a classical anthelmintic, pyrvinium pamoate, as an anti-cancer drug targeting mitochondrial respiration. *Front. Oncol.* **2,** (2012).
197. Shang, S., Hua, F. & Hu, Z. W. The regulation of β-catenin activity and function in cancer: Therapeutic opportunities. *Oncotarget* **8,** 33972–33989 (2017).
198. Staal, F. J. T., Famili, F., Perez, L. G. & Pike-Overzet, K. Aberrant Wnt signaling in leukemia. *Cancers* **8,** (2016).
199. Wei, A. H. & Tiong, I. S. Midostaurin, enasidenib, CPX-351, gemtuzumab ozogamicin, and venetoclax bring new hope to AML. *Blood* **130,** 2469–2474 (2017).
200. FDA Approves 2 Drugs for Acute Myeloid Leukemia (AML). Available at: https://www.cancer.org/latest-news/fda-approves-2-drugs-for-acute-myeloid-leukemia-aml.html. (Accessed: 6th November 2019)
201. Sun, W., Sanderson, P. E. & Zheng, W. Drug combination therapy increases successful drug repositioning. *Drug Discovery Today* **21,** 1189–1195 (2016).
202. Capparelli, E. V., Bricker-Ford, R., Rogers, M. J., McKerrow, J. H. & Reed, S. L. Phase I clinical trial results of auranofin, a novel antiparasitic agent. *Antimicrob. Agents Chemother.* **61,** (2017).
203. Smith, T. C., Kinkel, A. W., Gryczko, C. M. & Goulet, J. R. Absorption of pyrvinium pamoate. *Clin. Pharmacol. Ther.* **19,** 802–806 (1976).
204. Roder, C. & Thomson, M. J. Auranofin: Repurposing an Old Drug for a Golden New Age. *Drugs R D* **15,** 13–20 (2015).
205. Huang, R. *et al.* The NCATS Pharmaceutical Collection: a 10-year update. *Drug Discov. Today* (2019). doi:10.1016/j.drudis.2019.09.019
206. Momtazi-borojeni, A. A., Abdollahi, E., Ghasemi, F., Caraglia, M. & Sahebkar, A. The novel role of pyrvinium in cancer therapy. *J. Cell. Physiol.* (2017). doi:10.1002/jcp.26006
207. Hanahan, D. & Weinberg, R. A. The hallmarks of cancer. *Cell* **100,** 57–70 (2000).
208. Debnath, A. *et al.* A high-throughput drug screen for Entamoeba histolytica identifies a new lead and target. *Nat. Med.* **18,** 956–960 (2012).
209. Donnelly, N., Gorman, A. M., Gupta, S. & Samali, A. The eIF2α kinases: Their structures and functions. *Cellular and Molecular Life Sciences* **70,** 3493–3511 (2013).
210. Costa, R. *et al.* Impaired Mitochondrial ATP Production Downregulates Wnt Signaling via ER Stress Induction. *Cell Rep.* **28,** 1949–1960.e6 (2019).
211. Harada, Y., Ishii, I., Hatake, K. & Kasahara, T. Pyrvinium pamoate inhibits proliferation of myeloma/erythroleukemia cells by suppressing mitochondrial respiratory complex I and STAT3. *Cancer Lett.* **319,** 83–88 (2012).
212. Horndasch, M. *et al.* The C/EBP homologous protein CHOP (GADD153) is an inhibitor of Wnt/TCF signals. *Oncogene* **25,** 3397–3407 (2006).
213. Verras, M., Papandreou, I., Lim, A. L. & Denko, N. C. Tumor Hypoxia Blocks Wnt Processing and Secretion through the Induction of Endoplasmic Reticulum Stress. *Mol. Cell. Biol.* **28,** 7212–7224 (2008).

# 6 Appendix

During the first year of my PhD studentship, while I was setting up the conditions for the HTS drug repurposing screen, I had worked on a project entitled "Cell-therapy using extracellular vesicles isolated from genetically-engineered cell lines expressing the transmembrane TNF-Related Apoptosis-Inducing Ligand (mTRAIL)", which was meant to be my thesis project. Unfortunately, the experiments repeatedly yielded conflicting results, and the hypothesis that TRAIL-expressing EVs can constitute an anti-cancer treatment was not confirmed, especially *in vivo*, as detailed below. This led me to change my thesis project, with the approval of my supervising team.

In this appendix, I have included a brief summary of this project, as requested by the SEMM rules.

## 6.1 Cell-therapy using extracellular vesicles isolated from genetically-engineered cell lines expressing the transmembrane TNF-Related Apoptosis-Inducing Ligand (mTRAIL)

### Outline of the project

### Background

In recent years, several therapeutic strategies that promote tumour cell death have been developed. Indeed, the best therapeutic strategy for cancer treatment is the use of agents that are capable of killing cancer cells without affecting normal cells. Tumour necrosis factor (TNF)-related apoptosis-inducing ligand (TRAIL), a member of the TNF superfamily, is able to initiate apoptosis selectively in cancer cells rendering it an appealing candidate for the development of targeted cancer therapy. TRAIL binds to five different receptors including the DR4 and DR5 agonist receptors that induce apoptotic

response.[1] Several studies reported promising results *in vitro*; thus, recombinant human TRAIL/Apo-2L (Dulanermin) was tested, in phase I/II clinical trials recruiting patients affected by different type of cancers. Dulanermin was generally well tolerated by patients, but the majority of the studies reported relatively little clinical efficacy.[1]

Recent studies demonstrated that TRAIL has a more potent anti-cancer activity when it is bound to cell membrane (mTRAIL) compared to its soluble form.[2,3] Cell-based therapy is a promising but challenging approach: side effects associated with the infusion of cells and cell accumulation in lungs and kidneys have to be considered. One possible alternative approach is the used of cell-free systems such as liposomes and extracellular vesicles (EVs). EVs mediate intercellular communication through the transmission of various substances such as proteins, bioactive lipids and nucleic acids influencing physiological and pathological functions of target cells.[4,5]

EVs are isolated from the vast majority of cell types and biological fluids. Moreover, they can be classified based on their origin in exosomes, micro-vesicles and apoptotic bodies. EVs are 100 or 1000 times smaller than a cell, thus less toxic effects and a uniform distribution in the organism may be expected.

## Project design

The project originated from the observation that mTRAIL has a potent antitumour activity and is able to selectively target cancer cells. EVs, a cell free system, may represent a valid delivery method for the TRAIL molecule.

The aim of the project was to determine the efficacy of TRAIL-expressing EVs against different types of cancer cells adopting a multidisciplinary approach, both *in vitro* and *in vivo*. For the achievement of this goal, the following tasks were performed:

1. Generation of TRAIL-expressing cell lines (HL60, K562 and mesenchymal cells) and evaluation of EV production

2. Assessment of treatment efficacy with TRAIL-expressing EVs on different cancer cell lines *in vitro*
3. Assessment of treatment efficacy *in vivo*

## Summary of results

Generation of TRAIL-expressing cell lines and EVs production

For EVs production, we initially used standard non-adherent cell lines that are easy to grow in unlimited quantities. HL60 and K562 cell lines were selected and infected with a TRAIL-expressing lentiviral vector. TRAIL expression was assessed by flow cytometry and western blotting **(Figure 6.1 A and B)**. Infected and non-infected cells were grown for 48h in low-serum medium and the resulting conditioned medium harvested and ultracentrifuged to recover TRAIL+ (TRAIL) and TRAIL- (WT) EVs. We evaluated TRAIL expression by the EVs using western blot analysis **(Figure 6.1 B)**.

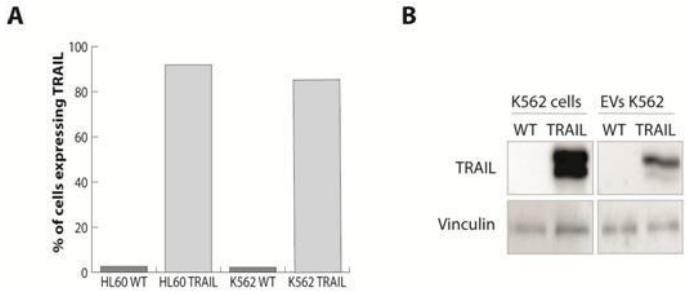


***Figure 6.1: Detection of TRAIL expression in cell lines and EVs isolated from them***
*(A) Flow cytometry analysis of TRAIL expression on HL60 and K562 cell lines. Cells were harvested and labelled with PE-TRAIL antibody. Histogram illustrates the percentage of TRAIL positive cells. (B) Representative immunoblot analysis to confirm TRAIL expression on K562 cells and EVs derived from them. The expression of TRAIL was analysed by SDS-PAGE and western blotting. Vinculin levels were used as a loading control.*

Assessment of treatment efficacy *in vitro* and *in vivo*

We next determined the efficacy of TRAIL EVs in inhibiting growth of MDA-MB-231 breast cancer and MEL1300 melanoma cell lines, both *in vitro* and *in vivo*. The *in vitro* survival test showed a modest efficacy of TRAIL EVs **(Figure 6.2)**. Moreover, their efficacy was variable from one production to the next.

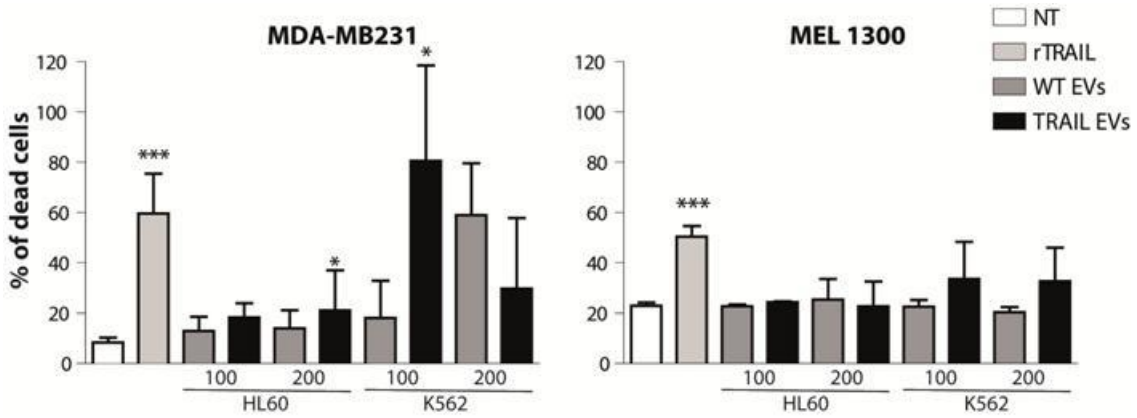


***Figure 6.2: EVs induce apoptosis of cancer cells***
*Effect of TRAIL EVs on different cancer cell lines. MDA-MB231 and MEL1300 were cultured in a six-well plate and treated for 24 h with EVs (WT and TRAIL) isolated from conditioned medium of HL60 and K562 cell lines at two different concentrations (100 μg/ml and 200 μg/ml), or treated with 100 ng/ml of recombinant TRAIL (rTRAIL). Cells were harvested and labelled with Annexin V-AF647 and PI for apoptosis assay by flow cytometry. Data represent averages ± SD. * $p < 0.05$, ** $p < 0.01$ compared to not treated cells (NT) by Student t-test.*

---

Given that the response to treatment with TRAIL EVs was limited and different for the two cell lines, we assessed the expression of TRAIL receptors, namely DR4 and DR5, by real time RT-PCR and flow cytometry, as it is known that TRAIL induces apoptosis through these two main receptors. We noticed a difference between the amount of mRNA and the protein for the MEL1300 cells, but we confirmed the expression of one of the two death receptors in both the cell lines tested **(Figure 6.3 A and B)**.

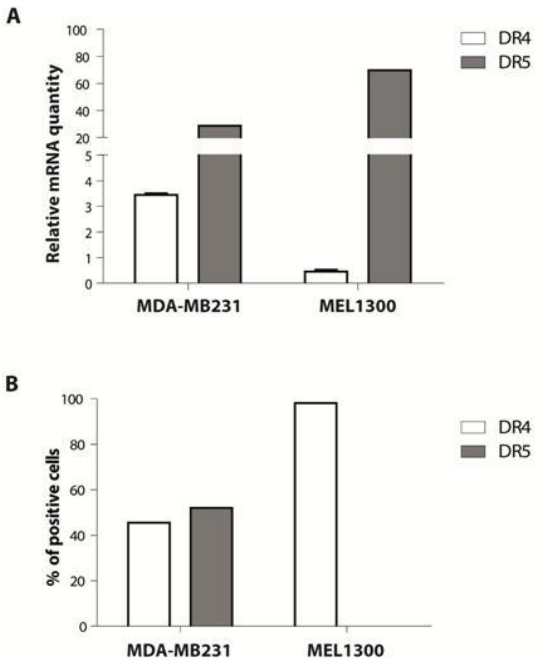


***Figure 6.3: Detection of DR4 and DR5 expression in different cancer cell lines***
*(A) The relative mRNA levels of DR4 and DR5 receptors were quantified by real-time RT-PCR. All values were normalized using TBP as internal control. Values are presented as mean ± SD. (B) Flow cytometry analysis of DR4 and DR5 expression on MDA-MB231 and MEL1300 cell lines. Cells were harvested and labelled with FITC-DR4 and PE-DR5 antibodies. Histogram illustrates the percentage of DR4 and DR5 positive cells.*

---

The *in vivo* experiments were conducted on a subcutaneous *xenograft* model created by inoculating MDA-MB231 and MEL1300 into immunocompromised mice. Briefly, we injected $2x10^6$ of MDA-MB-231 or $2x10^5$ of MEL1300 cells in two different spots on the abdomen of NOD-scid IL2Rgamma$^{null}$ (NGS) mice, one on the right and one of the left. After a week from injection, all tumours were palpable, tumour volume was then measured and mice were randomized into five experimental groups that possessed the same average tumour volume. The groups included mice treated with TRAIL or WT EVs obtained from HL60 and K562 cell lines and with PBS as a control. Treatment was performed according to the therapeutic scheme illustrated in **Figure 6.4 A**. Tumour growth was monitored weekly by manually measuring the *xenografts* with a calliper. After 30 days from the beginning of treatment, mice were sacrificed due to the large size of tumours.

The treatment with TRAIL EVs produced from either cell line showed no significant effect on tumour growth in mice treated with TRAIL EVs compared to controls (PBS, only) **(Figure 6.4 B and C)**.

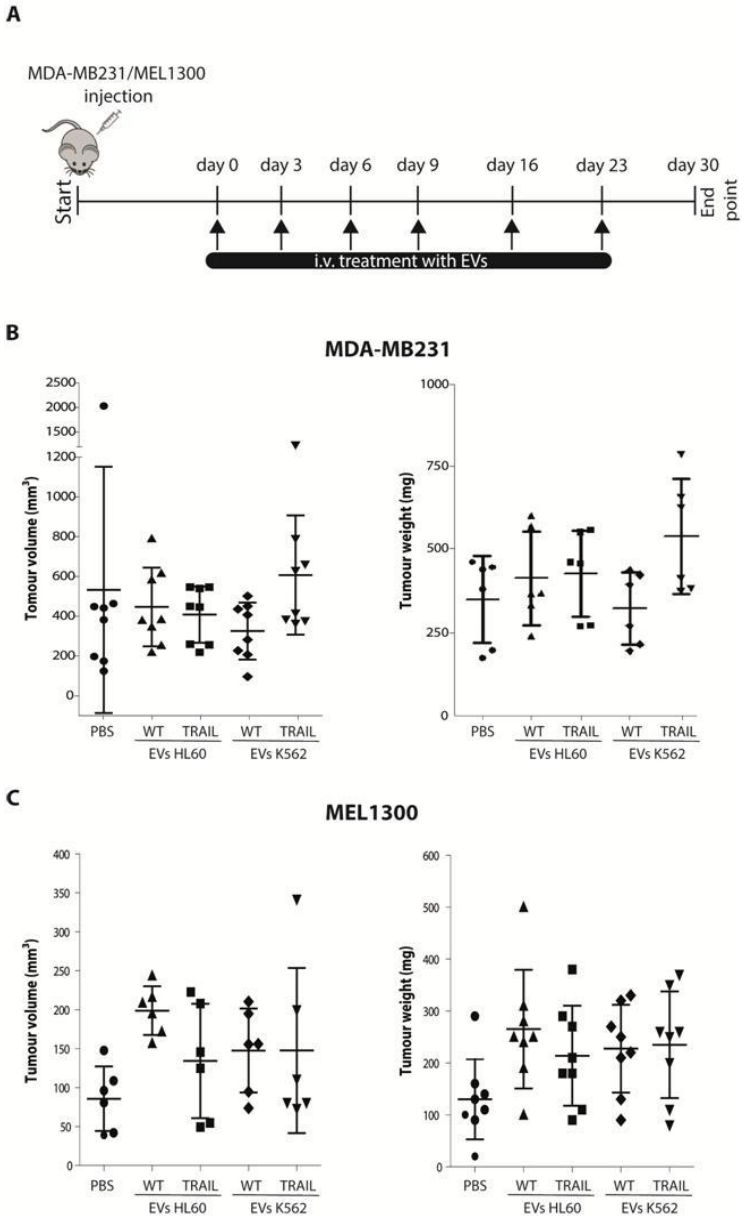


***Figure 6.4: In vivo effect of EVs***
*(A) Schematic representation of the experimental protocol used for the treatment with EVs. Mice were inoculated with MDA-MB231 or MEL1300 cells and treated with 200 µg of EVs at the indicated time points. (B) Left-hand side panel – tumour volume; right-hand side panel – tumour weight of tumours resected from mice inoculated with MDA-MB231 and treated with 200 µg EVs (WT and TRAIL) isolated from conditioned medium of HL60 and K562 cell lines. Means ± SD are reported. (C) Left-hand side panel – tumour volume; right-hand side pane l– tumour weight of tumours resected from mice inoculated with MEL1300 and treated with 200 µg EVs (WT and TRAIL) isolated from conditioned medium of HL60 and K562 cell lines. Means ± SD are reported.*

---

Despite a minimal effect at the macroscopic tumour growth level, immunohistochemical analysis revealed areas of extensive necrosis and apoptosis with haemorrhagic zones in

tumours removed from mice treated with TRAIL EVs and not in the control tumours suggesting TRAIL-dependent effect on tumour vasculature **(Figure 6.5 A and B)**.

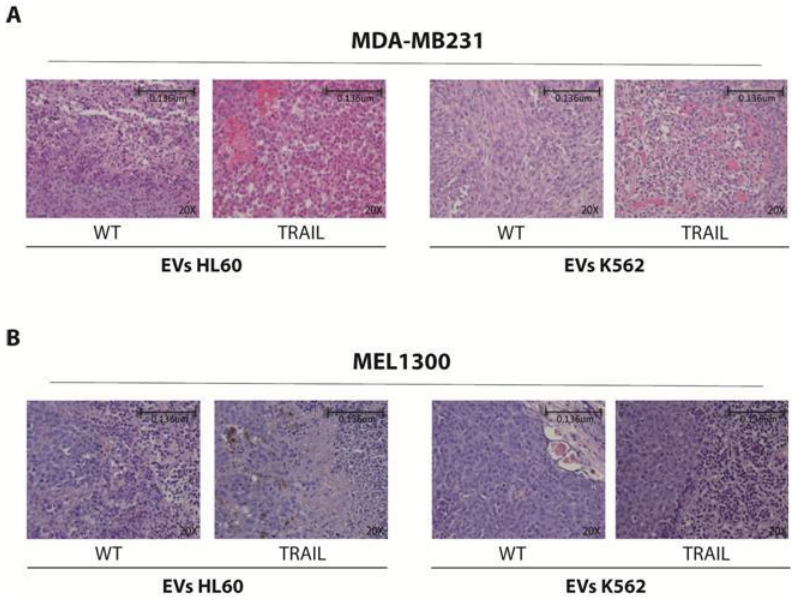


***Figure 6.5: Immunohistochemical analysis of xenograft tumours***
*Haematoxylin-eosin stained histological sections of xenograft tumours with MDA-MB231(A) and MEL1300 (B) upon EVs treatment.*

---

To further investigate this observation, we performed a third *in vivo* experiment using IVIS Illumina bioimaging system in order to refine the method of outcome measurement. Moreover, we tested if there was a synergistic effect between bevacizumab, a monoclonal antibody that inhibits angiogenesis, and TRAIL EVs produced from K562 on the MDA-MB-231 *xenograft* tumours. Two-hundred μg of EVs either WT and TRAIL were injected i.v. two times a week combined with 100 μg of bevacizubam injected i.p. No clear synergy was seen and bevacizumab alone was more efficacious than the EVs alone **(Figure 6.6)**. Taken together, these results show that EVs produced from common cell lines such as K562 and HL60 cannot be used for TRAIL EV therapy.

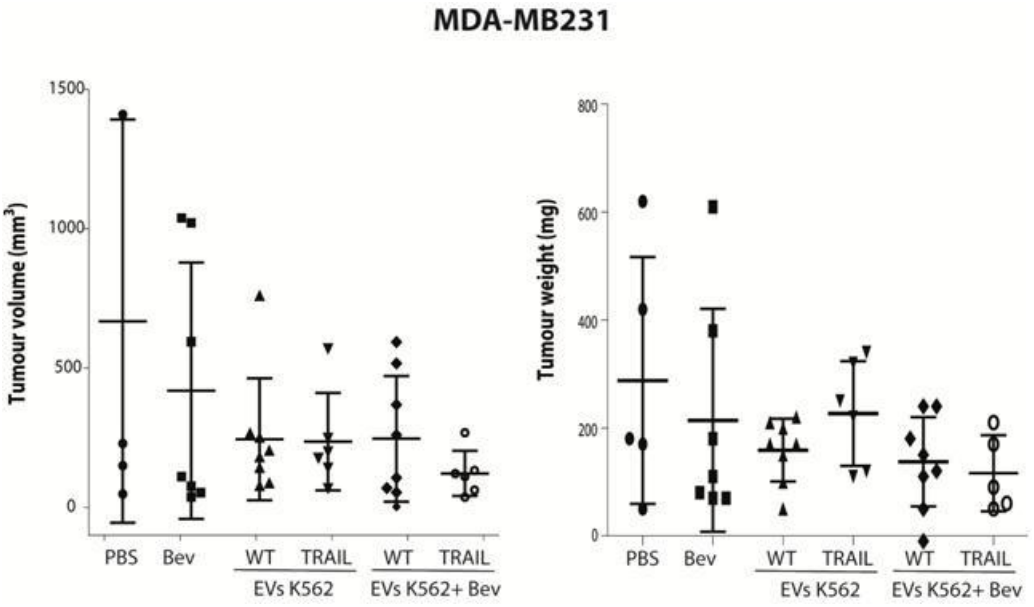


***Figure 6.6: In vivo effect of EVs***
*Left-hand side panel – tumour volume; right-hand side panel – tumour weight of tumours resected from mice inoculated with MDA-MB231 and treated with EVs (WT and TRAIL) isolated from conditioned medium of K562 cell line alone or in combination with bevacizumab. Means ± SD are reported.*

---

Generation of TRAIL-expressing MSC and EVs production

We next decided to adopt mesenchymal stem cells (MSC) as a source of EVs. Bone marrow samples were taken from 10 patients and MSC lines established. MSC were infected with the lentiviral TRAIL-expressing vector previously used for both HL60 and K562 cell lines. Infected and non-infected cells were grown for 72h in nonadherent condition and the resulting conditioned medium was harvested and ultracentrifuged to recover TRAIL and WT EVs. We confirmed TRAIL expression in MSC cells and in the corresponding EVs by western blotting **(Figure 6.7)**.

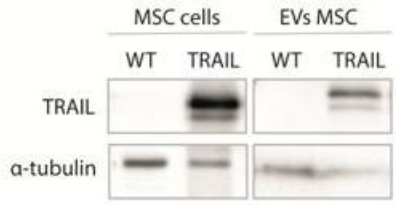


***Figure 6.7: Detection of TRAIL expression in MSC cells and EVs isolated from them***
*Representative immunoblot analysis to confirm TRAIL expression on MSC cells and EVs derived from them. The expression of TRAIL was analysed by SDS-PAGE and western blotting. α-tubulin levels were used as a loading control.*

---

Assessment of treatment efficacy *in vitro* and *in vivo*

We observed that TRAIL MSC-EVs reduced the viability of MDA-MB231, MEL1300 and SUDHL-4 cells more efficiently than cell-line-derived-EVs as confirmed by CellTiter-Glo (CTG) assay **(Figure 6.8)** and flow cytometry analysis upon AnnexinV/PI staining (data not shown).

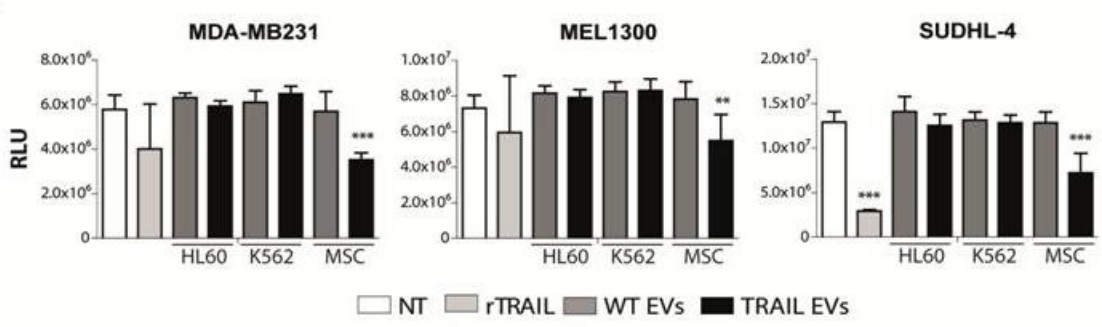


***Figure 6.8: Comparison of the effect of EVs isolated from cell lines and MSCs***
*Effect of TRAIL EVs on different cancer cell lines. Cells were cultured in 96-well plate and treated for 24 h with 50 µg/ml of EVs (WT and TRAIL) isolated from conditioned medium of HL60, K562 and MSC cells, or treated with 100 ng/ml of recombinant TRAIL (rTRAIL). Viability was evaluated using the CTG assay. Data represent averages ± SD. ** p < 0.01, *** p<0.001 compared to not treated cells (NT) by Student t-test.*

---

Unfortunately, primary MSC cells undergo senescence and, as expected, after 10 passages MSC cells stopped growing, changed morphology and became frankly senescent as

attested to by p16 expression **(Figure 6.9)**. Thus, they cannot be use for large-scale EVs production as they grow slowly and have a limited lifespan.

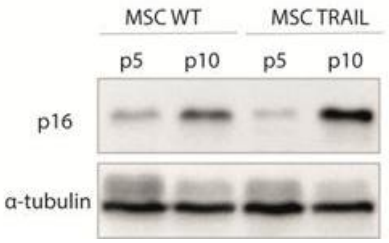


***Figure 6.9: MSC cells become senescence after limited passage number***
*Representative immunoblot analysis to confirm p16 expression on MSC cells both WT and TRAIL. The expression of p16 was analysed by SDS-PAGE and western blotting. α-tubulin levels were used as a loading control. p5, five passage number; p10 ten passage number.*

---

A hTERT-immortalised MSC (hTERT MSC) cell line[6] was sought and transduced with TRAIL. EVs were isolated using the same protocol as described above. The expression of TRAIL was confirmed both in cells and EVs derived from them **(Figure 6.10)**. We confirmed the efficacy of TRAIL EVs derived from hTERT MSC by performing Annexin V/PI staining (data not shown) and CTG luminescence assay **(Figure 6.11).**


***Figure 6.10: Detection of TRAIL expression in MSC hTERT cells and EVs isolated from them.***
*Representative immunoblot analysis to confirm TRAIL expression on MSChTERT cells and EVs derived from them. The expression of TRAIL was analysed by SDS-PAGE and western blotting. α-tubulin levels were used as a loading control.*

---

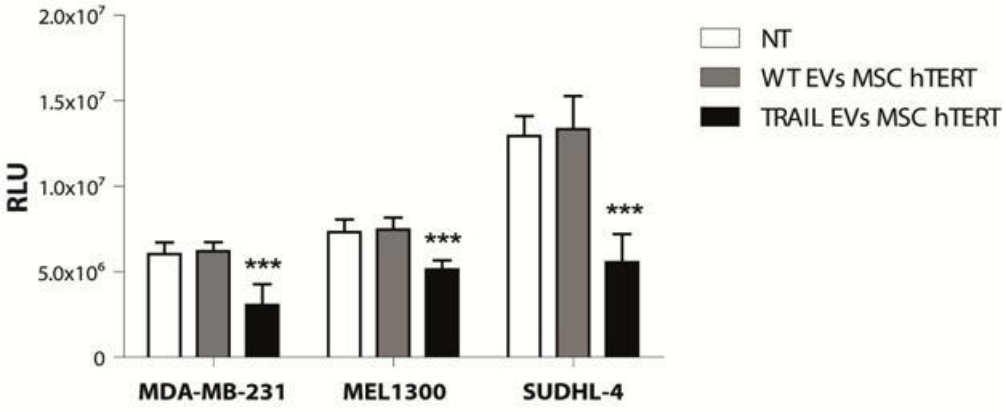


***Figure 6.11: Effect of EVs isolated from MSC hTERT cell line***
*Effect of TRAIL EVs on different cancer cell lines. Cells were cultured in 96-well plate and treated for 24 h with 50 µg/ml of EVs (WT and TRAIL) isolated from conditioned medium of MSC hTERT cells. Viability was evaluated using the CTG assay. Data represent averages ± SD. *** p <0.001 compared to not treated cells (NT) by Student t-test.*

---

The *in vivo* experiments were conducted creating subcutaneous *xenograft* model of the MEL1300 cell line. Briefly, we injected $2x10^5$ of MEL1300 cells in two separate spots of the abdomen of NGS mice. After ten days from injection all tumours were palpable, tumour volume was then measured and mice were randomized into three experimental groups: i) TRAIL EVs obtained from hTERT MSC ii) WT EVs obtained from hTERT MSC iii) PBS. Treatment was performed according to the therapeutic scheme illustrated in **(Figure 6.4A).** No therapeutic effect was observed as attested by lack of difference of tumour volume measurements in mice treated with TRAIL EVs compared to control **(Figure 6.12)**.

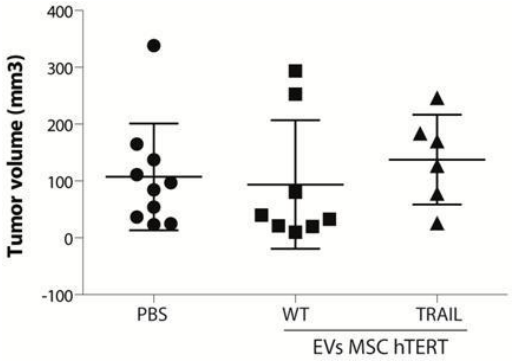


***Figure 6.12: In vivo effect of EVs derived from MSC hTERT***
*Tumour volume of mice inoculated with MEL1300 and treated with 200 µg of EVs (WT and TRAIL) isolated from conditioned medium of MSC hTERT cell line. Means ± SD are reported.*

---

Although MSC cells represent a valid source of EVs that express stably TRAIL protein upon transduction, some weaknesses have to be considered. First, the yields of EVs from MSC are very low. We tried to increase the yield by replacing the common culture flasks with bioreactors that allow cells to be cultivated at high density. Unfortunately, the number of particles measured by Nanoparticle Tracking Analysis (NTA) was equal for samples from bioreactor and flask. In addition, we observed that the EVs produced in bioreactors comprised a more homogeneous population in terms of average molecule size as measured by NTA (data not shown). The significance of this observation remains unknown, even though the EVs preparation from bioreactors was sticky and forms a gelatinous pellet that is very difficult to dissolve. The efficacy of EVs produced in bioreactor, instead, was comparable to EVs produced in flask, although much of the production has to be filtered out due to solubility issues. Second, it seemed that only 10% of EVs derived from MSC cells expressed TRAIL as attested to by FACS analysis performed by Prof. Luca Gianni and collaborators (data not shown). This could provide an explanation for the unsuccessful *in vivo* data and the variability of the *in vitro* results. An optimisation of EVs production, a better strategy for their purification, an adjustment of the *in vivo* dosage and administration, and finally a better characterization of EVs and their content would be required.

# References

1. Amarante-Mendes GP, Griffith TS. Therapeutic applications of TRAIL receptor agonists in cancer and beyond. Pharmacology & therapeutics. [Review]. 2015 Sep 5.
2. Lavazza C, Carlo-Stella C, Giacomini A, Cleris L, Righi M, Sia D, et al. Human CD34+ cells engineered to express membrane-bound tumor necrosis factor-related apoptosis-inducing ligand target both tumor cells and tumor vasculature. Blood. 2010 Mar 18;115(11):2231-40.
3. Carlo-Stella C, Lavazza C, Di Nicola M, Cleris L, Longoni P, Milanesi M, et al. Antitumor activity of human CD34+ cells expressing membrane-bound tumor necrosis factor-related apoptosis-inducing ligand. Human gene therapy. 2006 Dec;17(12):1225-40.
4. Andaloussi SEL, Mager I, Breakefield XO, Wood MJ. Extracellular vesicles: biology and emerging therapeutic opportunities. Nature reviews Drug discovery. 2013 May;12(5):347-57.
5. Raposo G, Stoorvogel W. Extracellular vesicles: exosomes, microvesicles, and friends. The Journal of cell biology. [Research Support, Non-U.S. Gov'tReview]. 2013 Feb 18;200(4):373-83.
6 Mihara K, Imai C, Coustan-Smith E, Dome JS, Dominici M, Vanin E, Campana D. Development and functional characterization of human bone marrow mesenchymal cells immortalized by enforced expression of telomerase. Br J Haematol. 2003 Mar;120(5):846-9.

# Publications arising from work during my PhD studentship not directly related to these projects

## Original papers

Barbieri E, Deflorian G, Pezzimenti F, **Valli D**, Saia M, Meani N, Gruszka A. M, Alcalay M. The leukemogenic nucleophosmin mutant modulates Wnt signaling during zebrafish development.Oncotarget. 2016 Jul 28. doi: 10.18632/oncotarget.10878. IF 5.008

Saia M, Termanini A, Rizzi N, Mazza M, Barbieri E, **Valli D**, Ciana P, Gruszka AM, Alcalay M. AML1/ETO accelerates cell migration and impairs cell-to-cell adhesion and homing of hematopoietic stem/progenitor cells. Sci Rep. 2016 Oct 7;6:34957. doi: 10.1038/srep34957. IF 5.228

Derenzini E, Mondello P, Erazo T, Portelinha A, Liu Y, Scallion M, Asgari Z, Philip J, Hilden P, **Valli D**, Rossi A, Djaballah H, Ouerfelli O, de Stanchina E, Seshan VE, Hendrickson RC, Younes A. BET Inhibition-Induced GSK3β Feedback Enhances Lymphoma Vulnerability to PI3K Inhibitors. Cell Rep. 2018 Aug 21;24(8):2155-2166. doi: 10.1016/j.celrep.2018.07.055. IF 8.032.

## Reviews

Gruszka A. M, **Valli D**, & Alcalay M. Understanding the molecular basis of acute myeloid leukemias: where are we now? Int. J. Hematol. Oncol. (2017) 6(2), 43–53. IF NA.

Gruszka AM, **Valli D**, Restelli C, Alcalay M. Adhesion Deregulation in Acute Myeloid Leukaemia. Cells. 2019 Jan 17;8(1). pii: E66. doi: 10.3390/cells8010066. IF 5.656

Gruszka A. M, **Valli D**, & Alcalay M. Wnt signalling in acute myeloid leukaemia. Cells. 2019 Nov 7;8(11). pii: E1403. doi: 10.3390/cells8111403. IF 4.829